UNIVERSITY OF CALIFORNIA SAN DIEGO

The Role of TREM2 in Myocardial Injury and Transcriptional Regulation of Macrophage Phenotypes

A Dissertation submitted in partial satisfaction of the requirements
for the degree Doctor of Philosophy

in

Biomedical Sciences

by

Thomas Andreas Prohaska

Committee in charge:

Professor Christopher Glass, Chair
Professor Ronald Evans
Professor Åsa Gustafsson
Professor Amit Majithia
Professor Joseph Witztum

2022

The Dissertation of Thomas Andreas Prohaska is approved, and it is acceptable in quality and form for publication on microfilm and electronically.

University of California San Diego

2022

TABLE OF CONTENTS

LIST OF FIGURES

LIST OF TABLES

LIST OF ABBREVIATIONS

DAMP	damage-associated molecular pattern
PAMP	pathogen-associated molecular pattern
TLR	toll-like receptor
IL	interleukin
TNF	tumor necrosis factor
TGF	transforming growth factor
PDGF	platelet-derived growth factor
IGF-1	insulin-like growth factor 1
VEGF	vascular endothelial growth factor
MMP	matrix metalloprotease
scRNA-seq	single-cell RNA sequencing
IRF	interferon regulatory factor
MITF	melanocyte inducing transcription factor
TF	transcription factor
LXR	liver X receptor
NFκB	nuclear factor κ B
LPS	lipopolysaccharide
NASH	non-alcoholic steatohepatitis
TREM2	triggering receptor expressed on myeloid cells 2
DAP	DNAX activation protein
TYROBP	TYRO protein tyrosine kinase-binding protein
SYK	spleen tyrosine kinase
PI3K	phosphatidylinositol 3-kinase
DAM	disease-associated microglia
LAM	lipid-associated macrophages
KC-N	Kupffer cells in NASH
SAM	scar-associated macrophages
GWAS	genome wide association study
KO	knockout
GLS	global longitudinal strain
LAD	left anterior descending coronary artery
BMDM	bone-marrow derived macrophages
TPM	transcripts per million
ATAC-seq	assay for transposase-accessible chromatin using sequencing
ChIP-seq	chromatin immunoprecipitation followed by sequencing
M-CSF	macrophage colony-stimulating factor
GM-CSF	granulocyte-macrophage colony-stimulating factor
FACS	fluorescence-activated cell sorting
H3K27ac	histone 3 lysine 27 acetylation
KLA	Kdo2-Lipid A
gRNA	guide RNA
CIM	conditionally immortalized macrophages
FDR	false discovery rate

ACKNOWLEDGEMENTS

I would like to acknowledge Dr. Christopher Glass for his mentorship throughout the past three years, for the inspiring scientific discussions we have had, and for the scientific nurture he provided at all stages for me to pursue my own ideas, while still always gently guiding me into the right direction.

I would also like to thank my first scientific mentor, Dr. Margarethe Geiger, for providing the opportunity to carry out my own project as a junior medical student in Vienna. I am thankful for the mentorship of Dr. Christoph Binder who led by example as an outstandingly successful young investigator and as a mentor who was always ready to provide supportive career and scientific advice. I particularly want to express my gratitude to Dr. Nai-Wen Chi who laid the foundation for me to come to UC San Diego first as a postdoctoral fellow and later as a resident physician in Internal Medicine. Additionally, I want to thank my postdoctoral mentor Dr. Joseph Witztum, whose continuous support as a mentor made a career as a physician-scientist possible for me. All of the above are role models of successful physician-scientists and mentors who fundamentally helped to shape the direction both of my career and my personal life.

I want to express my gratitude to all members of the Glass Laboratory who have made these past three years an enjoyable experience and have always provided valuable scientific input and discussions. I want to particularly thank Mashito Sakai, Nathan Spann, Yohei Abe, Christian Nickl, and Mohnish Alishala for their invaluable help and contributions to my projects.

While the professional mentorship and support I have received has been

crucial for my career, there are many other people who have provided tremendous support during the past few years. First, I want to thank my wife Vi who has unconditionally supported me through the often challenging years of “endless training” of a postdoctoral fellowship, clinical residency, clinical fellowship, and a research fellowship including formal PhD training. I want to thank my parents Ingrid and Gottfried, and my sister Elisabeth for their continuous loving support from infancy to fellowship. I am grateful to my aunt Christa and uncle Hanns who have always supported my professional endeavors. Furthermore, I would like to thank my friends in San Diego who have become like family over the past years.

Research in this dissertation was supported by NIH grants T32 DK007044, R01 DK091183, and P01 HL147835.

Chapter 2 is coauthored with Jason Duran, Christian Nickl, Ty Troutman, David Calcagno, Yusu Gu, Kevin King, Eric Adler, and Christopher Glass. The dissertation author was the primary author of this chapter.

Chapter 3 is coauthored with Nathanael Spann, Yohei Abe, Johannes Schlachetzki, Mohnish Alishala, Sydney O’Brien, Mashito Sakai, and Christopher Glass. The dissertation author was the primary author of this chapter.

VITA

2022 Doctor of Philosophy in Biomedical Sciences, University of California San Diego

2013 Doctor of Medicine, Medical University of Vienna

PUBLICATIONS

Shen Z, Li RZ, Prohaska TA, Hoeksema MA, Spann NJ, Tao J, Fonseca GJ, Le T, Stolze LK, Sakai M, Romanoski CE, Glass CK. Systematic analysis of naturally occurring insertions and deletions that alter transcription factor spacing identifies tolerant and sensitive transcription factor pairs. *Elife.* 2022 Jan 20;11:e70878

Que X, Hung MY, Yeang C, Gonen A, Prohaska TA, Sun X, Diehl C, Määttä A, Gaddis DE, Bowden K, Pattison J, MacDonald JG, Ylä-Herttuala S, Mellon PL, Hedrick CC, Ley K, Miller YI, Glass CK, Peterson KL, Binder CJ, Tsimikas S, Witztum JL. Oxidized phospholipids are proinflammatory and proatherogenic in hypercholesterolaemic mice. *Nature.* 2018; 558: 301–306

Prohaska TA, Que X, Diehl CJ, Hendrikx S, Chang MW, Jepsen K, Glass CK, Benner C, Witztum JL. Massively Parallel Sequencing of Peritoneal and Splenic B Cell Repertoires Highlights Unique Properties of B-1 Cell Antibodies. *J Immunol.* 2018 Mar 1;200(5):1702-1717.

Harmon DB, Srikakulapu P, Kaplan JL, Oldham SN, McSkimming C, Garmey JC, Perry HM, Kirby JL, Prohaska TA, Gonen A, Hallowell P, Schirmer B, Tsimikas S, Taylor AM, Witztum JL, McNamara CA. Protective Role for B-1b B Cells and IgM in Obesity-Associated Inflammation, Glucose Intolerance, and Insulin Resistance. *Arterioscler Thromb Vasc Biol.* 2016 Apr;36(4):682-91.

Rosenfeld SM, Perry HM, Srikakulapu P, Grewal S, Das D, McSkimming C, Gonen A, Prohaska TA, Taylor A, Tsimikas S, Witztum JL, Bender TP, McNamara CA. B-1b cells secrete atheroprotective IgM and attenuate atherosclerosis. *Circ Res.* 2015 Jul 17;117(3):e28-39.

Tsiantoulas D, Perkmann T, Afonyushkin T, Mangold A, Prohaska TA, Papac-Milicevic N, Millischer V, Bartel C, Hörkkö S, Boulanger CM, Tsimikas S, Fischer MB, Witztum JL, Lang IM, Binder CJ. Circulating microparticles carry oxidation-specific epitopes and are recognized by natural IgM antibodies. *J. Lipid Res.* 2015 Feb;56(2):440-8.

Prohaska TA*, Wahlmüller FC*, Furtmüller M, Geiger M
Interaction of Protein C Inhibitor with the Type II Transmembrane Serine Protease Enteropeptidase. *PLoS ONE* 2012, 7(6): e39262.
*contributed equally

ABSTRACT OF THE DISSERTATION

The Role of TREM2 in Myocardial Injury and Transcriptional Regulation of Macrophage Phenotypes

by

Thomas Andreas Prohaska

Doctor of Philosophy in Biomedical Sciences

University of California San Diego, 2022

Professor Christopher Glass, Chair

TREM2 (Triggering Receptor Expressed on Myeloid Cells 2) is a transmembrane receptor that has recently been established as a key regulator of macrophages in multiple disease models. It is highly expressed in distinct macrophage populations in models of Alzheimer's Disease, non-alcoholic steatohepatitis, and obesity. In this study, we interrogated the effect of deletion of TREM2 or treatment with a TREM2-activating antibody in myocardial injury models. To understand how TREM2 itself is regulated and how it mediates its effects on transcription, we established a conditionally immortalized monocyte progenitor cell

line that constitutively expresses Cas9 and is able to differentiate into macrophages. We used this cell line to delete the intergenic enhancer of TREM2 and to knock out TREM2 as well as transcription factors. Thereby, we identified transcription factors mediating the effects of TREM2 on gene expression. Overall, in this work we demonstrate the role of TREM2 in myocardial injury, interrogate regulation of *Trem2* expression, and identify transcription factors downstream of TREM2 signaling.

.

CHAPTER 1: INTRODUCTION

Discovery of Basic Functions of Macrophages

Macrophages were first described at the end of the 19th century by Ilya Mechnikov when he described a cell type in starfish larvae he termed “phagocyte”. He demonstrated that they are able to engulf foreign material and that bacteria attract leukocytes isolated from blood (1). Macrophages are resident cells in most organs of the body and can either originate from fetal development or from circulating monocytes differentiating into a macrophage upon entry into a tissue (2).

Previously it had been thought that most or all tissue macrophages originate from monocytes (3). However, fate-mapping experiments in the 21st century have demonstrated that many tissue-resident macrophages have their origins during embryonic development from the yolk sac or fetal liver (2, 4-8). Depending on the tissue, varying proportions of macrophages are either embryonic (yolk salk or fetal liver) or adult (monocytes) in origin. While some tissue macrophage populations such as microglia in the brain are almost exclusively composed of self-renewing macrophages of embryonic lineage, the liver, lung, and heart receive monocytes contributing to their macrophage populations, which thereby are of mixed lineage (4, 9, 10).

Macrophages are traditionally known for their function to phagocytose microorganisms in response to infection. Additionally, they were described as the cells taking up lipids via scavenger receptors and turning into foam cells in atherosclerosis (11, 12). While they previously have been studied as classically (M1) or alternatively (M2) activated macrophages, recent studies have identified much more complexity of macrophage populations in various disease models *in vivo* that cannot be explained by

these polarized cell activations (13-15). They have been shown to play major functions in the inflammatory response and repair to any form of tissue injury, including non-alcoholic steatohepatitis, Alzheimer's Disease, and myocardial infarction (16-18). In addition, they also occupy most tissues of the body at homeostasis (2, 10). There they often have unique functions such as facilitating electrical conduction in the heart or removing aged erythrocytes in the spleen (19, 20).

Macrophage Origins and Development

Tissue resident macrophages are derived from three different lineages. First, in early embryogenesis, the yolk sac gives rise to macrophage progenitors (5). Following that, the fetal liver takes over hematopoiesis and gives rise to monocytes (21). Eventually, hematopoiesis starts in the bone marrow, which is the source of monocytes throughout life (22). Initially it was thought that all macrophages are derived from circulating monocytes originating from the bone marrow. However, based on lineage-tracing experiments it is now known that adult tissue macrophages have diverse origins and the composition of each tissue's resident population at homeostasis varies substantially. For example, microglia are by and large derived from yolk sac precursors with minimal contribution from other sources (4). On the other hand, skin Langerhans cells are mostly derived from fetal liver (23). Other organs, such as the spleen, liver, kidney, or heart are initially populated from yolk sac precursors, and later to varying extents replaced by macrophages derived from circulating monocytes (2, 9, 21). Circulating monocytes can enter tissue, differentiate first into a F4/80^{lo} macrophage, followed by further differentiation into a F4/80^{hi} macrophage similar to tissue

macrophages derived from the yolk sac (24). Thus, depending on the tissue and physiological or pathophysiological contexts, tissue macrophages can be derived from multiple sources.

Role of Macrophages in Tissue Repair

Any form of tissue injury releases damage-associated molecular patterns (DAMPs) or pathogen-associated molecular patterns (PAMPs), released from injured cells or microorganisms (25-28). These trigger an inflammatory response consisting of proliferation of immune cells and recruitment of various cell types to the injured tissue (29-32). Depending on the nature of the response, it may be well orchestrated and resolve quickly or it may result in chronic complications of inflammation, such as fibrosis and impaired tissue function (33-35). Monocytes are recruited to the site of injury from the bloodstream via chemokines and differentiate into macrophages after their arrival. Generally, first $Ly6C^{hi}$ monocytes are recruited, followed later by $Ly6C^{lo}$ monocytes (31, 36). Additionally, local macrophages proliferate and contribute to the immune response to the injury (30, 33). Initially, macrophages are activated through DAMPs and/or PAMPs binding to pattern recognition receptors such as toll-like receptors (TLRs) 2 and 4 and express pro-inflammatory cytokines such as interleukin 1β (IL-1β), IL-6, and tumor necrosis factor alpha (TNF-α), attract other chemokines, and secrete matrix metalloproteases (37-39). After this early pro-inflammatory response, the predominant phenotype generally turns towards a “reparative” macrophage secreting proteins like transforming growth factor β (TGF-β) inducing production of collagen in fibroblasts or myofibroblasts and platelet-derived growth factor (PDGF) promoting cell proliferation

(40, 41). This change of macrophage phenotype has been highlighted in different diseases models. For example, in CCl_4-induced liver injury, ablation of CD11b-expressing macrophages during CCl_4 treatment decreased the extent of injury to the liver. In contrast, ablation of macrophages after CCl_4 treatment was completed, increased the degree of fibrosis (39). This study highlighted the potentially detrimental pro-inflammatory effect of macrophages early in the process and the beneficial contribution in the reparative phase of tissue injury.

The pro-inflammatory initial macrophage response is characterized by secretion of IL-1β, IL-6, and TNF-α (42). IL-1β accelerates atherosclerosis in mouse models and a randomized clinical trial of canakinumab, a monoclonal antibody targeting IL-1β, has shown a reduction in cardiovascular events in patients with cardiovascular disease (43, 44). TNF-α secretion by macrophages is dysregulated in rheumatoid arthritis leading to inflammation of the synovial membrane (45). Inhibition of TNF-α has shown a benefit in randomized clinical trials of patients with rheumatoid arthritis (46-48). A trial using the IL-6 antagonists tocilizumab and sarilumab in patients with Covid-19 showed an increase in cardiovascular or respiratory organ support-free days (49). This highlights the detrimental effect excessive action of these cytokines can have and the beneficial effect of antagonizing them in certain disease processes in animal models or humans. In addition, macrophages can produce cytokines stimulating the proliferation and activation of T cells further contributing to inflammation (50, 51). While this inflammatory response may be beneficial in clearing pathogenic microorganisms, excessive or prolonged responses can cause significant tissue damage and/or lead to harmful chronic inflammatory processes (33, 42).

After the initial response, pro-inflammatory macrophages either undergo apoptosis or switch to a reparative or anti-inflammatory phenotype that promotes wound healing and recover of function of the tissue (52, 53). This macrophage subtype stimulates fibrosis through TGF-β, parenchymal regeneration and proliferation through growth factors such as insulin-like growth factor 1 (IGF-1) or PDGF, angiogenesis through VEGF-α, and tissue renewal from progenitors or stem cells through Wnt3a (40, 41, 54, 55). These processes contribute to healing after the initial pro-inflammatory response.

Additionally, macrophages can also promote fibrosis. This is assumed to be mediated through activation of collagen production in fibroblasts by TGF-β secretion but a TGF-β independent mechanism mediated by IL-13 has also been identified (56, 57). In a model of bleomycin-induced pulmonary fibrosis, depletion of macrophages led to a decrease in lung collagen and fibrosis by histologic assessment, showcasing the importance of macrophages in the development of fibrosis (58). In addition to directly stimulating collagen production, macrophages also contribute to the survival of myofibroblasts (59). Furthermore, macrophages secrete matrix metalloproteases (MMPs), some of which can contribute to fibrosis. IL-13 induces secretion of the elastase MMP12 by macrophages. Knockout of *Mmp12* in mice led to a reduction in pulmonary and hepatic fibrosis (60). In summary, macrophages play a key role in regulating fibrosis after tissue injury through multiple mechanisms.

Transcriptional Regulation of Macrophages

Tissue resident macrophages exhibit diverse gene expression as evidenced by the analysis using single-cell RNA-seq (scRNA-seq) (30, 61-64). While there is a core set of genes that are expressed in most macrophages, there are a variety of genes expressed that are mediated by the environment the macrophage resides in (64, 65). This diversity is often connected to tissue-specific functions such as iron homeostasis or toxin removal in Kupffer Cells of the liver, synaptic monitoring and pruning of microglia, or clearance of aged erythrocytes by splenic macrophages.

Macrophage gene expression is regulated both by lineage determining transcription factors and signal-dependent transcription factors. In general, lineage determining factors bind to DNA and create the accessible chromatin landscape by dislocating nucleosomes and making promoters and enhancers accessible to collaborative binding of signal-dependent factors (66, 67). These complexes can then activate transcription based on signals from the environment the cell resides in (e.g., Notch ligands in Kupffer Cells) and signals derived from injury (e.g., DAMPs and PAMPs). The activation of transcription is often associated with acetylation of histone 3 at the lysine 27 site (H3K27ac) (68). The macrophage lineage determining factor PU.1 is expressed in all macrophages and together with the C/EBP family of factors represents the major lineage determining transcription factors in macrophages (69-71). Some other transcription factor families are broadly expressed throughout macrophages in multiple tissue environments (e.g., AP-1, IRF, TFE/MITF) (67, 72). Each transcription factor preferentially binds to a specific DNA sequence represented computationally by a “motif” that is typically 10-15 bases long (73). Of each motif, some bases are more

conserved and essential for transcription factor-binding while others may be flexible and can be replaced with other bases without major effect on transcription factor binding (74).

While promoters are necessary for initiating transcription of genes into mRNA, information from enhancers is needed to control the level of gene expression dependent on the cell type and signals received from the environment (67). In macrophages, binding of a relatively small number of lineage-determining transcription factors, mostly PU.1 together with members of the C/EBP, AP-1, and RUNX families, creates the enhancer landscape (75, 76). Depending on signals derived from the environment, the enhancer landscape is modified further by signal-dependent transcription factors in collaboration with lineage-determining transcription factors. For example, in Kupffer cells, the Notch ligand DLL4, TGF-β, and desmosterol induce the recruitment of the transcription factors RBPJ, SMAD family, and LXR-α to create the enhancer landscape and induce transcriptional programs specific to Kupffer Cells (65). Depending on the existing enhancer landscape, each cell type then responds with different transcriptional programs to external signals derived from pathogens, inflammation, or disease contexts (67).

Bacterial lipopolysaccharide (LPS) induces a pro-inflammatory transcriptional program in macrophages initially started by binding of LPS to toll like receptor 4 (TLR4), a pattern recognition receptor. This leads to a recruitment of interferon response elements such as IRF3 and nuclear factor κ B (NFκB) to enhancers, eventually leading to the expression of pro-inflammatory cytokines such as IL-1β, IL-6, and TNF-α, inducing a pro-inflammatory effect also in the surrounding cells or tissue (77).

In non-alcoholic steatohepatitis (NASH), Kupffer cells activate vastly different transcriptional programs compared to homeostatic Kupffer cells characterized by decreased expression of Kupffer cell identity genes, decreased survival of homeostatic Kupffer cells, and an increase in NASH-specific genes. These effects are at least partly mediated by increased binding of AP-1 (e.g., ATF3) and EGR family members binding to enhancers of genes specific to NASH Kupffer cells and reprogramming LXR activity in Kupffer cells (30). Equivalent processes involving changes in transcriptional regulation are present in macrophages in other settings of signals from pathogens or tissue injury (67, 78).

TREM2 as a Key Regulator of Macrophages in Tissue Injury

TREM2 (Triggering Receptor Expressed on Myeloid cells-2) is a transmembrane receptor expressed in macrophages binding a variety of ligands, including DNA, bacterial lysates, phospholipids, and lipoproteins (79, 80). The majority of ligands are products present during tissue damage. TREM2 has an extracellular domain with a V-type immunoglobulin domain and a short cytosolic domain without any motifs relevant to signal transduction (80). The extracellular domain can be cleaved by the metalloproteases ADAM10 and ADAM17, removing the ligand-binding site from TREM2 and rendering it inactive on the cell surface (81). The effects of the cleaved and now soluble part of TREM2 itself are thus far largely unknown (82). TREM2 mediates its effects through DAP12 (DNAX activation protein 12), also known as TYROBP (TYRO protein tyrosine kinase-binding protein), or DAP10 (Figure 1) (83, 84). After binding of ligands to TREM2 and the formation of heterodimers of TREM2 with a DAP protein,

DAP12 then activates the tyrosine kinase SYK and DAP10 activates PI3K (phosphatidylinositol 3-kinase) (84, 85). However, the following steps in signal transduction leading to gene expression changes mediated by TREM2 are unknown.

TREM2 expression in healthy human tissue obtained from organ donors is mostly limited to macrophages in adipose tissue and microglia, the tissue-resident macrophage of the brain (80). With the recent advances in single-cell RNA sequencing, macrophage populations with high expression of *Trem2* have been identified in models of Alzheimer's Disease (disease-associated microglia, DAM), metabolic syndrome in adipose tissue macrophages (lipid-associated macrophages, LAM), and in Kupffer cells during NASH (KC-N) (17, 67, 86, 87). In humans, Ramachandran et. al identified a population of macrophages that expressed high levels of *TREM2* and *CD9* by single-cell RNA-sequencing of livers from patients with cirrhosis (62). By immunofluorescence, they discovered that this population is located close to areas of collagen/fibrosis and therefore named them scar-associated macrophages (SAM) (62). As they were identified by RNA sequencing, these cells all have a distinct expression profile compared to homeostatic macrophages in the same tissue, including genes related to lipid metabolism, phagocytosis, and inflammatory regulation (80). One of the markers that is co-expressed with *Trem2* in all of the above macrophage populations is *Cd9* (17, 62, 67, 86, 87). CD9 is an inhibitor of ADAM17, the major protease cleaving TREM2 off the cell surface (88). By this action, CD9 may act to potentiate the effect of TREM2 in these cells.

In vitro, TREM2 is highly expressed in macrophages in tissue cultures. Early studies with knockout models of TREM2 showed that TREM2 suppressed the

inflammatory response of macrophages to external stimuli. The production of TNF-α and IL-6 in response to lipopolysaccharide, zymosan, and CpG was markedly increased in macrophages lacking TREM2 (89, 90). Additionally, TREM2 increased phagocytosis of apoptotic neurons in microglia and overexpression of both TREM2 and DAP12, but not overexpression of either alone, markedly increased the phagocytic capacity of Chinese Hamster Ovary cells that are intrinsically non-phagocytic (91, 92). Thus, TREM2 both dampens the pro-inflammatory response and increases phagocytosis in cultured cells.

In vivo, development of the DAM population goes through two stages, with the first (stage 1 DAM) being TREM2 independent and the second (stage 2 DAM) being dependent on TREM2. Knockout of TREM2 therefore leads to loss of stage 2 DAM (17). Additionally, TREM2 deficiency in Alzheimer's Disease mouse models lead to an increase in amyloid β plaques and loss of neurons (93, 94). Furthermore, genome wide association studies (GWAS) have identified a missense mutation of TREM2 that is strongly associated with the development of Alzheimer's Disease in humans, further strengthening the evidence for a beneficial effect in microglia (95, 96). The rare human disease associated with loss of TREM2 or DAP12 function, Nasu-Hakola Disease or polycystic lipomembranous osteodysplasia with sclerosing leukoencephalopathy, leads to bone cysts with recurrent fractures and a severe frontal dementia that usually leads to death from dementia complications by age 50 (97, 98). This illustrates not only the effect of TREM2 in Alzheimer's Disease but also in human brain homeostasis.

By single-cell RNA-seq, a substantial proportion of TREM2-expressing LAM appeared in adipose tissue after 12 weeks of high-fat diet feeding. These cells are

defined by high expression of *Trem2* and *Cd9*. Knockout of TREM2 led to adipocyte hypertrophy, increased glucose levels, reduced insulin sensitivity, and hypercholesterolemia (86). This indicates that TREM2 in adipose tissue macrophages has an overall beneficial effect on metabolic parameters in metabolic syndrome.

While *Trem2* is only minimally expressed in Kupffer cells in healthy livers, in NASH, Kupffer Cells and macrophages recruited to the liver express high levels of *Trem2* (67). Additionally, in humans with cirrhosis, there is a subset of *TREM2*-expressing scar-associated macrophages, co-localizing with fibrotic areas (62). However, while in most other tissues TREM2 exerts a mostly protective effect, further studies are needed to determine if TREM2 has a beneficial, neutral, or harmful effect in NASH.

TREM2 is also expressed on tumor-associated macrophages (TAM). TAM are usually considered anti-inflammatory and activate T regulatory cells suppressing the immune response to the tumor environment. TREM2 seems to potentiate this effect in two recent studies, showing that knockout of TREM2 decreases tumor growth by increasing the inflammatory response to the cancer (99, 100). Therefore, while activation of TREM2 may be desired in neurodegenerative or metabolic disease, in cancer, suppression of TREM2 may be a viable therapeutic strategy, similar to current therapies like PD-1 and PD-L1 inhibitors that augment the immune response to cancer (101).

Overall, TREM2 acts as a key regulator of macrophage function in multiple disease contexts, and either activation or suppression may be viable therapeutic strategies, depending on the disease context.

The Immune Response to Myocardial Infarction

Myocardial infarction (MI) is a cardiovascular event with substantial morbidity, mortality, and economic costs, both in the U.S. and around the world (102). It usually results from atherosclerotic plaque development in the coronary arteries, followed by plaque rupture and thrombosis, which result in occlusion or critical narrowing of the artery (103, 104). This leads to ischemia, tissue hypoxia, and cell death of cardiomyocytes in the tissue supplied by the culprit artery (105). Despite novel therapeutics for atherosclerotic vascular disease, about 805,000 people suffer from MI in the United States each year and the annual economic burden is estimated to be around $85 billion from medical procedures and lost productivity (102, 106, 107). Despite the additional advancement of early reperfusion with primary percutaneous coronary intervention as treatment for ST-elevation MI, in-hospital mortality remains high at 5-9% and congestive heart failure develops in 20-30% of patients within a year following MI, leading to delayed morbidity and mortality (108-113). No therapy currently exists that directly targets the wound-healing process after MI, creating a vacuum for novel therapeutics in this area to decrease morbidity and mortality.

MI leads to extensive recruitment of immune cells to the infarcted area in multiple waves. First, resident cardiac macrophages secrete CXCL2 and CXCL5 to attract neutrophils within hours (114). Monocytes arrive at the heart first as “pro-inflammatory” $Ly6C^{hi}$ macrophages within 3-10 days and later as “reparative” $Ly6C^{lo}$ macrophages within 7-14 days either by differentiation from $Ly6C^{hi}$ macrophages or via recruitment through CX3CR1 (31, 115, 116). Initially, macrophages remove necrotic tissue and produce pro-inflammatory cytokines such as IL-1β and IL-6 (117). When the tissue

environment changes to the reparative phase, macrophages express fewer pro-inflammatory cytokines, but stimulate the conversion of fibroblasts into myofibroblasts through TGF-b and angiogenesis through VEGF (31, 118).

In the heart, macrophages can have both beneficial and harmful effects. Inhibition of CCR2 improved infarct healing and left ventricular function (119). On the other hand, knockout of the macrophage transmembrane receptor MerTK worsened myocardial wound healing and MerTK also maintains function in normal hearts by taking up exophers filled with defective mitochondrial products from cardiomyocytes (120, 121). Additionally, cardiac stem cell infusion was found to exert its protective effects in mice by activating the innate immune response, highlighting the potential of modulating macrophages *in vivo* (18). Despite these findings showing that modulation of the immune response can have beneficial or harmful effects, there is no current therapy specifically targeting macrophages in the wound-healing process after MI.

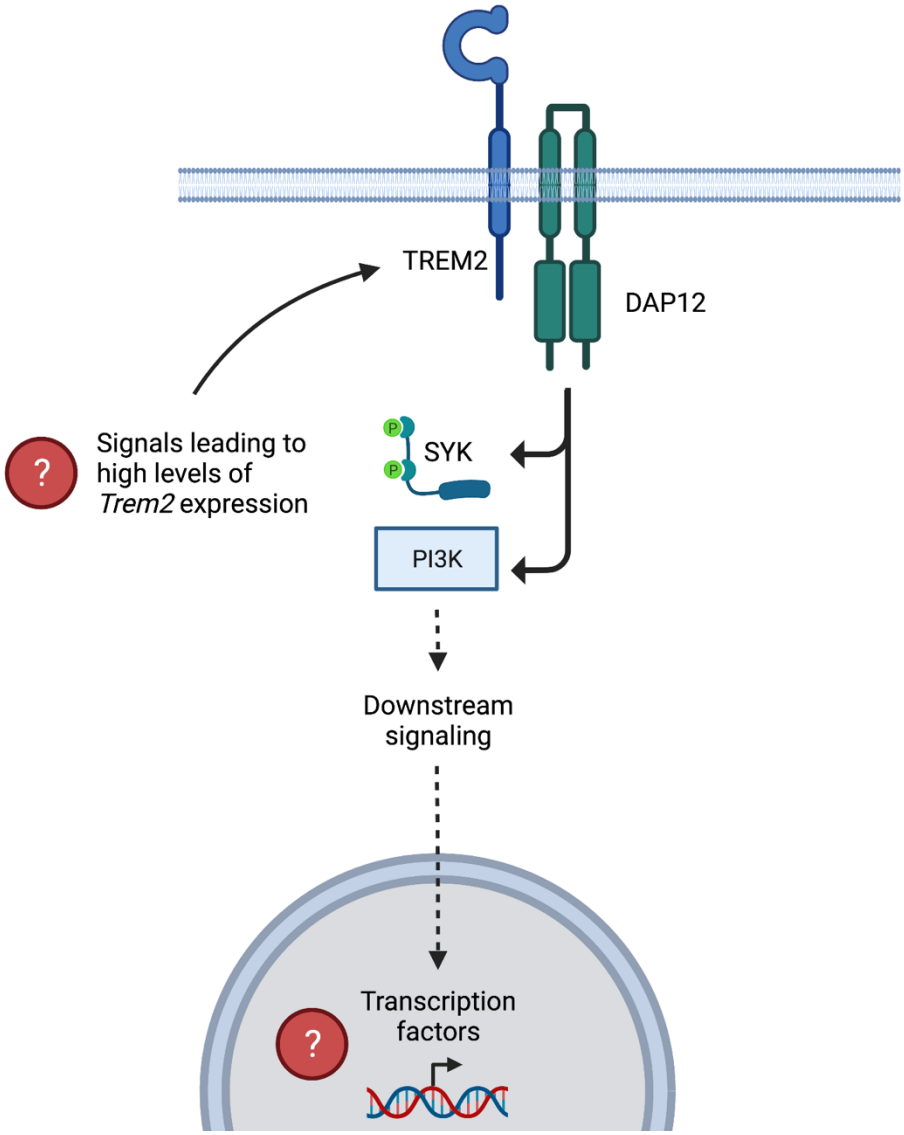

Figure 1: Knowledge of the TREM2 signaling pathway prior to this study
While parts of the initial signaling cascade were known, no studies had addressed how *Trem2* expression is upregulated or which transcription factors TREM2 employs to mediate its effect on gene expression. Adapted from Dezykowska, Weiner, and Amit, *Cell* 2020 (80).

CHAPTER 2: TREM2 IN MYOCARDIAL INJURY

Abstract:

TREM2 (Triggering Receptor Expressed on Myeloid Cells 2) is a transmembrane receptor that has recently been established as a key regulator of macrophages in multiple disease models. It is highly expressed in distinct macrophage subsets identified by single-cell RNA-seq in models of Alzheimer's Disease (disease-associated microglia/DAM), obesity (lipid-associated macrophages/LAM), or non-alcoholic steatohepatitis (scar-associated macrophages/SAM). However, it has remained unknown how TREM2 activates these gene expression programs.

We analyzed published single-cell RNA-seq data and found that TREM2 is highly expressed in cardiac macrophages after myocardial injury with a peak around 7 days after LAD ligation but is not substantially expressed at baseline or in the uninjured area. We used TREM2 KO (knockout) mice to evaluate the function of TREM2 in cardiac macrophages. Loss of TREM2 led to a substantial increase in mortality in male mice compared to wild-type. All female mice survived until euthanasia 8 weeks after injury but loss of TREM2 worsened left ventricular global longitudinal strain measured 6 weeks after injury. These findings demonstrate that TREM2 exerts a protective effect after myocardial injury.

To address whether pharmacologic activation of TREM2 is a therapeutic strategy with translational potential, we administered TREM2-activating antibody or isotype in a cohort of mice undergoing ischemia/reperfusion injury with 60 minutes of LAD ligation. Treatment with TREM2-activating antibody did not lead to significant changes in cardiac function, left ventricular volume, or heart weight. Therefore, pharmacologic modulation

of factors downstream of TREM2 may have better translational potential and could be tested in the future.

Overall, we show that TREM2 is expressed in macrophages after myocardial injury, loss of TREM2 worsens cardiac mortality after LAD ligation in male mice and left ventricular function in female mice, but administration of a TREM2-activating antibody did not lead to any change in cardiac parameters after ischemia/reperfusion injury.

Introduction:

Ischemic heart disease is the leading cause of death worldwide and the morbidity associated with its complications causes suffering and major economic impacts (102, 107). In most cases, myocardial infarction is caused by rupture of an atherosclerotic plaque followed by superimposed thrombosis leading to occlusion or critical stenosis of the artery (103, 104). This further leads to ischemia of the supplied cardiac tissue and cell death of cardiomyocytes (105). The necrotic cells release large amounts of damage-associated molecular patterns (DAMPs) causing activation of the innate immune system, followed by influx of neutrophils into the heart within hours of infarction and thereafter the recruitment of circulating monocytes that differentiate to macrophages upon entering the tissue (31). Inflammatory cells can be activated by DAMPs through pattern recognition receptors such as toll-like receptors (TLRs) (28, 77). This leads to the production of pro-inflammatory cytokines such as TNF-α, IL-1β, and IL-6 (122). While there is an association between inflammation and poor outcomes both in animal models and humans, anti-inflammatory treatment with glucocorticoids or non-steroidal anti-inflammatory drugs during the acute period after myocardial infarction has not shown benefits in humans (123). Thus, a better understanding of factors

contributing to and counteracting inflammation, may lead to the discovery of novel therapeutic targets to target the immune system after myocardial infarction.

TREM2 is a surface receptor of macrophages expressed during multiple types of tissue injury and has been shown to be protective in models of Alzheimer's Disease and metabolic syndrome (86, 94). It is expressed on the cell surface of macrophage subsets with distinct gene expression profiles compared to other macrophages, e.g., disease-associated microglia (DAM) in Alzheimer's Disease, scar-associated macrophages (SAM) in cirrhosis, and lipid-associated macrophages (LAM) in metabolic syndrome (17, 62, 86). In genome-wide association studies, a missense variant of TREM2 has been shown to substantially increase the risk of developing Alzheimer's Disease in humans (95, 96). TREM2 can be cleaved off the cell surface by metalloproteases (81). It has a small extracellular tail with no catalytic domains and mediates its functions by binding to DAP12 which in turn activates intracellular signaling pathways such as phosphatidylinositol-3-kinase (80). It binds a variety of ligands that are present during any form of tissue injury, including phospholipids and free DNA, many of them also present after myocardial infarction (79). Despite it being identified as a key regulator of macrophages in multiple disease models, little is known about what mediates its expression, how it mediates its effects on gene expression, and if it plays a role in myocardial injury.

This study aimed to address if TREM2 is expressed in models of myocardial infarction, similar to other disease models causing significant tissue damage. Additionally, we tested the effect of TREM2 knockout and treatment with the TREM2-activating 4D9 antibody on cardiac function and/or mortality in myocardial injury models.

Results:

TREM2 is expressed in macrophages after myocardial infarction

To test whether TREM2 is expressed in macrophages after myocardial injury, we analyzed publicly available datasets available from single-cell data. Yokota et al. carried out LAD ligation in C57BL/6 mice and generated both single-cell and bulk RNA-seq data (124). In our analysis of the datasets, we identify *Trem2* to be highly expressed in macrophages but not in other cell types 7 days after LAD ligation (Figure 2A). In a time course analysis of bulk-tissue from the infarcted area, *Trem2* expression in the injured area is notable after 3 days, peaks at 7 days, and is decreased again by 14 days (Figure 2B). Notably, Trem2 expression is essentially absent in bulk tissue from uninjured areas of the heart. In addition, we analyzed data from Mouton et al., who carried out isolation of macrophages by magnetic beads after LAD ligation in C57BL/6 mice (125). In their dataset, *Trem2* was lowly expressed at baseline in macrophages, but expression substantially increased by day 5-7 (Figure 2C). Overall, these findings indicate that, similarly to other disease models such as metabolic syndrome and non-alcoholic steatohepatitis, TREM2+ macrophages are present in the heart after myocardial infarction in the response to tissue injury, but not in areas unaffected by infarction. Similarly, *Trem2* is not or only minimally expressed in the heart at baseline, in the absence of injury.

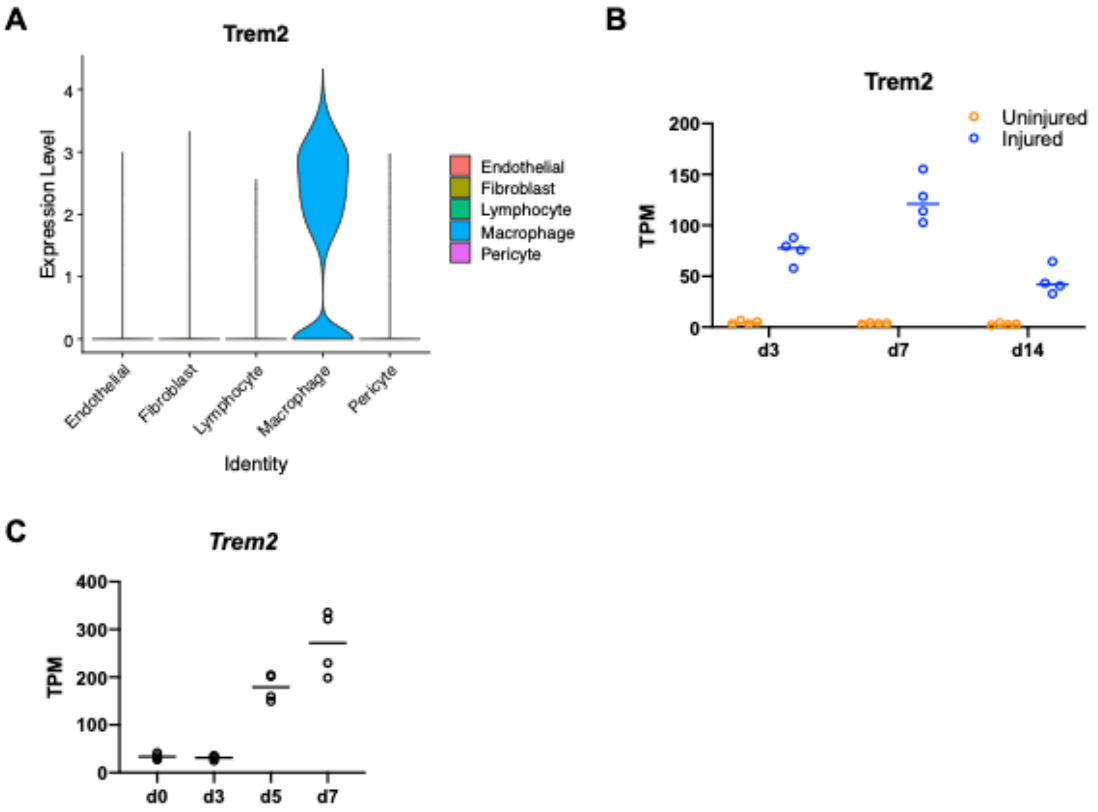

Figure 2: *Trem2* is expressed in macrophages in myocardial infarction models
A. Analysis of single-cell RNA-seq data from Yokota et al. shows high expression of *Trem2* 7 days after myocardial infarction. Expression of *Trem2* is limited to macrophages.
B. Analysis of bulk RNA-seq data from Yokota et al. shows a time course of *Trem2* expression in the infarcted area of the heart after LAD ligation. Gene expression is noted after 3 days, peaks at 7 days, and decreases by day 14. Notably, in the uninjured area of the same heart, there is only minimal expression of *Trem2*.
C. Analysis of RNA-seq data from Mouton et al. indicates minimal expression of *Trem2* in macrophages at baseline with a substantial increase after LAD ligation.

Loss of TREM2 increases mortality in male mice and worsens left ventricular function in female mice after myocardial infarction

To assess whether TREM2 has a beneficial, neutral, or detrimental effect after myocardial injury, we used TREM2 KO mice to undergo LAD ligation. Male and female age-matched sex-matched C57BL6/J mice underwent baseline echo, followed by permanent LAD ligation by an experienced operator, and were assessed for survival for 8 weeks on a daily basis. Serial echocardiograms were done in surviving mice 2 and 6 weeks after LAD ligation. Mice were sacrificed 8 weeks after LAD ligation to assess hearts by morphometry. All procedures and analyses were carried out with the operator blinded to the genotype of the mice. As expected, at baseline, there was no significant difference in left ventricular function between TREM2 knockout and wild-type mice.

After undergoing LAD ligation, male TREM2 KO mice showed increased mortality (87.5%) compared to male wild-type mice (33.3%, p=0.02 by two-tailed log-rank test). The curves of the Kaplan-Meier plot started to diverge around 5-10 days, consistent with the increased expression of *Trem2* during that time (Figure 3A). The last death occurred on day 14 when recruited macrophages have decreased again substantially in numbers after the initial model. Overall, the presence of TREM2 appears to be decreasing mortality in male mice in a permanent LAD ligation model. However, due to the high mortality in the TREM2 KO mice, a comparison between male TREM2 KO and wild-type mice was not possible by echocardiography or morphometry.

Female mice are known to be more resistant to the effects of myocardial infarction compared to male mice (126). In our study, all female mice in both the TREM2 KO and the wild-type groups survived. This allowed for interrogation with serial

echocardiograms followed by morphometry. We used global longitudinal strain (GLS) to assess left ventricular function, a sensitive method that has been shown to be a strong predictor of adverse outcomes in humans. This decision was made as image quality in the short axis views necessary to assess fractional shortening was limited in multiple mice and the long-axis views provided good quality images in all mice to use for left ventricular strain analysis. Left ventricular GLS was not different at baseline prior to LAD ligation and worsened substantially in both groups 2 weeks after LAD ligation (more negative values are indicative of better function) (Figure 3B). At that time point, there was no significant difference between the groups. However, at 6 weeks after LAD ligation, left ventricular function was worse in TREM2 KO mice compared to wild-type mice (-2.4% $\pm$ 1.0% vs. -4.7% $\pm$ 2.0%, mean $\pm$ SD, p=0.03 by two-tailed t test). This indicates that presence of TREM2 leads to a modest increase in cardiac function 6 weeks after LAD ligation compared to female mice lacking TREM2, suggesting that TREM2 plays a beneficial role in long-term remodeling. On postmortem morphometry, there was no statistically significant difference in heart weight normalized to tibia length or body weight. However, consistent with worsening numerical strain, the average normalized heart weight was higher in TREM2 KO mice compared to wild-type controls (Figure 3C). In summary, in an LAD ligation model, loss of TREM2 dramatically increased mortality in male mice while in female mice it led to a modest decrease in left ventricular function by global longitudinal strain.

Figure 3: Loss of TREM2 increased mortality in male mice and led to a modest decrease in left ventricular function in female mice after LAD ligation.

A. Kaplan-Meier plots showing increased mortality in male TREM2 KO mice (n=9 wild-type, n=8 TREM2 KO). All female mice survived until the study endpoint (n=7 in each group).
B. Assessment of left ventricular function by GLS in female mice. TREM2 KO mice showed no significant difference in function at baseline and 2 weeks after LAD ligation but showed a significant decrease in function 6 weeks after LAD ligation compared to wild-type mice (n=7 in each group).
C. Morphometry of female mice at time of euthanasia 8 weeks after LAD ligation. There was no statistically significant difference between wild-type and TREM2 KO mice, but the average heart weight normalized to tibia length or body weight was numerically higher in TREM2 KO mice.

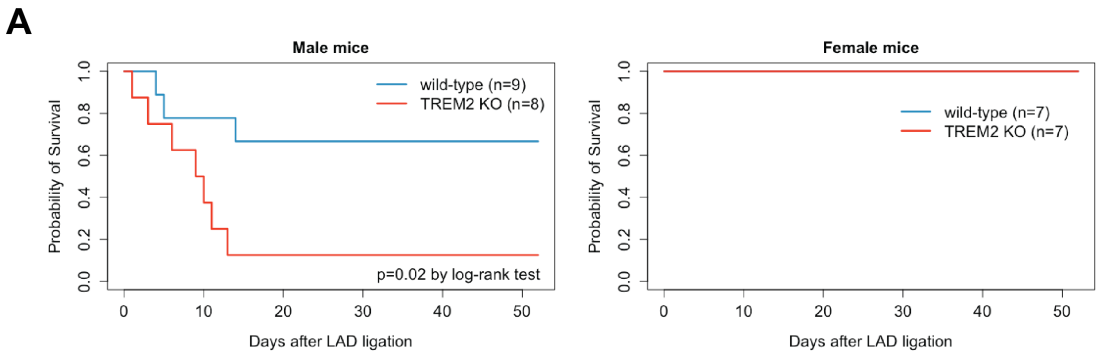
A
Male mice
Probability of Survival
wild-type (n=9)
TREM2 KO (n=8)
p=0.02 by log-rank test
Days after LAD ligation
Female mice
wild-type (n=7)
TREM2 KO (n=7)
Days after LAD ligation

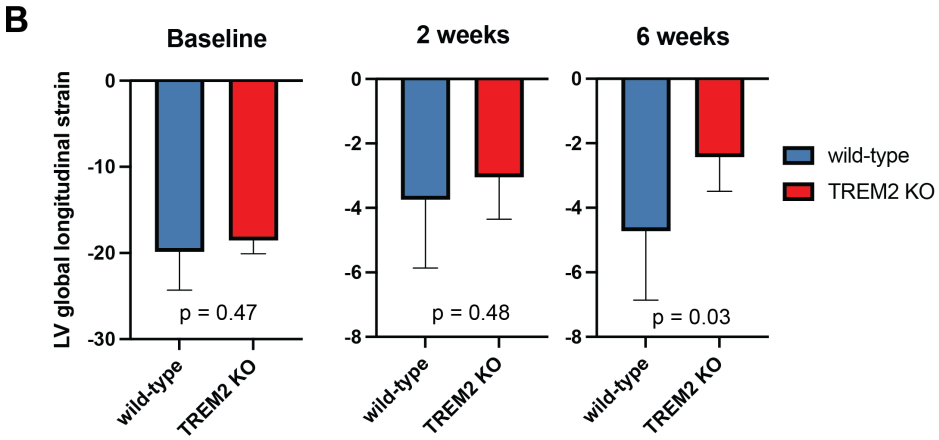
B
Baseline
2 weeks
6 weeks
LV global longitudinal strain
p = 0.47
p = 0.48
p = 0.03
wild-type
TREM2 KO

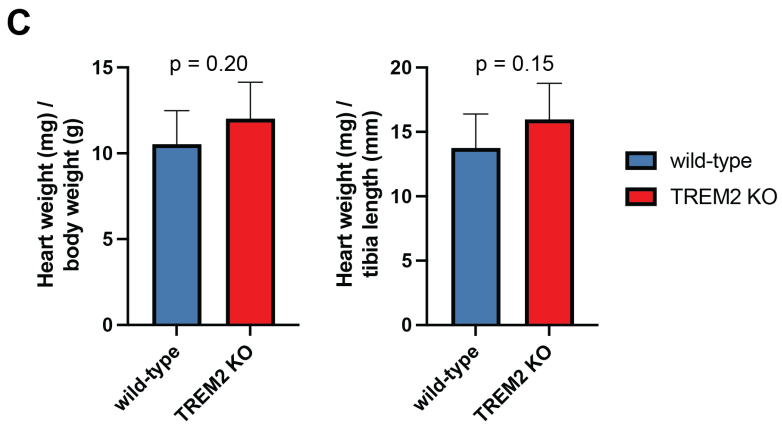
C
Heart weight (mg) / body weight (g)
p = 0.20
Heart weight (mg) / tibia length (mm)
p = 0.15
wild-type
TREM2 KO

TREM2 is expressed in cardiac macrophages after ischemia/reperfusion injury

While loss of TREM2 has detrimental effects after LAD ligation, we aimed to test if additional pharmacologic activation of TREM2 could have beneficial effects. To test this, we chose to use an ischemia/reperfusion model. As in the previous experiments, this model includes ligation of the LAD but with removal of the suture after 60 minutes to allow for reperfusion. This model has the advantage that it will lead to restored perfusion of the infarcted area and supply the area with an administered therapy. Additionally, this model also recapitulates the process that most commonly in humans. Since the advent of reperfusion therapy, most patients with myocardial infarction due to complete occlusion of the culprit vessel are taken to the cardiac catheterization laboratory emergently and reperfusion is achieved by balloon angioplasty with subsequent stent placement. Alternatively, they can receive reperfusion therapy with thrombolytic therapies if no catheterization laboratory is available.

Thus, we aimed to investigate whether *Trem2* is expressed in cardiac macrophages after ischemia/reperfusion injury. We used single-cell RNA-seq data available from Dr. Kevin King's laboratory in mice prior to and 4 days after ischemia/reperfusion injury. While a relatively small proportion of macrophages expresses *Trem2* at baseline, after 4 days a substantial number of macrophages expresses high levels of *Trem2* (Figure 4). This makes ischemia/reperfusion a feasible model that can be used to test if pharmacologic activation leads to beneficial effects after myocardial injury.

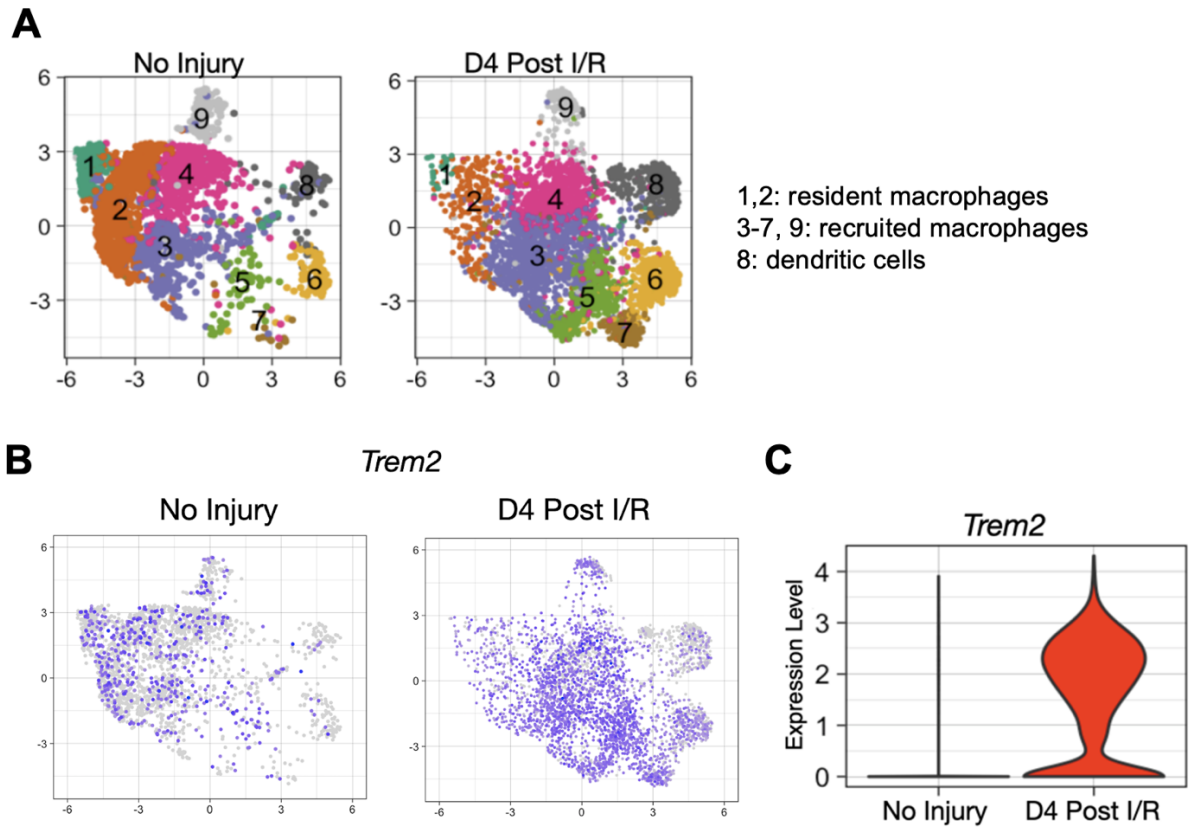

Figure 4: Single-cell RNA-seq demonstrates substantial expression of Trem2 in cardiac macrophages 4 days after ischemia/reperfusion injury.

A. UMAP plots of innate immune cells at baseline and 4 days after 60 minutes of ischemia/reperfusion injury. Ischemia/reperfusion leads to a sizeable expansion of the populations of recruited macrophages in the heart.
B. UMAP plot with *Trem2* expression annotated in purple. After ischemia/reperfusion injury there is widespread expression of *Trem2*, highest in recruited macrophages.
C. Expression of *Trem2* in macrophages is substantially increased after myocardial injury 4 days after ischemia/reperfusion injury compared to baseline.

Treatment with a TREM2-activating antibody does not change left ventricular function after ischemia/reperfusion injury

The next aim of our studies was to assess whether pharmacologic activation of TREM2 can improve cardiac function after myocardial injury. 4D9 is an antibody that binds to TREM2 and prevents its cleavage from the cell surface by blocking the access of metalloproteases and itself activates signaling through TREM2 evidenced by an increase in phosphorylated SYK (127). In an Alzheimer's model, treatment with the antibody led to a reduction in amyloid pathology. To test the effects of the antibody in a myocardial injury model, we designed a rigorous trial (Figure 5A). We used 16 male mice per group for a power of at least 80% to find a 20% difference in a parameter with 25% standard deviation and a two-tailed p value of 0.05. The primary endpoint was left ventricular function at 6 weeks after ischemia/reperfusion as assessed by left ventricular ejection fraction. We used male wild-type C57BL6/J mice as males are more susceptible to the adverse effects of myocardial injury. Mice received a baseline echo, 60 minutes of ischemia/reperfusion injury, and were then randomized to 4D9 treatment or an isotype control (4D5). Treatment with 4D9 antibody or isotype control was administered intraperitoneally at a dose of 5 mg/kg at postoperative day 1, day 7, and day 13. This dose was chosen as it led to supramaximal plasma concentrations for multiple days in pharmacokinetic experiments performed by the laboratory of Dr. Christian Haass, where the antibody was first developed. Only the laboratory technician preparing the antibody solution for injection was aware of the treatment groups, the operator and everyone involved in data analysis were blinded until all data acquisition

and echocardiographic analysis was complete. One mouse was excluded prior to randomization as the suture could not be removed and permanent LAD ligation ensued.

There was no difference between the groups at baseline in echocardiographic parameters of left ventricular ejection fraction, fractional shortening, or left ventricular end-diastolic volume. As expected, after ischemia/reperfusion injury, there was a decrease in ejection fraction and fractional shortening, as well as an increase in left ventricular end-diastolic volume in both groups compared to baseline. However, at both time points (2 and 6 weeks after ischemia/reperfusion injury), there was no significant difference between the two groups in left ventricular function or dimensions (Figure 5B). Additionally, heart weight normalized to body weight area was not significantly different between the two groups at time of euthanasia (Figure 5C). In summary, treatment with a TREM2-activating antibody after ischemia/reperfusion injury did not alter left ventricular function or heart weight.

Figure 5: Administration of a TREM2-activating antibody (4D9) does not alter left ventricular function after ischemia/reperfusion injury.

A. Outline of the study protocol. Mice underwent baseline echocardiography and ischemia/reperfusion injury with an ischemic time of 60 minutes. Mice were then randomized to receive 3 doses of either 5mg/kg of TREM2-activating antibody 4D9 or an isotype control. One mouse had to be removed due to technical problems during surgery, so 31 mice were randomized.
B. Left ventricular function measured by ejection fraction (%) at baseline, 2 weeks after ischemia/reperfusion injury, and 6 weeks after ischemia/reperfusion injury (mean ± SD, n=15 in 4D9 group, n=16 in isotype control group).
C. Left ventricular end-diastolic volume (µl) at baseline, 2 weeks after ischemia/reperfusion injury, and 6 weeks after ischemia/reperfusion injury (mean ± SD, n=15 in 4D9 group, n=16 in isotype control group).
D. Morphometry at 10 weeks after ischemia/reperfusion injury (mean ± SD, n=15 in 4D9 group, n=16 in isotype control group).

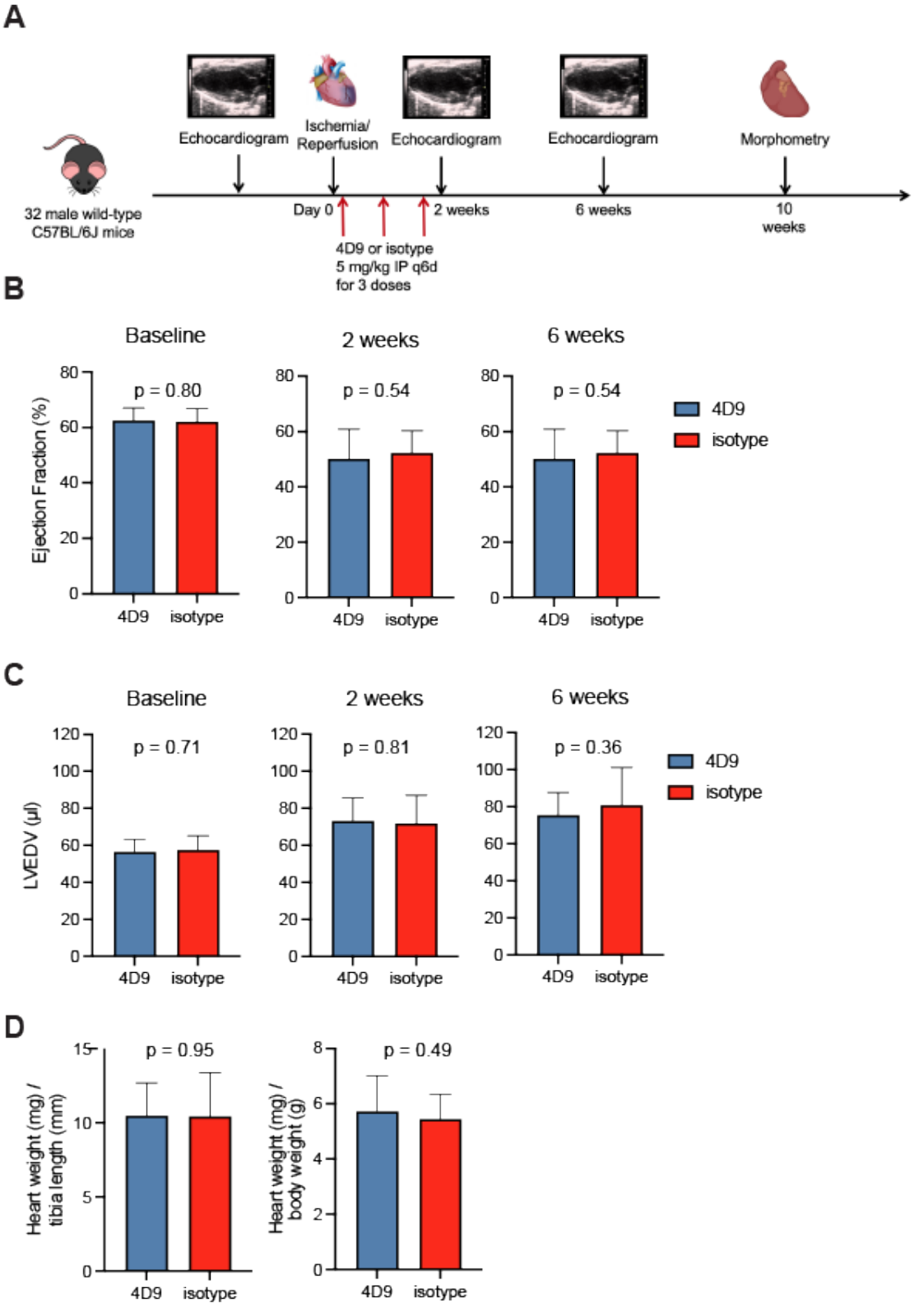
A
Echocardiogram
Ischemia/
Reperfusion
Echocardiogram
Echocardiogram
Morphometry
32 male wild-type
C57BL/6J mice
Day 0
2 weeks
6 weeks
10
weeks
4D9 or isotype
5 mg/kg IP q6d
for 3 doses
B
Baseline
2 weeks
6 weeks
Ejection Fraction (%)
p = 0.80
p = 0.54
p = 0.54
4D9
isotype
C
Baseline
2 weeks
6 weeks
LVEDV (µl)
p = 0.71
p = 0.81
p = 0.36
4D9
isotype
D
p = 0.95
p = 0.49
Heart weight (mg) /
tibia length (mm)
Heart weight (mg) /
body weight (g)
4D9
isotype

Discussion:

In this study, we investigated the effect of TREM2 in myocardial injury models and tested whether activation may have a benefit. First, we found that *Trem2* is highly expressed in macrophages within 3-5 days after myocardial infarction and peaks around 7 days. Coinciding with the decrease in macrophage numbers in the heart, *Trem2* expression decreases around 14 days. This acute expression of *Trem2* contrasts with the other disease models in which *Trem2* has been found to be expressed, which are models of chronic diseases with ongoing tissue injury, such as metabolic syndrome or Alzheimer's Disease (17, 30, 86). In these diseases, the *Trem2*-expressing macrophages cluster together as distinct populations in UMAP or t-SNE plots of single-cell RNA-seq. In comparison, in our analyzed datasets 4 days after ischemia/reperfusion injury or 7 days after LAD ligation TREM2 seems to be widely expressed throughout macrophage populations without distinct sets of gene expression profiles in TREM2+ macrophages at the time. This may be a fundamental difference between the acute model of myocardial injury and the more chronic disease models, or it may indicate that it takes longer for the fundamental changes in gene expression to occur.

We identified that loss of TREM2 in male mice leads to an increase in mortality after permanent LAD ligation. One possible explanation may be that TREM2 is required to induce a phagocytic phenotype in macrophages and lead to clearance of debris and apoptotic cells, as another study found the prophagocytic receptor MerTK to be necessary for the development of reparative macrophages after myocardial infarction and to contribute to the uptake of defective mitochondria and normal myocardial

function at tissue homeostasis (120, 121). TREM2 may play a similar role by inducing a prophagocytic phenotype. Additionally, TREM2 dampens the inflammatory response *in vitro* and in cancer models, where through its anti-inflammatory properties TREM2 has a pro-tumorigenic effect by suppressing the T cell immune response (89, 90, 99, 100). In the heart, an excessive proinflammatory immune response has been identified to be detrimental to wound healing and knockout of IRF3 decreased mortality in mice after LAD ligation (117). Therefore, TREM2 may exert its effects at least partially through dampening inflammation after myocardial infarction. Of note, these effects are still not severe enough to cause mortality in female mice, but rather a modest change in left ventricular strain 6 weeks after LAD ligation. Future studies will need to address how TREM2 modulates macrophage function, including the transcriptomic profile and transcriptional regulation in macrophages. Additionally, studying how TREM2+ macrophages affect cardiomyocyte function and metabolism or fibrosis development through myofibroblasts will be of importance.

In the rigorous trial of an activating TREM2 antibody versus isotype control in wild-type mice, we hypothesized that additional pharmacologic activation of TREM2 may prove beneficial after myocardial injury, as loss of TREM2 had detrimental effects. However, we did not observe a significant difference in left ventricular function, left ventricular dimension, or heart weights. There are multiple reasons for why treatment with the antibody may not have had an effect. First, there may not be enough antibody reaching the infarct area and border zone of the heart, which is where most of the macrophage infiltration occurs. While this cannot be ruled out, it is unlikely as the dose given reaches supramaximal plasma levels based on prior pharmacokinetic analyses

and the fact that all animals included in the study had the suture removed after 60 minutes of LAD ligation, thereby restoring adequate blood flow. Second, there may have not been additional activation of TREM2 beyond physiologic states. There is an abundance of potential TREM2 ligands after substantial necrosis occurs with myocardial injury (e.g., necrotic cells, phospholipids, free DNA). These ligands may saturate the available TREM2 and further stimulation with an exogenous molecule may not be possible in this acute setting. By binding to TREM2, these endogenous ligands may also prevent cleavage of TREM2 at the surface. Third, the effect of the antibody may not be strong enough to have a substantial effect in such an acute disease model. Given these limitations of TREM2 antibody treatment and possible saturation of the receptor, understanding what leads to upregulation of TREM2 and which transcription factors mediate the disease will be important to study, as it will have relevance in multiple disease processes beyond myocardial infarction. Additionally, there are disease processes where TREM2 activation is desired (e.g., myocardial infarction, Alzheimer's Disease, metabolic syndrome) and other diseases such as cancer where TREM2 plays a malignant role for the host. Therefore, the identification of factors downstream and upstream of TREM2 will provide new targets to test in myocardial injury models to assess if the pathways related to TREM2 have therapeutic potential.

Materials and Methods:

Mice

All animal studies were approved by the University of California San Diego Animal Care and Use Committee in accordance with the University of California San Diego research guidelines for the care and use of laboratory animals. Mice were maintained under a 12-hour light and 12-hour dark cycle at constant temperature with *ad libitum* access to food and water. Mice were fed a regular chow diet (T8604, Envigo). TREM2 knockout mice on a C57BL6/J background were obtained from The Jackson Laboratory (Strain # 027197, Bar Harbor, ME) and then maintained and bred in our vivarium facilities.

Genotyping

The primers used in the PCR reaction to genotype mice in the TREM2 knockout studies were the following:

Forward: 5'-TCAGGGAGTCAGTCATTAACCA-3'

Reverse: 5'- AGTGCTTCAAGGCGTCATAAGT-3'

Reverse mutant: 5'- CAATAAGACCTGGCACAAGGA-3'

The product was assessed by gel electrophoresis on a 1.5% agarose gel. A 254 base pair product was generated from the wild-type allele and a 396 bp product from the mutant allele.

Permanent LAD ligation experiments

For myocardial infarction studies, male and female TREM2 knockout and age-matched sex-matched wild-type control mice were used. All mice were on the C57BL6/J background. Genotype of the mice was identified by genomic DNA from earpieces at

the beginning of the study. Additionally, confirmatory genotyping was performed after death from tail samples. Mice were 20-22 weeks old at the time of permanent LAD Ligation. Mice received baseline echocardiogram prior to LAD ligation. After LAD ligation mice were monitored at least daily and assessed for distress or death. Mice received echocardiogram 2 weeks and 6 weeks after surgery. The operator at the Seaweed Canyon core who performed echocardiograms and surgeries was not aware of the genotype of the mice undergoing the procedures. Mice were euthanized 8 weeks after surgery and hearts flushed and rinsed. They were extracted and weights measured for morphometry. Tibias were extracted for tibia length for normalization of heart weights.

Ischemia/reperfusion experiments with 4D9 antibody treatment

As determined by power analysis with a minimum power of 80% to find a 20% difference in a parameter with 25% standard deviation and a two-tailed p value cutoff of 0.05, 16 male wild-type C57BL6/J mice (Jackson) per group to undergo ischemia/reperfusion injury. Mice were 16-18 weeks old at the time of surgery. All mice received a baseline echocardiogram prior to undergoing surgery. After successful completion of ischemia/reperfusion injury, mice were randomly assigned to treatment with 4D9 antibody (Denali Therapeutics) or isotype control (4D5, Denali Therapeutics). One mouse was excluded prior to randomization as reperfusion was not achieved. Treatment was given intraperitoneally at 5 mg/kg at post-operative days 1, 7, and 13. Only the laboratory technician preparing the antibody was aware of the study arm assignment until acquisition of all data was complete. Mice were monitored at least daily for distress or death after undergoing ischemia/reperfusion surgery. Echocardiograms

were performed 2 weeks and 6 weeks after injury to assess left ventricular function and dimensions. Mice were euthanized 10 weeks after injury and hearts flushed, rinsed, and extracted for morphometric analysis, along with tibias to normalize heart weight to tibia length. After completion of all data acquisition and echocardiographic analysis, treatment arms were revealed, and statistical analysis performed.

Surgical procedures

Permanent or transient LAD coronary artery ligations were be performed by an experienced project scientist in the Seaweed Canyon Laboratory. Mice were anesthetized with ketamine (50 mg/kg) and xylazine (5 mg/kg) intraperitoneally followed by inhaled isofluorane (0.75 – 1.5%). Anesthesia was monitored by visual examination of spontaneous movement, blinking, respiratory parameters on the ventilator, as well as the response to gentle stimuli. Mice were intubated and ventilated with a pressure ventilator administering inhaled isofluorane. A skin incision was made at the left chest and heart visualized between 3rd and 4th rib. LAD artery was ligated by tying a suture. Successful ligation was confirmed by blanching of the LAD territory along with ST elevation on electrocardiogram. For permanent ligation, the chest was closed at this point and monitored postoperatively as below. For ischemia/reperfusion injury, the mouse was kept warm with a warming pad and an additional dose of xylazine and ketamine given along with normal saline. After 60 minutes, the suture was released and reperfusion confirmed by visual return of blood flow in the LAD territory. Thereafter, the chest was closed with sutures and Nexaband topical tissue adhesive. Mice received buprenorphine (0.1 mg/kg) intraperitoneally immediately following surgery. Thereafter mice were monitored daily thereafter to assess for distress and mortality.

Transthoracic Echocardiography

Animals were anesthetized with 5% isoflurane for 30 seconds and then maintained at 0.5% throughout the examination. Small needle electrodes for simultaneous electrocardiogram were inserted into one upper and one lower limb. Images were acquired in M-mode, 2- dimensional and Doppler modalities using the FUJIFILM VisualSonics Inc., Vevo 2100 high-resolution ultrasound system. All images were acquired and analyzed without knowledge of the genotype or treatment arm of the mice.

Single-cell RNA-seq analysis

Single-cell RNA-seq datasets were obtained from publicly available sources or collaborators as indicated and analyzed using the Seurat R toolkit for single cell genomics (128, 129).

Acknowledgements:

Chapter 2 is coauthored with Jason Duran, Christian Nickl, Ty Troutman, David Calcagno, Yusu Gu, Kevin King, Eric Adler, and Christopher Glass. The dissertation author was the primary author of this chapter.

CHAPTER 3: TRANSCRIPTIONAL REGULATION RELATED TO TREM2

Abstract:

TREM2 (Triggering Receptor Expressed on Myeloid Cells 2) is a transmembrane receptor that has recently been established as a key regulator of macrophages in multiple disease models. It is highly expressed in distinct macrophage subsets in models of Alzheimer's Disease (disease-associated microglia/DAM), obesity (lipid-associated macrophages/LAM), and non-alcoholic steatohepatitis (NASH Kupffer cells/KC-N). However, it has remained unclear how expression of *Trem2* is activated or how TREM2 mediates its effects on gene expression.

To understand these questions, we generated a conditionally immortalized monocyte progenitor line from a Rosa26-Cas9 mouse. These cells are immortalized at a monocyte progenitor stage that can terminally differentiate into macrophages. We generated a line with a deletion of the intergenic enhancer of Trem2, whose accessibility strongly correlates with expression of *Trem2*, and multiple lines with disruption of the ATF3 motif, a transcription factor strongly binding to this enhancer *in vivo*. Surprisingly, deletion of the enhancer or disruption of the motif had only minimal effects on gene expression of Trem2, indicating that other parts of its cis-regulatory system are determining its levels of expression or that redundancies are in place. We also created TREM2 KO clones and found 212 genes upregulated in wild-type vs. TREM2 KO, 90 of which are also upregulated in DAM, LAM, and/or KC-N *in vivo*. We identified active enhancers by ChIP-seq for H3K27 acetylation and found 4243 enhancers with increased H3K27 acetylation in wild-type vs. TREM2 KO cells. In these enhancers, the DNA-binding motifs of the MITF/TFE family and the AP-1 family (of

which ATF3 is a member) were enriched compared to enhancers with unchanged H3K27 acetylation. We found that TREM2 signaling led to rearrangement of binding of MITF/TFE factors and ATF3 to gene regulatory elements. While most MITF/TFE factors and ATF3 showed increased binding in enhancers activated downstream of TREM2, TFEC binding was slightly decreased. TREM2 KO led to a substantial loss of TFEB peaks and a substantial gain of TFEC peaks, suggesting a diverging effect of TREM2 on the two factors. Additionally, we created TFEB KO cells and discovered that multiple signature genes of DAM, LAM, and KC-N (e.g., *Cd9*, *Myo1e, Atf3)* were similarly changed with KO of TFEB as with KO of TREM2. These findings show that, unexpectedly, the intergenic enhancer of *Trem2* is not required for high expression of its mRNA and that ATF3 and the MITF/TFE transcription factor family are downstream of TREM2 signaling.

Introduction:

TREM2 is a major regulator of macrophage function in multiple disease models, including Alzheimer's Disease, metabolic syndrome, and cancer (17, 86, 94, 99, 100). Subsets of macrophages that highly express *Trem2* appear in tissue injury, e.g., disease-associated microglia (DAM) in Alzheimer's Disease, lipid-associated macrophages (LAM) in metabolic syndrome, and Kupffer Cells (KC-N) in non-alcoholic steatohepatitis (NASH) (17, 30, 86). TREM2 exerts a protective effect in the 5xFAD model of Alzheimer's Disease and has been found essential for the full transition of microglia to DAM (17, 94). Additionally, a missense mutation in humans (R47H) has been found to be strongly associated with the development of Alzheimer's Disease in

genome-wide association studies, signifying the importance in humans (95, 96). TREM2 is a transmembrane receptor on macrophages that exerts its effects through binding of DAP12, which in turn activates phosphatidylinositol 3 kinase (80). Nonsense mutations of TREM2 or DAP12 cause the rare Nasu-Hakola Disease, leading to early onset frontal dementia with death from dementia complications usually by age 50 (97). This highlights that TREM2 plays not only a role during disease, but also during homeostasis of human brains. Additionally, TREM2 KO mice exhibit worsened metabolic parameters and adipocyte hypertrophy in a model of metabolic syndrome (86). On the other hand, deletion of TREM2 has pro-inflammatory effects on tumor-associated macrophages and leads to a reduction in tumor size (99, 100). These studies exhibit the importance of TREM2-expressing macrophages in the development and pathophysiology of multiple disease processes. However, it is currently unknown how expression of *Trem2* itself is regulated and how TREM2 mediates its effects on transcriptional regulation to mediate the distinct gene expression profile of TREM2-expressing macrophages such as DAM. Previous results from a NASH model show that Kupffer cells gain accessibility to an intergenic enhancer downstream of the *Trem2* gene during NASH that is not accessible in Kupffer cells of healthy livers, when transcription of *Trem2* is low. This enhancer also shows substantial binding of the transcription factor ATF3 with high expression during NASH (30). We generated conditionally immortalized macrophages with deletion of the enhancer and ATF3 motif disruptions to study if and how this enhancer may regulate *Trem2* expression. Additionally, we generated TREM2 KO lines to examine how TREM2 affects gene regulation and KO lines of transcription factors that may be downstream of TREM2.

Results:

Generation of Cas9-expressing conditionally immortalized macrophage cell line

To investigate how TREM2 is regulated and how it mediates its effects on transcriptional regulation, we established conditionally immortalized monocyte progenitors from the bone marrow of a Rosa26-Cas9 mouse. These cells are immortalized by HoxB8 at a monocyte progenitor stage while supplemental estradiol is present in the culture media (130). After removal of estradiol and addition of macrophage colony-stimulating factor (M-CSF), the cells can differentiate into macrophages. This makes them a useful tool to study macrophage biology. Due to constitutive expression of Cas9, genetic modifications can be carried out at the monocyte progenitor stage with introduction of guide RNA (gRNA) by lentivirus. These modifications with subsequent cell sorting and generation of clones are not possible in conventional bone-marrow derived or peritoneal macrophages as they terminally differentiate within 1-2 weeks after removal from the body.

After generation of the ER-HoxB8 monocyte progenitors, we differentiated them into macrophages to assess them for similarities with bone-marrow derived macrophages, particularly in relation to *Trem2* expression and the gene regulatory locus of the *Trem2* gene. We first carried out RNA-seq to assess gene expression before and after differentiation, and to compare the cells with conventional bone-marrow derived macrophages (Figure 6A). Expectedly, the differentiation from ER-HoxB8 progenitors to ER-HoxB8 macrophages massively alters their transcriptional pattern, with upregulation of macrophage genes such as *Cd68*, *Csf1r*, *Lyz2*, and *Itgam*, as well as downregulation of monocyte genes such as *Ccr2* and *Ly6c2*. While there were differences in gene

expression, key macrophage genes were substantially expressed both in ER-HoxB8 macrophages and bone-marrow derived macrophages, with the notable of *Apoe*, which was only lowly expressed in ER-HoxB8 macrophages (Figure 6B). Important for this study, *Trem2* is expressed at high levels above 1,000 TPM (transcripts per million) in differentiated ER-HoxB8 cells, comparable to bone-marrow derived macrophages. *Cd9*, which is also highly expressed in DAM, LAM, and SAM subsets, is also expressed at high levels in differentiated ER-HoxB8 cells (Figure 6B). Importantly, these cells responded to stimulation with ligands that activate bone-marrow derived macrophages Treatment with KLA (Kdo2-Lipid A), a key component of LPS, led to large transcriptomic changes with more than 2,000 differentially expressed genes after 6 hours (Figure 7A). The pro-inflammatory genes *Il1b*, *Il6*, and *Tnf* were massively upregulated with essentially no expression at baseline (Figure 7B). We also tested differentiation into osteoclasts. In a protocol equivalent to the derivation of bone-marrow derived osteoclasts with 4 days of RANKL treatment, the ER-HoxB8 cells also expressed high levels of osteoclast genes, e.g., *Ocstamp*, *Ppargc1b*, *Acp5*, and *Jdp2*, comparable to osteoclasts differentiated directly from bone marrow cells (Figure 7C). Overall, this demonstrates that macrophage gene expression is comparable in ER-HoxB8 macrophages and bone-marrow derived macrophages and that ER-HoxB8 macrophages respond to stimuli similarly to bone-marrow derived macrophages. Thus, they are suitable to be used as macrophage or osteoclast models that allow for introduction of mutations with CRISPR gRNA and rapid generation of large amounts of cells necessary for assays of transcriptional regulation such as ChIP-seq (chromatin immunoprecipitation followed by sequencing).

Figure 6: Gene expression in ER-HoxB8 macrophages differs vastly from ER-HoxB8 monocyte progenitors and resembles bone-marrow derived macrophages and osteoclasts

A. Differential gene expression between undifferentiated ER-HoxB8 monocyte progenitors (HoxB8_undiff) and differentiated ER-HoxB8 macrophages (HoxB8_mps), as well as ER-HoxB8 macrophages and bone-marrow derived macrophages (BMDMs). Differentially expressed genes were defined as FDR < 0.05, fold-change > 2 or < -2 (n=2 per cell type).
B. Gene expression of monocyte/macrophage genes in ER-HoxB8 monocyte-progenitors (HoxB8_undiff), ER-HoxB8 macrophages (Hoxb8_mps), and bone-marrow derived macrophages (BMDMs). Mean ± SD, n=2 per cell type.

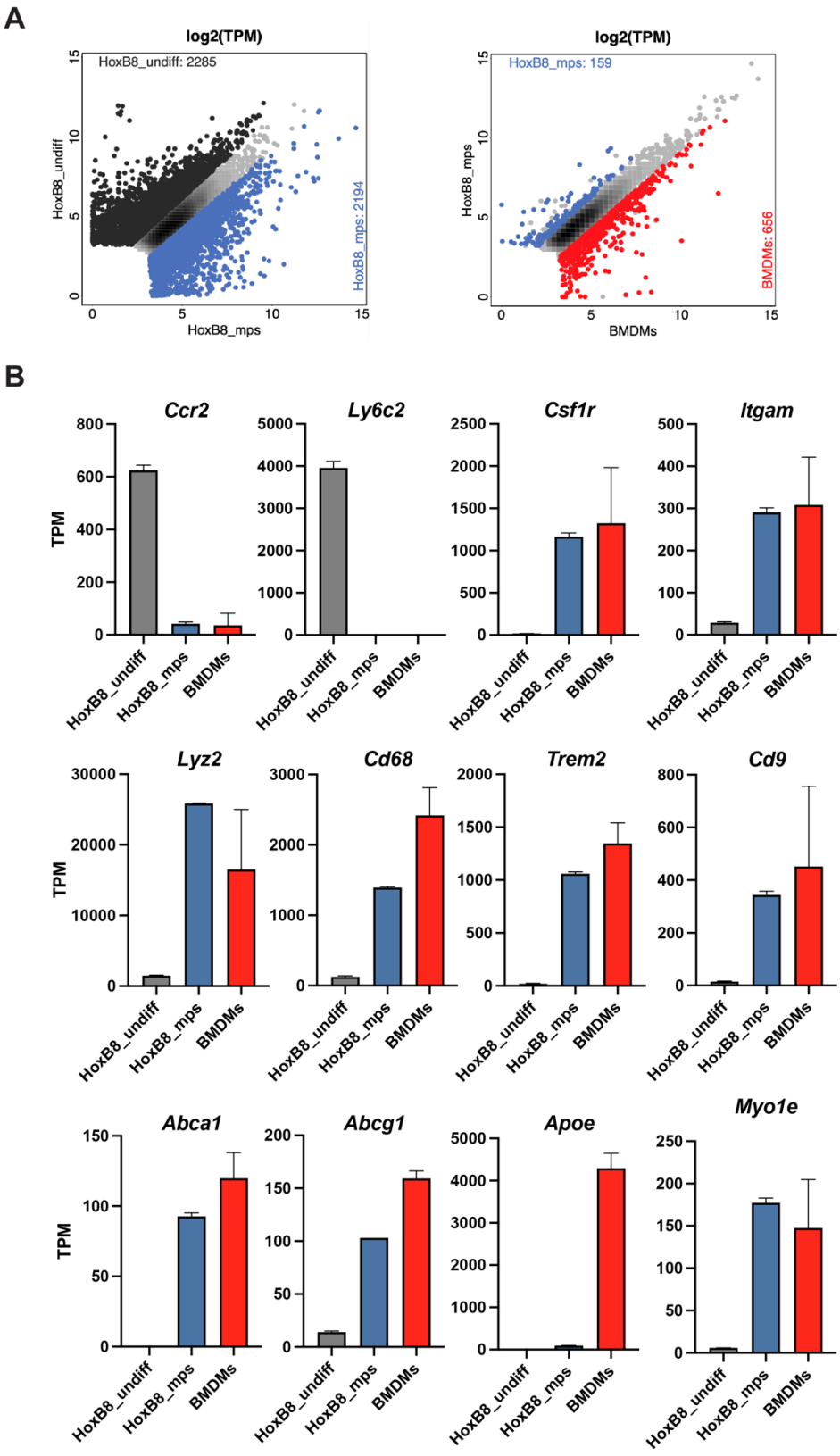
A
log2(TPM)
HoxB8_undiff: 2285
HoxB8_mps: 2194
HoxB8_undiff
HoxB8_mps
log2(TPM)
HoxB8_mps: 159
BMDMs: 656
HoxB8_mps
BMDMs
B
Ccr2
Ly6c2
Csf1r
Itgam
Lyz2
Cd68
Trem2
Cd9
Abca1
Abcg1
Apoe
Myo1e
TPM
HoxB8_undiff
HoxB8_mps
BMDMs

Figure 7: ER-HoxB8 macrophages respond to ligands of macrophages

A. Differential gene expression of ER-HoxB8 macrophages after 1 hour or 6 hours of stimulation with KLA (Kdo2-Lipid A), a key component of lipopolysaccharide. Differentially expressed genes were defined as FDR < 0.05, fold-change > 2 or < -2, and log2(TPM+1) > 4 in at least one group (n=2 per group).
B. Gene expression of inflammatory genes in ER-HoxB8 macrophages in response to 1 hour or 6 hours of stimulation with KLA (mean ± SD, n=2 per group).
C. Gene expression of osteoclast genes in ER-HoxB8 macrophages (HoxB8_mps), ER-HoxB8 osteclasts (ER-HoxB8_osteo) after 4 days of RANKL stimulation, bone-marrow derived macrophages (BMDMs) and bone-marrow derived osteoclasts after RANKL stimulation (BM_osteo) (mean ± SD, n=2 per group).

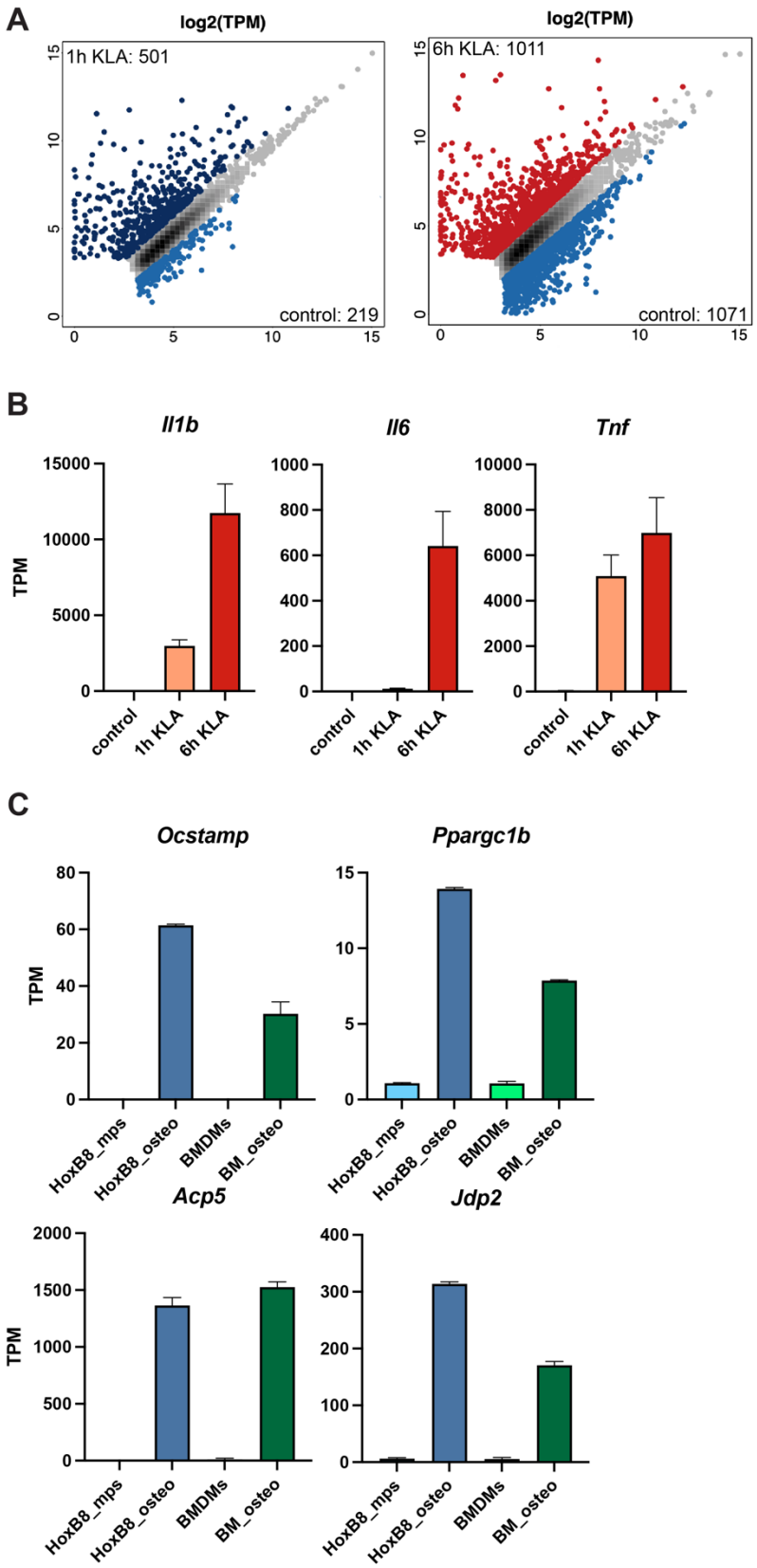
A
log2(TPM)
1h KLA: 501
control: 219
log2(TPM)
6h KLA: 1011
control: 1071
B
Il1b
Il6
Tnf
TPM
control
1h KLA
6h KLA
C
Ocstamp
Ppargc1b
Acp5
Jdp2
TPM
HoxB8_mps
HoxB8_osteo
BMDMs
BM_osteo

Deletion and Motif Disruption of the Intergenic Enhancer of *Trem2* in ER-HoxB8 cells

In addition to RNA-seq above, we carried out ATAC-seq (Assay for Transposase-Accessible Chromatin using sequencing) in differentiated ER-HoxB8 macrophages to ensure the gene regulatory locus of *Trem2* in ER-HoxB8 cells is similar to other cells that exhibit high levels of *Trem2* expression. We found that in ER-HoxB8 macrophages, both the intronic and intergenic enhancers are accessible, like in Kupffer cells during NASH and in bone-marrow derived macrophages (Figure 8A). As *Trem2* is highly expressed and the intergenic enhancer is accessible, these cells are suitable to investigate if the intergenic enhancer is necessary for high levels of *Trem2* expression. To test the hypothesis that accessibility of the intergenic enhancer is required for high expression of *Trem2*, we designed gRNA targeting sequences at both flanks of the accessible region as defined by ATAC-seq (Figure 8B). We transduced ER-HoxB8 monocyte progenitors with a lentiviral construct carrying the code for these two gRNAs as well as mCherrry. We then single-cell sorted mCherry-positive cells into 96 well-plates and grew clones.

As ChIP-seq data from Kupffer cells during NASH exhibits a strong increase in binding of ATF3 to the intergenic enhancer, we also hypothesized that the DNA binding site of ATF3 may be important for high expression of *Trem2*. Thus, we designed gRNA to the two ATF3 motifs within the enhancer to introduce varying insertions and deletions and disrupt binding of ATF3. We then introduced the gRNA and grew clones as above. We used a control gRNA sequence without any matching genomic DNA sequence on the same construct as control and isolated clones as above.

We carried out amplification of the genomic region of the intergenic enhancer after FACS sorting and identified one clone that exhibited recombination of the DNA causing homozygous enhancer deletion. This was evidenced by a ~500 bp reduction in size of a PCR product with primers flanking the enhancer and no visible PCR product using primers within the enhancers (Figure 8C). For ATF3, we identified three clones with various motif disruptions in either one or both ATF3 motifs.

We differentiated the cells into macrophages and carried out RNA-seq to assess for changes in *Trem2* and global gene expression. Surprisingly, neither the clone with homozygous enhancer knockout nor the motif disruptions exhibited a marked change in *Trem2* expression. All clones still expressed *Trem2* at levels of more than 1,000 TPM, indicating that the intergenic enhancer is not required for high levels of *Trem2* expression (Figure 8D). This may suggest redundancies between the intergenic and intronic enhancer or that binding of transcription factors to the intronic enhancers play a more major role in transcription factor binding. Future studies using CRISPR screen and *Trem2* reporter cells may help in defining which proteins and transcription factors are upstream of *Trem2* and inform how cells turn on high expression of *Trem2* during tissue injury.

Figure 8: The intergenic enhancer is accessible in ER-HoxB8 macrophages but homozygous deletion or ATF3 motif disruption do not markedly alter Trem2 expression

A. Genome browser track of ATAC-seq comparing the gene regulatory locus of ER-HoxB8 macrophages to Kupffer cells of healthy liver (KC-H, low *Trem2* expression, intergenic enhancer not accessible), Kupffer cells of NASH livers and bone-marrow derived macrophages (KC-N, BMDM, respectively; high *Trem2* expression, intergenic enhancer accessible).

B. CRISPR gRNA design targeting the *Trem2* enhancer and primers used to confirm enhancer deletion by PCR.

C. Gel electrophoresis confirming homozygous enhancer knockout (E-KO) by showing decreased size PCR product using flanking primers and no product using primers complementary to DNA within the enhancer region.

D. Gene expression of *Trem2* comparing control gRNA to enhancer deletion (E-KO) and ATF3 motif disruption (Motif-KO) (mean ± SD, n=2 each for control and E-KO, n=3 for Motif-KO).

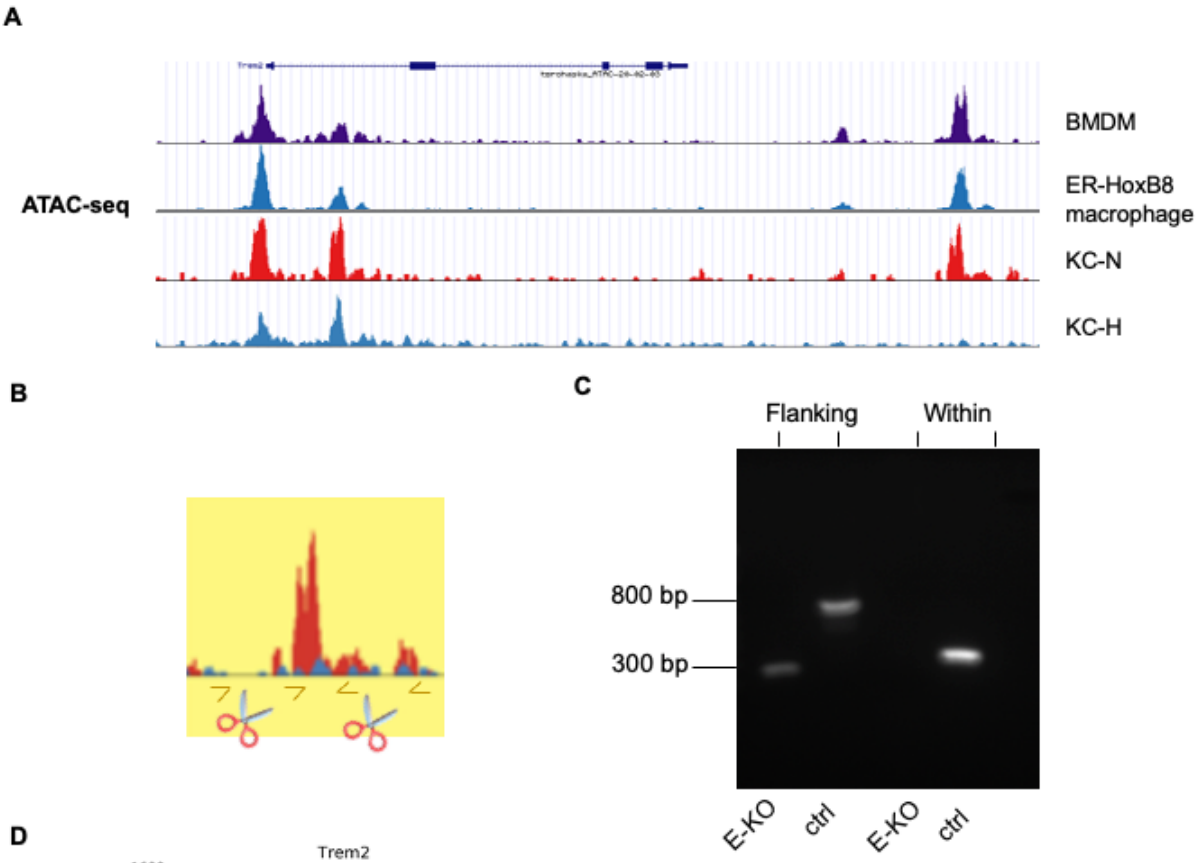
A
ATAC-seq
BMDM
ER-HoxB8 macrophage
KC-N
KC-H
B
C
Flanking
Within
800 bp
300 bp
E-KO
ctrl
E-KO
ctrl
D
Trem2
TPM
1600
1400
1200
1000
800
600
400
200
0
Control
E-KO
Motif-KO

Gene expression profile of macrophage subsets expressing high levels of *Trem2*

Recently multiple subsets of macrophages exhibiting high expression of *Trem2* have been identified *in vivo*. In mouse models that includes DAM in the brains in Alzheimer's Disease models, LAM in adipose tissue in metabolic syndrome, and Kupffer cells in NASH models. In human cirrhosis, scar-associated macrophages (SAM) have also been identified at the sites of fibrosis. Since all these *Trem2*-expressing cells cluster distinctly by single cell RNA-seq and there is evidence for TREM2 being required for formation of some of them, we hypothesized that TREM2 induces a distinct gene expression profile in macrophages.

We accessed publicly accessible data from previous studies to generate lists of upregulated genes in the murine *Trem2* expressing macrophages compared to homeostatic macrophages in the same tissue (17, 30, 86). We overlapped the gene lists of DAM, LAM, and KC-N and found that a limited number of 27 genes is upregulated in all subsets (Figure 9A). Of the genes upregulated in all subsets, some are related to phagocytic function, such as *Ctsd* and *Myo1e*, metabolism such as *Ldha* and *Aldoa*, as well as the transcription factor *Atf3* (Figure 9B). Additionally, the surface proteins *Cd9*, *Cd63*, and *Cd84* are increased in all three populations. Of note, CD9 is an inhibitor of metalloproteases ADAM17, the major protease cleaving TREM2 off the cell surface (81, 88). Thereby, CD9 may be potentiating the effect of TREM2.

Additionally, there were 192 gene upregulated in at least two of the subsets with more overlap between LAM and KC-N (Figure 9A). Overall, this analysis demonstrates genes that are likely downstream of TREM2 *in vivo*. However, some may also be

controlled by other environmental stimuli, as all three cell subsets were identified in models of tissue injury.

A

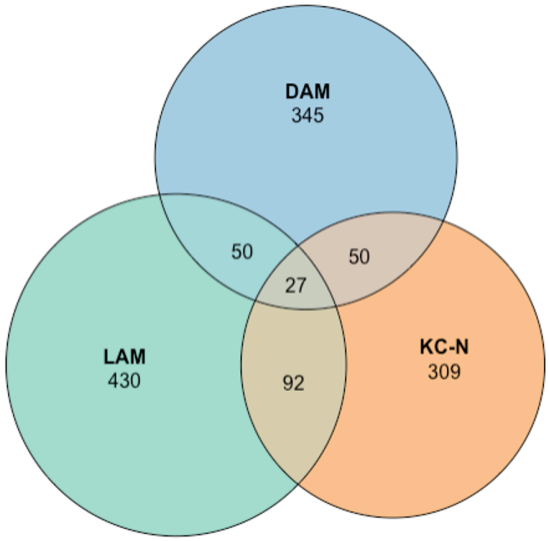

B

Genes upregulated in all subsets:

Trem2	*Gusb*
Cd9	*Nceh1*
Cd63	*Anxa5*
Cd84	*Myo1e*
Atf3	*Cadm1*
Ctsd	*Pld3*
Capg	*Aldoa*
Fabp5	*Vat1*
Ldha	*Atp6v0d2*
Fam20c	*Plin2*
Gnas	*Cstb*
Glipr1	*Cd300lb*
Ctsz	*Fblim1*
Fth1	

Figure 9: Gene expression profile of murine macrophage subsets with high expression levels of *Trem2*

A. Venn Diagram showing overlap of genes upregulated in DAM, LAM, KC-N macrophage populations.

B. List of genes that show increased expression in all three macrophage populations.

TREM2 knockout in ER-HoxB8 cells leads to deregulation of DAM, LAM, KC-N genes

To identify which genes are directly downstream of TREM2 in a neutral tissue culture environment without additional external stimuli from disease, we designed gRNA towards TREM2 to create TREM2 KO clones. We introduced gRNA with a lentiviral construct carrying an mCherry domain and single-cell sorted successfully transduced cells by FACS. We Sanger sequenced the growing clones and differentiated 3 clones with homozygous frameshift mutations in the *Trem2* gene. We confirmed successful gene knockout with Western Blot after macrophage differentiation showing no TREM2 signal while it was preserved in the control gRNA clones that were transduced and grown in parallel (Figure 10A).

The TREM2 KO clones clustered together on principal component analysis showing similar changes in global gene expression. In a direct comparison of TREM2 KO vs. control gRNA, 212 genes were expressed higher in wild-type macrophages and 118 genes were expressed higher in TREM2 KO macrophages (fold-change > 1.5, false discovery rate < 0.05) (Figure 10B). The 212 genes with increased expression in control gRNA are downstream of TREM2 *in vitro* without the influence and stimuli of a disease process causing additional changes in macrophage gene expression independent of TREM2.

Of the genes upregulated in the wild-type cells, we observed multiple signature genes of DAM/LAM/KC-N populations, e.g., *Cd9*, *Atf3*, *Myo1e*, *Lpl*, *Lrp1*, *Lrpap1*, and *Igf1* (Figure 10C). In total, 90 of the 212 genes found in vitro with TREM2 present are also upregulated in at least one of the *in vivo* subsets that highly express *Trem2* or are

TREM2-dependent (Figure 11A). Dissecting the overlap further, the expression profile correlates closer with LAMs and KC-N (61 and 55 genes) and less so with DAMs (19 genes) (Figure 11B, Tables 1 and 2). However, some of the genes that overlap with DAMs are DAM signature genes and have proposed functions in microglia. LRP1 for example is a receptor for apolipoprotein E and amyloid β, two key molecules in the pathophysiology of Alzheimer's Disease (131). Myosin-1e (*Myo1e*) has been identified as a key regulator of the phagocytic cap and to be upregulated in DAM (132, 133). The lipid droplet surface protein PLIN2 has been implicated in neuroinflammation via altering lipid metabolism in stressed hypertensive rats (134). Microglial lipoprotein lipase (LPL) has been associated with lipid uptake and suggested to prevent inflammatory lipid distribution and lipid droplet accumulation (135). In addition, albeit lowly expressed in this cultured macrophage model, the microglial homeostatic receptor genes *P2ry13* and *P2ry12* exhibited increased expression in the TREM2 KO cells, indicating that they are suppressed by TREM2, a finding similar to what is noted *in vivo* in DAMs (17). Overall, the gene expression profile in wild-type vs. TREM2 KO cultured macrophages recapitulates key aspects of the expression patterns observed in TREM2-expressing macrophages *in vivo*, making them a useful model to examine how these changes occur on a molecular level.

Figure 10: CRISPR knockout of TREM2 in ER-HoxB8 macrophages leads to loss of TREM2 on a protein level and to deregulation of DAM/LAM/KC-N signature genes

A. Western Blot in cells that were transduced in parallel with control gRNA or gRNA towards the TREM2 gene. TREM2 KO clones were Sanger sequenced and had homozygous frameshift mutations. There is loss of TREM2 protein in all TREM2 KO clones.
B. Volcano plot indicating differential gene expression in wild-type vs. TREM2 KO clones. Wild-type clones show an increased gene expression of multiple genes that are signature genes of DAM/LAM/KC-N macrophage populations *in vivo*. Differentially expressed genes were defined by FDR < 0.05, fold-change > 1.5 or < -1.5 (n=3 per genotype).
C. Bar plots of selected genes that are similarly regulated in DAM/LAM/KC-N populations (mean ± SD, n=3 per genotype).

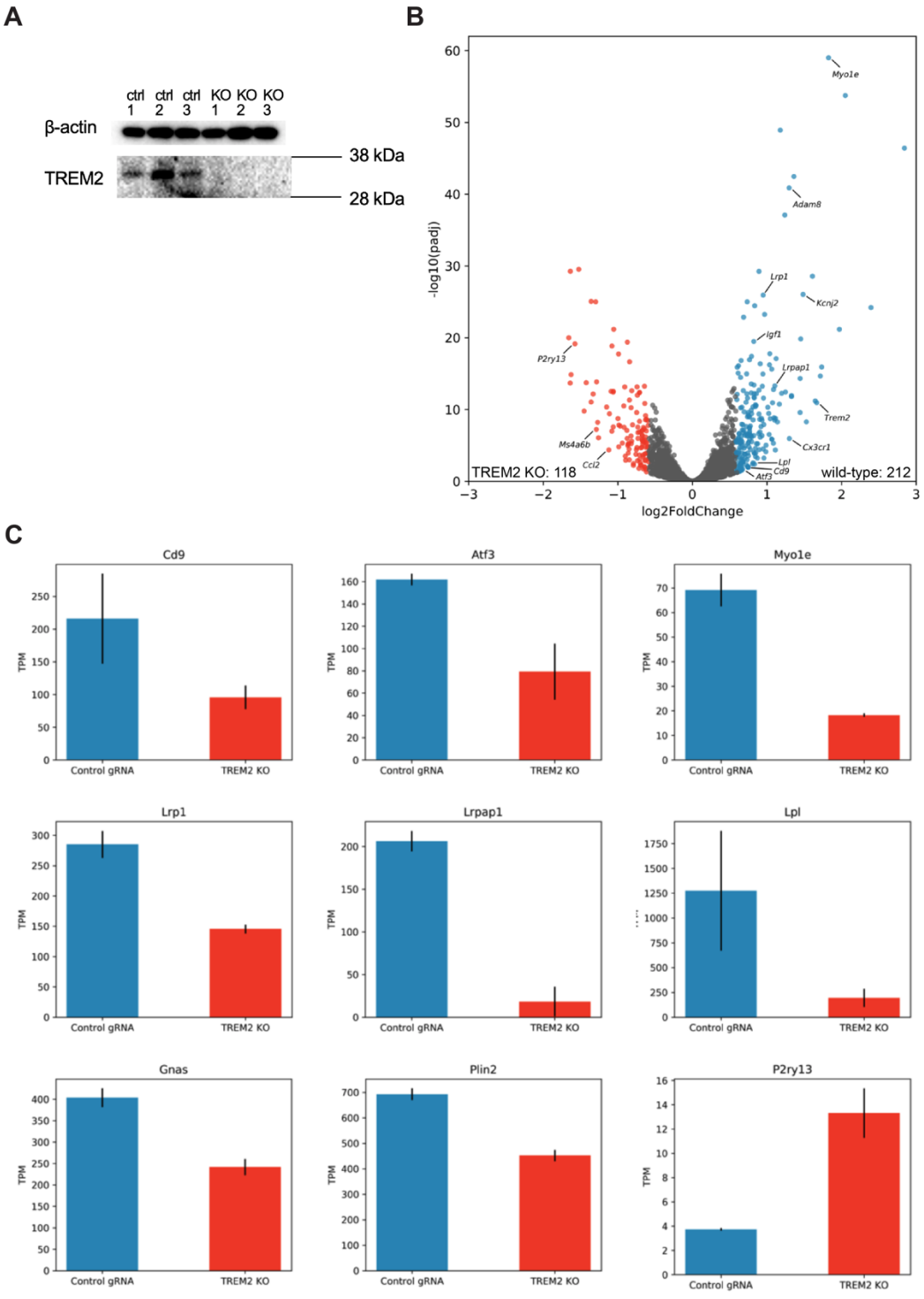
A
ctrl 1
ctrl 2
ctrl 3
KO 1
KO 2
KO 3
β-actin
TREM2
38 kDa
28 kDa
B
-log10(padj)
log2FoldChange
TREM2 KO: 118
wild-type: 212
Myo1e
Adam8
Lrp1
Kcnj2
Igf1
P2ry13
Lrpap1
Trem2
Ms4a6b
Ccl2
Cx3cr1
Lpl
Cd9
Atf3
C
Cd9
Atf3
Myo1e
Lrp1
Lrpap1
Lpl
Gnas
Plin2
P2ry13
TPM
Control gRNA
TREM2 KO

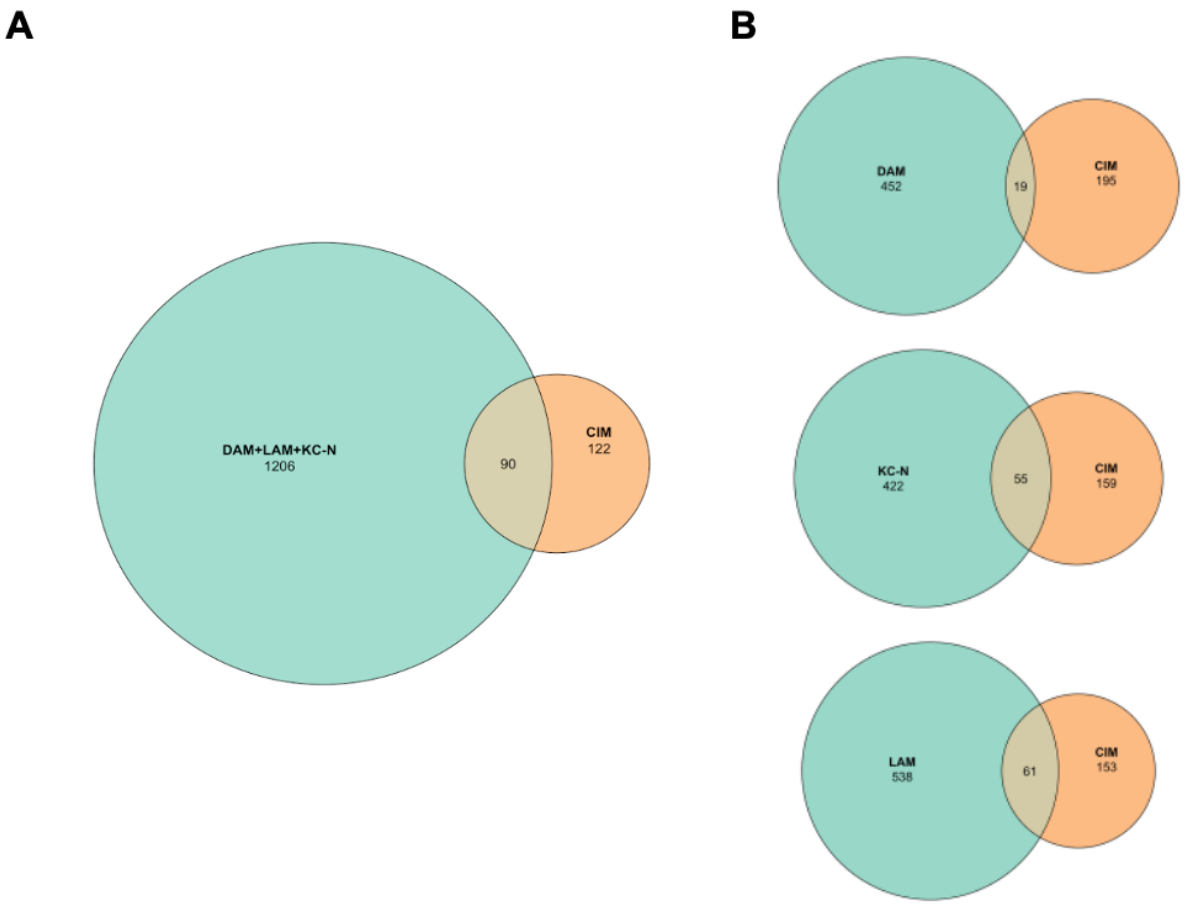

Figure 11: Overlap of genes increased in wild-type vs. TREM2 KO ER-HoxB8 macrophages with genes upregulated in DAM/LAM/KC-N populations in vivo

A. Overlap of downregulated genes in TREM2 KO conditionally immortalized macrophages (CIM) with at least any of the genes upregulated in DAM/LAM/KC-N populations.
B. Overlap of downregulated genes in TREM2 KO macrophages with DAM, LAM, and KC-N populations. Overlap is bigger with the KC-N and LAM populations compared to the overlap with DAM.

Table 1: Overlap of genes of the DAM/LAM/KC-N populations with genes downregulated in cultured macrophages with TREM2 KO.
Genes with increased expression in wild-type vs. TREM2 KO ER-HoxB8 cells in vitro that are increased as well in at least two of the murine in vivo populations of DAM, LAM, and KC-N.

DAM + LAM + KC-N	**LAM + KC-N**		**DAM + KC-N**	**DAM + LAM**
Trem2	*Lgals3*	*Asph*	*Ccl4*	*Lpl*
Cd9	*Anxa1*	*Metrnl*	*Csf2ra*	*Adssl1*
Atf3	*Clic4*	*Slc15a3*	*Cd83*	
Glipr1	*Rnh1*	*Dot1l*	*Inf2*	
Gnas	*Dpep2*	*Myof*	*Chst11*	
Plin2	*Atp6v1b2*	*Bcl2l1*	*Scd2*	
Myo1e	*Lilr4b*	*Actg1*	*Cd74*	
	Flna	*Anxa2*		
	Stap1	*Gsn*		
	Gpr137b-ps	*Vim*		
	Lrp1	*Lat2*		

Table 2: Genes expressed in a single LAM/DAM/KC-N subset that are also downregulated in cultured macrophages with TREM2 KO.
Genes with increased expression in wild-type vs. TREM2 KO ER-HoxB8 cells in vitro that are increased one of the murine in vivo populations of, LAM (columns 1 and 2), KC-N (columns 3 and 4), and DAM (column 5).

LAM		**KC-N**		**DAM**
Lilrb4a	*Pparg*	*Adam8*	*Cx3cr1*	*Igf1*
Dusp3	*Plekho2*	*Cdk18*	*Tgm2*	*Kcnj2*
Plk2	*S100a4*	*Nav2*	*Mafb*	*Lrpap1*
Rtn4	*Serpinb6b*	*Sema4d*		
Tlr13	*Id2*	*Oldfr111*		
Itgav	*Nap1l1*	*Xylt1*		
Ybx3	*Ckb*	*Pik3cb*		
Acer3	*Il7r*	*Tmem132a*		
Cd44	*Rhoc*	*Slc25a25*		
Gngt2	*S100a6*	*Tmem38b*		
Rab7b	*Tuba1b*	*Psen2*		
Gpx1	*Tuba1c*	*Lars2*		
Rgs1	*Rgs2*	*Hp*		
Ywhah	*S100a11*	*Tpcn2*		
Pcna		*Myadm*		

TREM2 leads to changes in transcriptional regulation

To understand how TREM2 leads to the changes in transcriptional programs observed in Figure 10, we started by carrying out ATAC-seq to define the landscape of accessible chromatin in ER-HoxB8 macrophages with or without TREM2 present. As expected, there was only a minimal change in the enhancer landscape with knockout of TREM2 (Figure 12A). Changes in accessible enhancer landscape usually are more subtle than changes in markers of enhancer modification, especially when interrogating cells of the same cell type. We merged the sites of accessible chromatin obtained from ATAC-seq and created a file with the enhancer landscape to use for H3K27 acetylation.

Acetylation of the lysine residue at the 27^{th} position of histone 3 is a marker of active enhancers and promoters, correlating with gene expression (68). We carried out ChIP-seq for H3K27 acetylation to interrogate how enhancer activation changes between wild-type and TREM2 KO ER-HoxB8 macrophages. We found that there were 4243 enhancers with increased acetylation at the H3K27 site within a 1000 bp region centered around the ATAC-seq peak (Figure 12B). Activation of these enhancers therefore appears to be downstream of TREM2. There were 127 gene regulatory regions that had increased acetylation at the H3K27 site with TREM2 KO. Therefore, activation of these sites appears to be suppressed by TREM2.

We carried out motif enrichment analysis of the enhancers that are downstream of TREM2. Transcription factor binding motifs are short repetitive sequences of DNA that mediate binding of transcription factors to DNA (73). By comparing enrichment of motif sequences with HOMER we identified transcription factor-binding motifs significantly enriched in enhancers that have more H3K27 acetylation in wild-type cells

(Figure 12C). When comparing motif enrichment in these enhancers to a random genomic background, we identified motifs for the two macrophage lineage-determining transcription factors PU.1 and TFEB to be significantly enriched, as expected when comparing the motifs in macrophage enhancers to genomic background. Additionally, motifs for three families signal-dependent transcription factors were also significantly enriched. Those were motifs for transcription factors of the AP-1 family, the MITF/TFE family, and the MEF2 family. When comparing the motifs with increased H3K27ac in TREM2+ cells with enhancers that are unchanged in H3K27 acetylation (i.e., are not affected by the presence of TREM2), as expected, the motifs for the lineage-determining factors PU.1 or C/EBP are not significantly enriched. However, the motifs for the signal-dependent factor families AP-1, MITF/TFE, and MEF2 are significantly enriched, suggesting that TREM2 mediates its effects on gene expression through factors of these families.

As ATF3 is a member of the AP-1 family and its gene expression is increased in all the TREM2-expressing populations of DAM, LAM, KC-N, and wild-type HoxB8 macrophages (compared to TREM2 KO), it is a factor likely downstream of TREM2. ATF3 has been described previously as a member of the AP-1 family that is specifically involved in resolving macrophages in the reparative phase of tissue injury, fitting with the prior findings that TREM2 dampens the pro-inflammatory response (33).

The MITF/TFE family has been described as being involved in regulating genes involved in autophagy, phagocytosis, and lysosomal function (136). They have been described as potential targets in neurodegenerative and lysosomal storage disorders

(137). Based on TREM2 having strong effects on phagocytosis *in vitro*, TREM2 mediating effects through factors of this family is also biologically plausible.

The role of the MEF2 family in macrophages still needs further investigation but reports so far have suggested a role in macrophage polarization and production of cytokines.

Overall, these results for the first time identify transcription factor families whose motifs are enriched in enhancers and are likely downstream of TREM2. After further validation, these may then serve as potential therapeutic targets in disease where TREM2 has been described to play a role, such as Alzheimer's Disease, metabolic syndrome, cancer, and myocardial infarction.

Figure 12: CRISPR knockout of TREM2 in ER-HoxB8 macrophages leads to differences in enhancer activation

A. ATAC-seq showed only minimal differences in the accessible chromatin landscape between TREM2 KO and wild-type cells (fold change > 2.0, FDR < 0.05).
B. ChIP-seq for H3K27ac shows differences in acetylation of H3K27 between TREM2 KO and wild-type cells. In wild-type cells 4243 regions of chromatin had more H3K27ac compared to TREM2-KO (fold change > 1.5, FDR < 0.05), suggesting that these regulatory regions are activated by TREM2. On the other hand, 127 regions had increased H3K27ac in TREM2 KO cells, indicating that these regulatory regions are suppressed by TREM2.
C. Motif analysis of gene regulatory regions downstream of TREM2. Regions that had more adjacent histone acetylation in wild-type cells were analyzed by motif analysis and first compared to random genomic regions. This expectedly found enrichment of motifs for lineage-determining factors (PU.1, C/EBP) of macrophages. Additionally, motifs of signal-dependent transcription factors (AP-1/ATF3, MITF/TFE, and MEF2) were identified. When comparing motif enrichment in enhancers with increased histone-acetylation to enhancers with unchanged histone acetylation between wild-type and TREM2 KO, only the motifs for the signal-dependent transcription factors remain enriched.

A

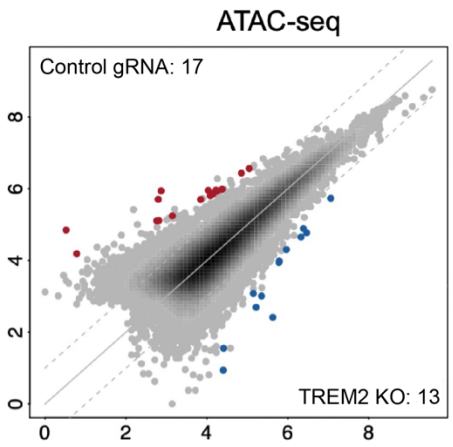

B

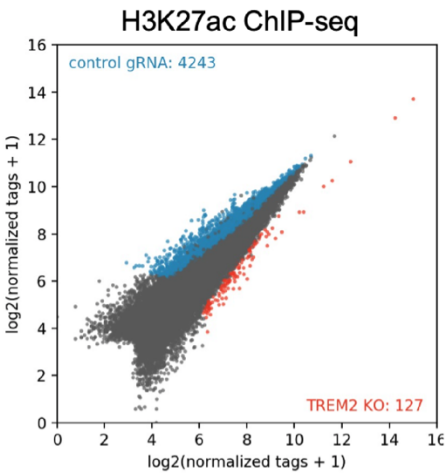

C

Background: generic genomic

Motif	p-value	%target/ %background	Best Match
	1e-375	45/16	PU.1
	1e-361	21/4	AP-1/ATF3
	1e-132	27/12	MITF/TFE
	1e-112	5/1	MEF2
	1e-91	21/10	CEBP

Background: enhancers with unchanged H3K27ac

Motif	p-value	%target/ %background	Best Match
	1e-78	24/13	AP-1/ATF3
	1e-61	6/2	MEF2
	1e-19	7/4	MITF/TFE

TREM2 leads to rearrangement of MITF/TFE members and ATF3 to regulatory regions of DNA

After identifying the motifs for the MITF/TFE and AP-1 family, we went on to further interrogate how the MITF/TFE family and ATF3 are expressed in different contexts and how DNA binding of these factors changes with the presence or absence of TREM2. First, we analyzed RNA-seq data that evaluated gene expression in undifferentiated ER-HoxB8 monocyte progenitors and differentiated ER-HoxB8 macrophages (Figure 13A). Gene expression of most factors increased substantially with macrophage differentiation with the exception of *Tfec*. *Tfec* was highly expressed in monocyte progenitors and expression was reduced considerably after differentiation, suggesting that its high expression may be involved in preventing macrophage differentiation. Between wild-type and TREM2 KO ER-HoxB8 macrophages, we observed comparatively small changes in gene expression, with Atf3 higher expressed in wild-type macrophages and *Tfec* higher expressed in TREM2 KO macrophages (both meeting the statistical significance criteria of fold-change > 1.5 and FDR < 0.05) (Figure 13B). This indicates that TREM2 suppresses expression of *Tfec*, induces expression of *Atf3*, but has no effect on expression levels of *Tfeb*, *Mitf*, and *Tfe3*.

As DNA binding of transcription factors is often rather post-translationally regulated than at a level of transcription, we carried out ChIP-seq for the MITF/TFE family and ATF3 in TREM2-KO and wild-type ER-HoxB8 macrophages. On a global scale, we found that binding of ATF3, TFEB, MITF, and TFE3 was substantially increased in enhancers with increased H3K27ac in wild-type macrophages, suggesting that some of the activation in these enhancers may stem from increased binding of

these factors to them (Figure 13C). Interestingly however, TFEC binding to these enhancers was reduced when TREM2 was present, indicating that activation of the cell through TREM2 leads to displacement of TREM2 from DNA and to the binding of other MITF/TFE family transcription factors. When focusing on the gene regulatory regions of DAM/LAM/KC-N genes, we observed a similar effect (Figure 14D). In enhancers of *Cd9*, *Atf3*, and *Myo1e*, we noted decreased H3K27ac and decreased binding of ATF3 and most of the MITF/TFE family in the TREM2 KO cells but unchanged or slightly increased binding of TFEC.

When further interrogating ChiP-seq for transcription factors, we identified that 2241 TFEB peaks (defined as an at least 4-fold change in enrichment) were lost in the TREM2 KO cells and only 32 peaks gained (Figure 14A). This indicates that TREM2 leads to increased TFEB binding to gene regulatory regions in DNA. The lost peaks also exhibited decreased H3K27ac in the TREM2 KO cells, implying that TFEB binding is associated with an increase in enhancer activation. Additionally, these peaks also showed a decrease in binding of MITF and ATF3 while TFEC binding was slightly increased (Figure 14A). This again highlights the differential recruitment of TFEC to DNA compared to the remaining MITF/TFE factors and ATF3. Interrogation of differential TFEC peaks again demonstrated these differences. In contrast to TFEB, 3110 TFEC peaks were gained in the TREM2 KO cells while only 187 peaks were lost (Figure 14B). This indicates that TREM2 represses TFEC binding to gene regulatory elements. Interestingly, the peaks gained in the TREM2 KO cells were associated with decreased H3K27ac, suggesting that TFEC binding is associated with suppression of enhancer activation. Additionally, TFEB and ATF3 binding was decreased in the gained

peaks while MITF binding was unchanged. These findings again highlight the contrasting role TFEC appears to play in comparison to other MITF/TFE factors and ATF3 in relation to DNA binding and enhancer activation.

Overall, these results suggest that TREM2 activation leads to rearrangement of transcription factor binding to enhancers. TREM2 signaling leads to displacement of TFEC from DNA and increases binding of ATF3, TFEB, MITF, and TFE3 to enhancers that also become more active. These findings are reciprocated in enhancers of DAM/LAM/KC-N signature genes, implying that these factors are likely to play a role in the regulation of these genes.

Figure 13: CRISPR knockout of TREM2 in ER-HoxB8 macrophages leads to differences in binding of ATF3, and the MITF/TFE family to differentially active enhancers.

A. Gene expression by RNA-seq of ATF3 and the MITF/TFE family in undifferentiated ER-HoxB8 monocyte progenitors (HoxB8_undiff) and differentiated ER-HoxB8 macrophages (HoxB8-mps). Mean ± SD, n = 2 per cell type.
B. Gene expression by RNA-seq of ATF3 and the MITF/TFE family in wild-type (control gRNA) and TREM2 KO ER-Hoxb8 macrophages. Mean ± SD, n = 3 per genotype.
C. Binding of ATF3 and the MITF/TFE family to enhancers that were found to have increased H3K27ac (i.e., are more active) in wild-type vs. TREM2 KO macrophages.
D. Visualization of ATAC-seq and ChIP-seq for H3K27ac and transcription factors in regulatory regions of DAM/LAM/KC-N signature genes.

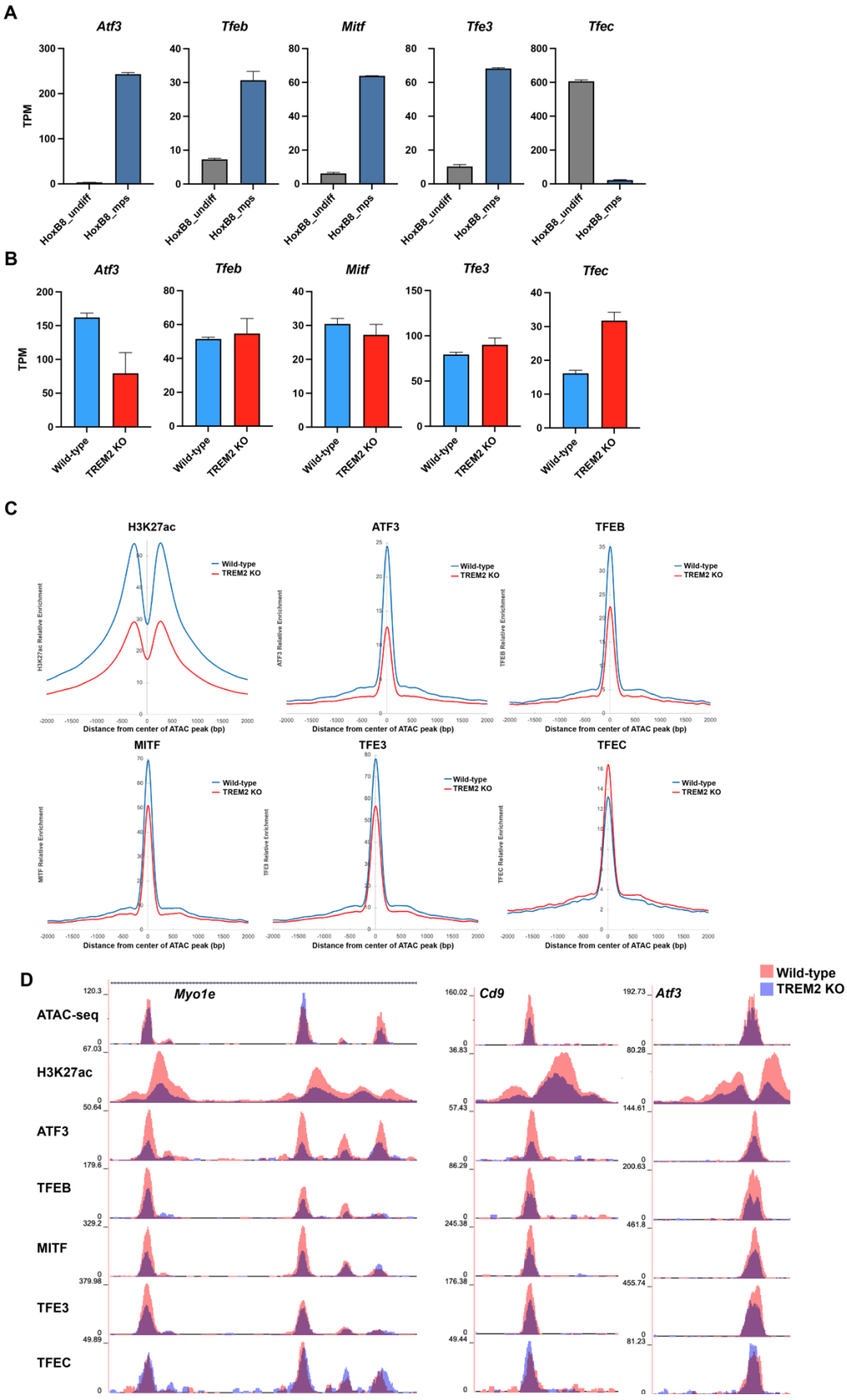
A
Atf3
Tfeb
Mitf
Tfe3
Tfec
TPM
HoxB8_undiff
HoxB8_mps
B
Wild-type
TREM2 KO
C
H3K27ac
ATF3
TFEB
MITF
TFE3
TFEC
Distance from center of ATAC peak (bp)
D
Myo1e
Cd9
Atf3
ATAC-seq
H3K27ac
ATF3
TFEB
MITF
TFE3
TFEC

Figure 14: TREM2 KO leads to different binding of ATF3 and ATF/TFE transcription factors to gene regulatory elements and leads to changes in H3K27 acetylation at these sites.

A. TREM2 KO leads to a substantial net loss of TFEB peaks (with 4-fold enrichment used as cutoff). The peaks lost in the TREM2 KO cells show a reduction in H3K27ac as well as a reduction in binding of MITF and ATF3, but a slight increase in binding of TFEC.
B. TREM2 KO leads to a substantial net gain of TFEC peaks (with 4-fold enrichment used as cutoff). The peaks gained in the TREM2 KO cells show a reduction in H3K27ac as well as a reduction in binding of TFEB, MITF, and ATF3.

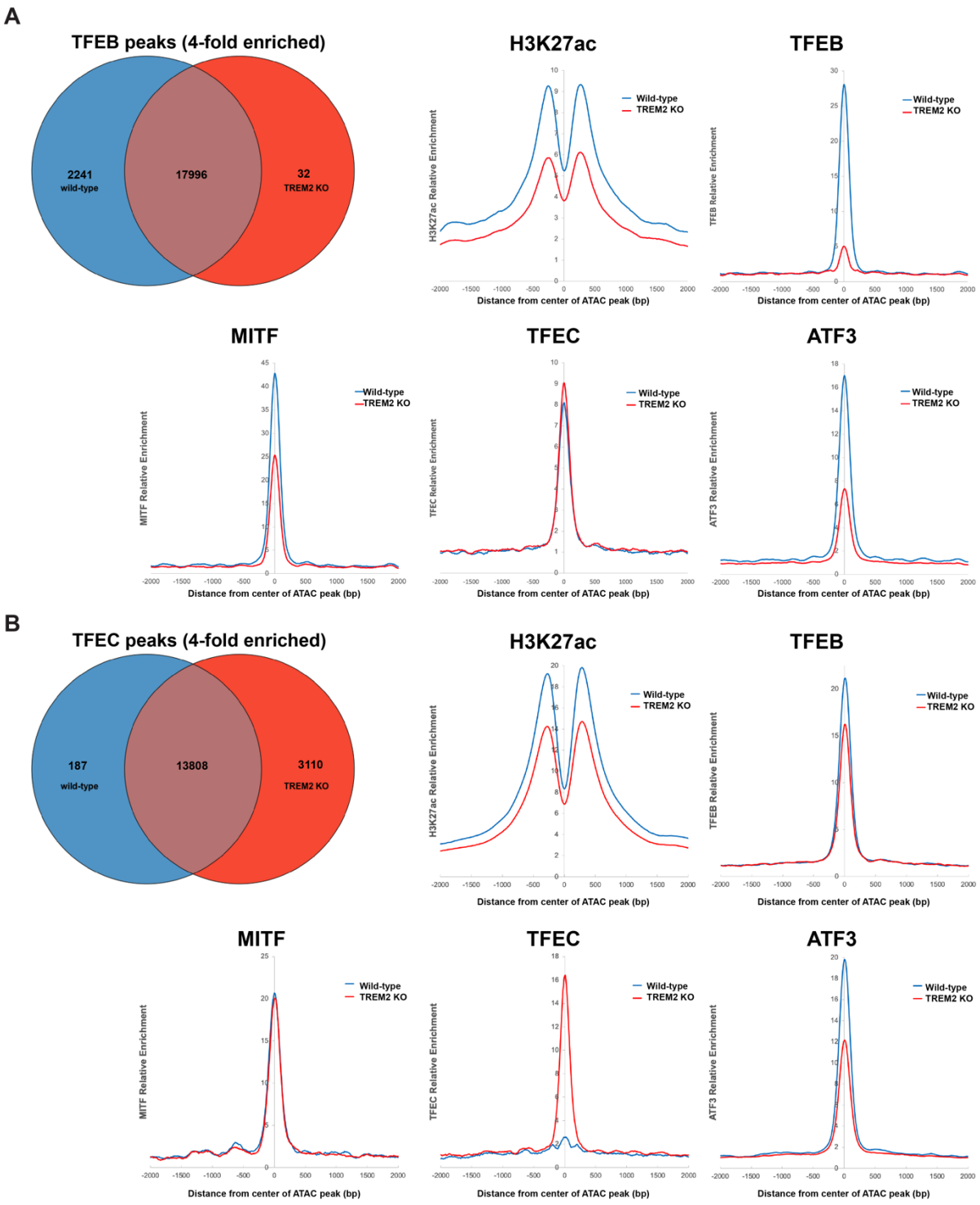
A
TFEB peaks (4-fold enriched)
2241
wild-type
17996
32
TREM2 KO
H3K27ac
TFEB
MITF
TFEC
ATF3
Wild-type
TREM2 KO
H3K27ac Relative Enrichment
TFEB Relative Enrichment
MITF Relative Enrichment
TFEC Relative Enrichment
ATF3 Relative Enrichment
Distance from center of ATAC peak (bp)
B
TFEC peaks (4-fold enriched)
187
wild-type
13808
3110
TREM2 KO

Loss of TFEB in ER-HoxB8 macrophages leads to downregulation of signature DAM/LAM/KC—N genes

To further validate whether MITF/TFE factors and ATF3 play a role in regulating transcription of genes downstream of TREM2, we used CRISPR to generate knockouts of TFEB and ATF3 with a strategy equivalent to knockout of TREM2 above. We generated the knockout in ER-HoxB8 monocyte progenitors using a lentiviral construct carrying gRNA towards TFEB or ATF3, as well as mCherry. Cells were single-cell sorted based on mCherry positivity, clones grown, and knockout confirmed with Sanger sequencing. Clones with homozygous frameshift mutations or large insertions/deletions were grown and differentiated into macrophages.

We carried out RNA-seq and found that loss of TFEB lead to a decrease in gene expression of 112 genes (gene expression activated by TFEB) and an increase in the expression of 125 genes (gene expression repressed by TFEB) (Figure 15A). The ATF3 knockout in this context had minimal effects on gene expression with only 6 genes differentially expressed (Figure 15A), suggesting the need for a perturbation to see effects of ATF3 or redundancies in place that can step into ATF3's role, such as other factors of the AP-1 family.

13 of the 112 genes exhibited decreased expression in both TREM2 KO and TFEB KO cells, suggesting activation by both TREM2 and TFEB. Of note, of the 6 genes besides *Trem2* that are upregulated in DAM/LAM/KC-N and wild-type (vs. TREM2 KO) ER-HoxB8 macrophages, *Cd9*, *Gnas*, *Atf3* were also increased in wild-type vs. TFEB KO ER-HoxB8 macrophages (Figure 15B, Table 1).

Interestingly, *Atf3* expression is increased in all TREM2-expressing cells above as well as in wild-type vs. TFEB KO cells, while KO of ATF3 itself did not have major changes on gene expression. Future studies could employ other approaches of knockout, certain perturbations that may rely more on ATF3 signaling, or double/triple KO of ATF3 together with other AP-1 family members.

Overall, these data add to the evidence that at least a subset of genes downstream of TREM2 is controlled by MITF/TFE family factors.

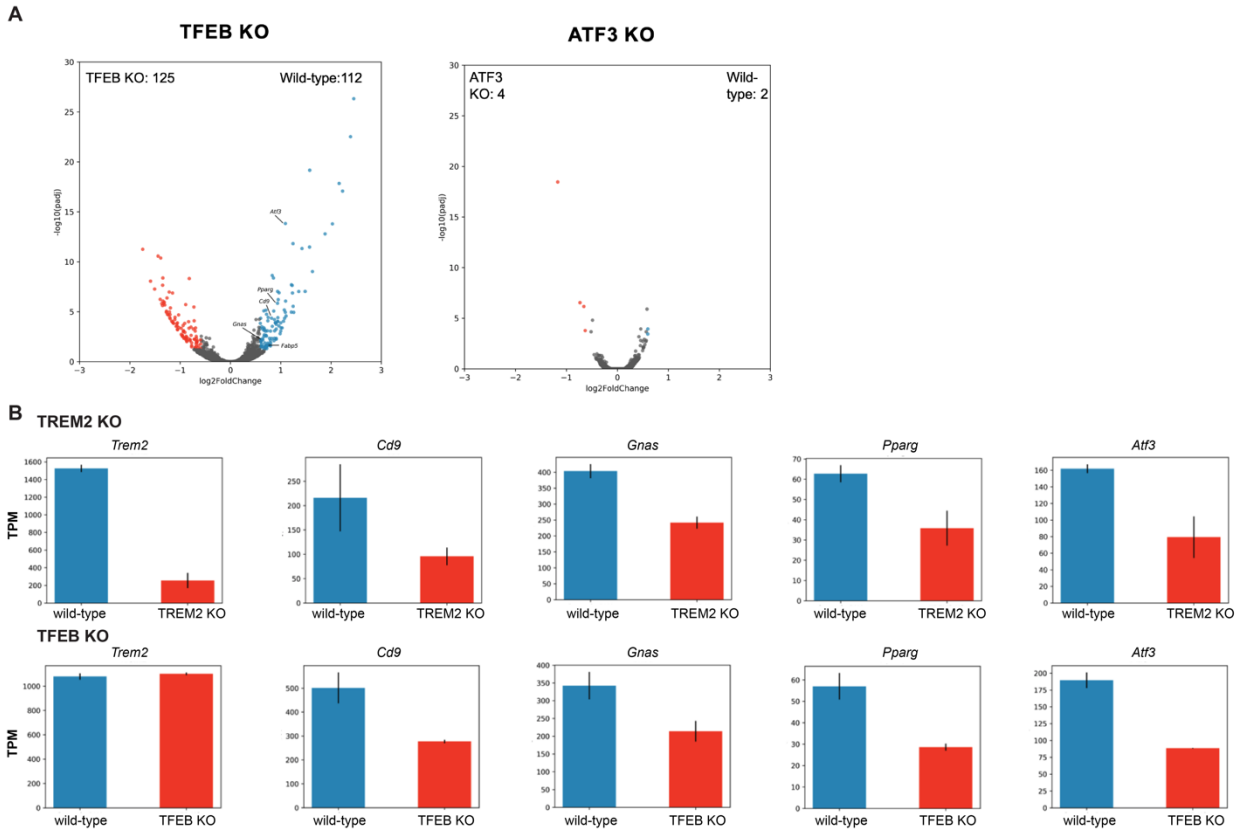

Figure 15: CRISPR knockout of TFEB in ER-HoxB8 macrophages leads to gene expression changes of DAM/LAM/KC-N genes similar to loss of TREM2

A. Volcano plot indicating differential gene expression in control vs. TFEB KO and ATF3 KO, respectively. Differentially expressed genes were defined by FDR < 0.05, fold-change > 1.5 or < -1.5, and log2(TPM+1) > 4 in at least one group (n=3 for control and ATF3 KO, n=2 for TFEB KO).

B. Expression of selected DAM/LAM/KC-N genes that are also increased in expression in control vs. TREM2 KO cells (mean ± SD).

Discussion:

In this study, we generated a conditionally immortalized myeloid cell line that constitutively expresses Cas9. As demonstrated in this study, these cells can differentiate into macrophages or osteoclasts similar in expression profile to bone-marrow derived cells while having some benefits over primary bone marrow cells. First, due to constitutive expression of Cas9, genetic modifications can be carried out at the monocyte progenitor stage with introduction of guide RNA (gRNA) by lentivirus. After the successful modification is confirmed, cells can then be differentiated into macrophages. Primary macrophages from the bone marrow or peritoneal cavity terminally differentiate within two to three weeks after being removed from the body, making these modifications more challenging. Furthermore, it is possible to generate very large numbers of cells in relatively short time, making it possible to carry out high-quality ChIP-seq for histone modifications and multiple transcription factors. Primary cells depend on a supply of mice of the desired genotype while these cells can be grown, and genetic modification made without the need for more study animals. Thus, these cells add an additional tool to the toolbox of macrophage research.

We used these cells to generate an enhancer deletion and ATF3 motif disruptions in the intergenic TREM2 enhancer. This enhancer is accessible during states of high level of *Trem2* expression in Kupffer cells in a NASH model (but not in healthy Kupffer cells with low levels of *Trem2* expression) and in bone-marrow derived macrophages, as well as ER-HoxB8 macrophages, which all express *Trem2* at high levels (30). Additionally, there was a substantial increase in ATF3 binding in NASH Kupffer cells compared to healthy cells. Thus, we had hypothesized that this enhancer,

and particularly binding of ATF3 to the enhancer, is necessary for high expression of *Trem2*. However, we found that deleting the whole enhancer or disrupting the ATF3 motif did not substantially change *Trem2* expression levels and it was still highly expressed at ~1,200 TPM. These experiments show that there might be redundancy in the intronic enhancer mediating high expression of *Trem2* or the enhancer may not be necessary. Future studies could target single knockouts of the intronic enhancer and adding a knockout of the intronic enhancer to the intergenic enhancer cell line to assess the effect of a double enhancer knockout. Additionally, a TREM2 reporter ER-HoxB8 cell line could be used in a CRISPR screen to assess which transcription factors may be necessary for high expression of *Trem2*.

We also used these cells to test how TREM2 itself regulates gene expression by knockout of the *Trem2* gene. We found that close to half of the genes that were upregulated in the wild-type cells *in vitro* were also upregulated in at least one of the DAM/LAM/KC-N populations *in vivo*, especially DAM/LAM/KC-N signature genes like *Cd9*, *Atf3*, *Lpl*, and *Myo1e*. Multiple of these genes also have proposed physiologic or pathophysiologic functions in microglia, making these a valuable model to improve our understanding of how TREM2 exerts its effects on gene regulation in macrophages.

We identified for the first time candidate transcription factors downstream of TREM2 by ChIP-seq. We discovered that the motifs of the MITF/TFE family, the AP-1 family, and the MEF2 family were enriched in enhancers that are more active (i.e., exhibit more H3K27 acetylation) when TREM2 is present. This suggests that factors of these families are likely the most important transcription factors mediating effects downstream of TREM2 in the cultured ER-HoxB8 macrophage model. As gene

expression of some signature DAM/LAM/KC-N genes is also upregulated in this context, these transcription factors are likely to contribute to the transcriptional program in these cells in Alzheimer's Disease, metabolic syndrome, and NASH. As the AP-1 family is large and *Atf3* is upregulated in DAM/LAM/KC-N populations, as well as wild-type vs. TREM2 KO cells, we focused on assessing ATF3 as a representative of the AP-1 family.

To further add to the evidence that these transcription factors are downstream of TREM2, we carried out factor-specific ChIP-seq for MITF/TFE family transcription factors and ATF3. We found that TREM2 leads to rearrangement of enhancer binding of MITF/TFE factors and ATF3. Their motifs are enriched in enhancers downstream of TREM2 and binding is increased in enhancers of DAM/LAM/KC-N genes when TREM2 is present. The MITF/TFE family is well described as regulating lysosomal function, autophagy, and phagocytosis, and TREM2 together with DAP12 is a strong inducer of phagocytosis (91, 92, 136, 137). Additionally, ATF3 plays a role in the resolution of inflammation in macrophages and TREM2 has been shown to dampen the pro-inflammatory response *in vitro* (33, 89, 90). Thus, these factors are also biologically plausible to be downstream of TREM2 signaling and may be possible therapeutic targets, as TREM2 itself may be saturated with ligands in certain disease contexts and challenging to further activate pharmacologically. Interestingly, we found opposing effects on factors of the MITF/TFE family, with TREM2 inducing DNA binding of TFEB, MITF, and TFE3 to active enhancers, while it reduces binding of TFEC. Additionally, we identified that a substantial amount of TFEB peaks is lost in the TREM2 KO while TFEC peaks are gained. Interestingly, TFEB binding was associated with increased enhancer

activation while the TFEC peaks gained associated with decreased enhancer activation as evidenced by H3K27ac. This suggests that in this context TFEB acts as an activator of gene regulatory elements while TFEC acts as a repressor. This shows that different factors of the MITF/TFE family may have distinctive effects on gene expression in macrophages. Interestingly, gene expression of *Tfec* during differentiation of ER-HoxB8 monocyte progenitors to macrophages also decreases, in contrast to the increase seen in other MITF/TFE factors. This may point towards generally differing effects of TFEC and the remaining MITF/TFE factors in macrophages. Of note, CRISPR deletion of TFEB led to a reduction in signature DAM/LAM/KC-N genes, similar to the effect of deletion of TREM2 itself in these genes, adding to the evidence that at least a subset of genes downstream of TREM2 are regulated by MITF/TFE factors. Generally, targeting specific factors downstream of TREM2 may add an additional benefit that is not achievable with activation of TREM2. However, the effect of these transcription factors first needs to be tested in loss and/or gain of function experiments in disease models where TREM2 has been shown to have an impact, i.e., Alzheimer's Disease, metabolic syndrome, cancer, and myocardial infarction (86, 94, 99, 100).

Overall, we find that the intergenic enhancer is surprisingly not required for high expression of *Trem2* and that TREM2 likelymediates its effect on gene expression at least partially through rearrangement of DNA binding of the MITF/TFE family and ATF3. These factors have the potential to be tested in disease models involving TREM2 and may serve as future therapeutic targets.

Materials and Methods:

Mice

Mice were maintained under a 12 hour light and 12 hour dark cycle at constant temperature with *ad libitum* access to food and water. Mice were fed a regular chow diet (T8604, Envigo). Rosa26-Cas9 knockin mice were obtained from The Jackson Laboratory (Strain No. 02855, Bar Harbor, ME) and maintained and bred in our vivarium.

Generation of the Cas9-expressing ER-HoxB8 conditionally immortalized monocyte progenitor cell line

A 12-week-old male Rosa26-Cas9 knockin mouse was euthanized by exposure to CO_2. Tibias and femurs were flushed with RPMI 1640 (Corning) containing 10% fetal bovine serum (FBS, Omega Biosciences) and 1% penicillin/streptomycin (Thermo Fisher Scientific). Cas9-expressing ER-HoxB8 conditionally immortalized monocyte progenitors were generated following established protocols (130). First, bone marrow cells were added to 10 ml of FACS buffer (phosphate-buffered saline (PBS) supplemented with 2% FBS and 1 mM EDTA) and then strained through a 40 μm filter. Then, cells were pelleted at 200g for 10 minutes, resuspended in 4 ml of FACS buffer and layered over 4 ml of Ficoll-Paque-Plus (Sigma-Aldrich) in a 15 ml conical. The interface with cells was collected, transferred to a new tube and cells were counted. After centrifugation, cells were resuspended at $2x10^{6/}$ml in RPMI 1640 supplemented with 10% FBS, 1% penicillin/streptomycin, and 10 ng/ml of each SCF, IL-3, and IL6 (all from PeproTech). $10x10^6$ cells were plated in one well of a six-well plate in 5ml of media. Cells were cultured for 48 hours and then transduced with retrovirus containing

an expression vector for the ER-HoxB8 construct. Murine stem cell virus-based expression vector for ER-Hoxb8 was gifted from Dr. David Sykes (Massachusetts General Hospital, Boston, MA).

For transduction, a 6-well culture plate was coated with fibronectin (Sigma-Aldrich) at a concentration of 1 mg/ml in PBS for one hour. 500,000 cells in 1 ml were transduced with 2 ml of ER-HoxB8 retrovirus (in DMEM with 30% FBS). Lentiblast A (OZ Biosciences), lentiblast B (OZ Biosciences) and polybrene (Sigma-Aldrich) were added to concentrations of 0.5 µg/ml, 2.5 µg/ml, and 8µg/ml, respectively. The culture plate containing the cells was centrifuged at 1,000 g for 90 minutes at 22 °C. 6 ml of ER-HoxB8 cell media (RPMI 1640 supplemented with 10% FBS, 1% penicillin/streptomycin, 0.5 µM β-estradiol (Sigma-Aldrich), and 20 ng/ml GM-CSF (PeproTech)) were added to the well and a half-media exchange with ER-HoxB8 cell media was performed the next day to dilute the polybrene. Successfully transduced cells were selected with G418 (Thermo Fisher Scientific) at 1 mg/ml for 48 hours. Thereafter, cells were passaged as needed and maintained in ER-HoxB8 cell media for 3 weeks. At this point, all cells except the transduced monocyte progenitors will have stopped dividing and vials of cells were frozen or used for further experiments such as macrophage differentiation or transduction with CRISPR guide RNA.

Macrophage and osteoclast differentiation

For differentiation into mature cells, ER-HoxB8 monocyte progenitors were washed twice with PBS and then resuspended at a concentration of $1x10^6$ cells/ml in DMEM with 10% FBS, 1% penicillin/streptomycin, and 16.7 ng/ml M-CSF (Shenandoa). Cells were plated at a density of $2x10^6$ per well of a 6-well plate or $30x10^6$ cells per 15

cm culture dish. Media was exchanged after 3 days and 5 days of culture and cells were collected at day 7. For osteoclast differentiation, 10 ng/ml M-CSF were used throughout the differentiation and at day 3 an additional 50 ng/ml RANKL (PeproTech) was added, and cells treated with RANKL for a total of 4 days. For KLA stimulation, cells were treated with 100 ng/ml KLA (Avanti Polar Lipids). Differentiated cells were then washed twice with PBS and either lysed/crosslinked in the culture plate (for RNA-seq or ChIP-seq) or scraped from the plate into PBS (for ATAC-seq or Western Blotting).

Single-cell sorting of ER-HoxB8 cells

To reduce variability between clones after CRISPR knockout, the starting culture was single-cell sorted by FACS to start with a clonal population of cells. For sorting, cells were collected from tissue culture flasks by pipetting up and down to detach loosely adherent cells. Cells were then centrifuged at 500 down, resuspended in FACS buffer and filtered through a 35 µm strainer into 5 ml polyprolylene FACS tubes. Cells were then single-cell sorted using a Sony MA 900 into 96-well plates filled with 100 µm of ER-HoxB8 cell media. After 7 days, another 100 µm of media was added and growing clones were subsequently moved to progressively larger cultures dishes or flasks and subsequently used for experiments or further characterization.

Generation of lentivirus encoding gRNA

For generation of lentivirus carrying a construct expressing gRNA, we used a modified version of lentiGuide-puro (Addgene) that has the puromycin-resistance gene replaced with mCherry. This plasmid was previously generated in our laboratory as described previously. The sequences for gRNA targets were constructed with the CHOPCHOP web tool for genome engineering (138-140). A full list of gRNAs can be

found in Table 3. Either one or two gRNAs were inserted for each vector into a BsmBI cleavage site. When two gRNAs were used, a sequence containing an H1 promoter was added between the two gRNA sequences as described previously by our laboratory. Annealed gRNA was ligated into the vector using T4 ligase. The vector was added to Stbl2 competent cells (Thermo Fisher), the mixture incubated on ice for 30 minutes, followed by 30 seconds of heat shock at 42 °C with return to ice thereafter for 2 minutes. Bacteria were cultured in 1ml S.O.C. media (Invitrogen) for one hour, spread onto an LB agar plate with ampicillin. Agar plates were cultured at 37 °C overnight. Colonies were picked with a 20 µl pipette tip and grown in 2 ml of LB media with ampicillin at 37 °C overnight with continuous agitation. The Zyppy Plasmid Miniprep Kit (Zymo Research) was used to extract plasmid DNA. DNA was then submitted for Sanger sequencing at Genewiz to confirm successful insertion of gRNA sequence(s).

Bacteria with confirmed gRNA were cultured overnight at 37 °C overnight with continuous agitation in 150 ml. Plasmid DNA was then extracted with NucleoBond Xtra Midi Plus EF (Takara) and quantified using a NanoDrop Microvolume Spectrophotometer. For transfection, Lenti-X 293T cells (Clontech) were added to a 10 cm culture plate coated with poly-D-lysin (Sigma-Aldrich) at a density of 3.5 million cells per plate in 10 ml DMEM containing 10% FBS and 1% penicillin/streptomycin. Cells were cultured overnight at 37 °C. Media was exchanged to 6 ml of DMEM containing 30% FBS the next morning and transfection carried out with 5 µg of lentiGuide-mCherry with gRNA, 3.75 µg of psPAX2 (Addgene) and 1.25 µg of pVSVG (Addgene) along with 20 µl of X-tremeGENE HP DNA Transfection Reagent (Roche). Cells were incubated overnight and media was replaced with 8 ml of DMEM with 30% FBS and 1%

penicillin/streptomycin. After another overnight incubation, media containing lentivirus was collected, filtered through a 0.45 μm filter. Media was exchanged again and another round of collection carried out the next day. Tubes with lentivirus were placed on dry ice immediately after collection, followed by storage at -80 °C.

Transduction of ER-HoxB8 cells with lentivirus

12-well plates were coated with fibronectin for an hour at 10 μg/ml. 500,000 cells in 500 μl of ER-HoxB8 cell media were then added to one well per lentivirus, one well for control gRNA lentivirus, and one well for control media (DMEM with 30% FBS and 1% penicillin/streptomycin, to use for gating during FACS). The transductions were carried out with 1 ml of lentiviral or control media, 0.5 μg/ml Lentiblast A, 2.5 μg/ml Lentiblast B, and 8 μg/ml polybrene. The plates were centrifugated at 1,000 g for 90 minutes at 22 °C. After completion of transduction, 3 ml of ER-HoxB8 cell media was added with a half-media exchange the following day. Cells were then transferred to T25 flasks. Successfully transduced cells (mCherry positive) were single-cell sorted into 96-well plates 4-6 days after transduction. After 7-10 days, 100 μl of ER-HoxB8 cell media was added to all wells. After 2-3 weeks, clones were passaged into increasingly larger tissue culture plates and genomic DNA isolated using the NucleoSpin Tissue Mini Kit (Macherey-Nagel). For gene knockouts, the region (150-300 bp) surrounding the gRNA target was then amplified with primers flanking the site. PCR products were identified by gel electrophoresis in 1.5% agarose gels, cut out, and extracted using the NucleoSpin Gel and PCR Clean-up Mini Kit (Macherey-Nagel), and submitted for Sanger sequencing (Genewiz). Sanger sequencing data was analyzed using CRISP-ID to identify clones with homozygous knockout deletions or large indels of more than 20

base pairs. Knockout was then confirmed at the protein level via Western Blotting with loss of bands at the size of the protein in the knockout clones compared to the clones that were transduced with control gRNA without binding site in the genome. For each round of knockouts experiments, transduction with control gRNA was performed in parallel and 3 independent clones of control gRNA were selected along with 2-3 clones with the gene knockout.

For TREM2 enhancer deletion, two sets of primers were used for PCR, one flanking the enhancer and one within the enhancer. PCR followed by gel electrophoresis demonstrated a reduction in size of the product by 500 bp using the flanking primers in one of the clones in addition to loss of the product using the primers within the enhancer. This confirmed homozygous deletion and this clone was further used in experiments as enhancer knockout.

Western Blotting

Whole cell lysates of knockout clones were prepared and sonicated in cell lysis buffer (50 mM HEPES-KOH (pH 7.9), 150 mM NaCl, 1.5 mM MgCl2, 1% NP40, 1 mM PMSF (Sigma-Aldrich), 1x protease inhibitor cocktail (Sigma-Aldrich)) by ultrasound homogenizer (Bioruptor) for 10 minutes at 4 °C. Aliquots were then boiled at 95 °C for 5 minutes in NuPage LDS Sample Buffer (Thermo Fisher) with NuPAGE Sample Reducing Agent (Thermo Fisher). Samples were then use for SDS-PAGE and transferred to immobilon-P transfer membranes (Merck Millipore). Antibody towards mouse TREM2 was MAB1729 (R&D Systems), followed by anti-rat secondary antibody (HAF005, R&D Systems). Bound antibodies were visualized using SuperSignal West

Femto Maximum Sensitivity Substrate (Thermo Fisher Scientific) and images were acquired with ChemiDoc XRS+System (Bio-Rad Laboratories).

RNA-seq library preparation

Library preparation for RNA-seq was essentially carried out as published previously (30, 141). Total RNA was isolated from differentiated ER-HoxB8 macrophages using the Direct-zol RNA MicroPrep Kit (Zymo Research). Plates were washed twice with PBS and then lysis was done with TRIzol reagent (Zymo Research) in the culture dish. RNA isolation was carried out according to manufacturer's instruction and was quantified using a NanoDrop Microvolume Spectrophotometer. 500 ng of RNA were then used for mRNA selection by incubation with oligo d(T) Magnetic Beads (NEB). mRNA was fragmented by incubation in 2X Superscript III first strand buffer (Thermo Fisher Scientific) with 10 mM DTT (Thermo Fisher Scientific) at 94 °C for 9 minutes, followed by immediate placement on ice. In the next step, 10 µl of fragmented mRNA was heated at 50 °C for one minute with 0.5 µl of Random primers (3 µg/µl stock) (Thermo Fisher Scientific), .5 µl of Oligo dT primer (50 µM) (Thermo Fisher Scientific), 0.5 µl SUPERase-In (Ambion), and 1 µl of dNTPs (10 mM). Following this step, 5.8 µl of nuclease-free water, 1 µl of DTT (100 mM) 0.1 µl Actinomycin D (2 µg/µl), 0.2 µl of 1% Tween-20 (Sigma-Aldrich) and 0.5 µl of SuperScript III (Thermo Fisher Scientific) were added and incubated in a PCR thermal cycler at 25 °C for 10 minutes and 50 °C for 50 minutes. The RNA/cDNA hybrid double-stranded nucleic acid was then purified with RNAClean XP beads (Beckman Coulter) according to the manufacturer's protocol. The purified nucleic acid was then eluted with 10 µl nuclease-free water and added to 1.5 µl of Blue Buffer (Enzymatics), 1.1 µl of dUTP mix (10 mM dATP, dCTP,

dGTP, and 20 mM dUTP), 0.2 µl of RNase H (5 U/µl), 1.05 µl of nuclease-free water, 1 µl of DNA polymerase I (Enzymatics) and 0.15 µl of Tween-20 (1%). This solution was incubated in a thermal cycler at 16 °C for 2 hours followed by 12 °C overnight to produce double-stranded DNA with one strand being marked with dUTP. This nucleic acid was then purified with 28 µl SpeedBeads (GE Healthcare) resuspended in 20% PEG8000 and 2.5M NaCl, resulting in a final concentration of 13% PEG. The purified DNA was then eluted with 40 µl EB buffer (10 mM Tris-Cl, pH 8.5) and end-repair, A-tailing, and adaptor ligation was carried out as previously described using barcoded adapters (Bioo Scientific). After adaptors were added, the dsDNA was amplified for 14 cycles with PCR and size-selected with SpeedBeads resuspended in 20% PEG8000 and 2.5M NaCl, resulting in a final concentration of 13% PEG. The completed libraries were then quantified using Qubit dsDNA HS Assay Kit (Thermo Fisher Scientific) and sequenced on an Illumina HiSeq 4000 or NovaSeq 6000 at the Institute for Genomic Medicine sequencing core at UC San Diego.

ATAC-seq library preparation

ATAC-seq libraries were prepared essentially as previously described (30, 142). Differentiated ER-HoxB8 macrophages in culture dishes were washed twice with PBS, scraped from the plate, centrifugated at 500 g for 5 minutes, and resuspended in cold lysis buffer (10 mM Tris-HCl, pH 7.4, 10 mM NaCl, 3 mM $MgCl_2$, 0.1% IGEPAL-CA630). After another centrifugation, cells were resuspended in 50 µl reaction buffer consisting of 25 µl Tagment DNA buffer, 2.5 µl Tagment DNA enzyme I (both from the Nextera DNA Library Preparation Kit, Illumina), and 22.5 µl of nuclease-free water. The reaction was performed for 30 minutes at 37 °C. DNA was purified immediately thereafter using

the ChIP DNA&Concentrator kit (Zymo Research). Amplification of DNA was carried out with the Nextera primer Ad1 and a unique Ad2.n barcoding primer using NEBNext High-Fidelity PCR Master Mix (NEB) for 14 cycles. Libraries were size selected by gel extraction of 175-225 base pair fragments, purified, and sequenced using an Illumina HiSeq 4000 at the Institute for Genomic Medicine sequencing core at UC San Diego.

Crosslinking of ER-HoxB8 macrophages

Plates with differentiated ER-HoxB8 macrophages were washed twice with PBS and cells then fixed. For H3K27ac ChIP-seq, cells were fixed with 1% formaldehyde (Thermo Fisher Scientific) in PBS at room temperature for 10 minutes. The reaction was quenched with glycine (Thermo Fisher Scientific) added to a final concentration of 125 mM. For transcription factor ChIP-seq, cells were crosslinked with 3mM DSG (ProteoChem) in PBS at room temperature for 30 minutes, followed by fixation with 1% formaldehyde (Thermo Fisher Scientific) in PBS for 10 minutes. As above, the reaction was quenched with glycine added to a final concentration of 125 mM. Following fixation and quenching, cells were scraped from the culture dish, washed with cold PBS and centrifugated at 700 g at 4 °C for 5 minutes. After removal of PBS, the pellet of crosslinked cells was flash frozen in liquid nitrogen and stored at -80 °C until ChiP-seq library preparation.

ChIP-seq library preparation

ChIP-seq libraries were prepared mostly as described previously (30, 143). The pellet of fixed cells was thawed on ice. For H3K27ac ChIP-seq, cells were resuspended in cold LB3 lysis buffer (10 mM Tris-HCl, pH 7.5, 100 mM NaCl, 1 mM EDTA, 0.5 mM EGTA, 0.1% sodium deoxycholate, 0.5% N-lauroylsarcosine, protease inhibitor cocktail,

and 1mM sodium butyrate). For transcription factor ChIP-seq, cells were resuspended in cold RIPA-NR1 lysis buffer (20 mM Tris-HCl, pH 7.5, 150 mM NaCl, 1 mM EDTA, 0.5 mM EGTA, 0.4% sodium deoxycholate, 0.1% SDS, 1% NP40, 1x protease inhibitor cocktail, 1 mM PMSF). Chromatin was sheared by sonication with a PIXUL Multi-Sample Sonicator (Active Motif) for 36 minutes for H3K27ac ChIP and 72 minutes for transcription factor ChIP. 10% Triton X-100 was added to each lysate to 1% final concentration. Samples were centrifugated at 20,000 g for 10 minutes at 4 °C and supernatant collected. The supernatant for each sample was brough up to 200 µl with LB3 buffer (H3K27ac ChIP) or RIPA-NR1 buffer (transcription factor ChIP). One percent of each lysate was kept as input and did not undergo chromatin immunoprecipitation.

For H3K27ac immunoprecipitation, 30 µl of Dynabeads protein A (Thermo Fisher Scientific) were bound to antibodies to H3K27ac (2 µg Active Motif 39133) and combined with diluted lysate of ~500,000 sonicated cells and rotated overnight at 4 °C. Beads were washed three times with wash buffer I (20 mM Tris-HCl, pH 7.5, 150 mM NaCl, 1% Triton X-100, 0.1% SDS, 2 mM EDTA, 1x protease inhibitor cocktail), wash buffer III (10 mM Tris-HCl, pH 7.4, 250 mM LiCl, 1% Triton X-100, 0.7% sodium deoxycholate, 1 mM EDTA, 1x protease inhibitor cocktail) and twice with TET (10 mM Tris-HCl, pH 7.5, 1 mM EDTA, 0.2% Tween-20, 1x protease inhibitor cocktail).

For transcription factor immunoprecipitation, 30 µl of Dynabeads protein A/G (Thermo Fisher Scientific) were bound to antibodies to ATF3 (2 µg Cell Signaling D2Y5W, 1 µg Invitrogen PA5-36244), MITF (1.5 µg Active Motif 91202), TFEB (1.5 µg Abcam ab2636, 9 µg Cell Signaling D2O7D), TFE3 (0.6 µg Abcam ab93808, 3 µl Abcam ab196681), and TFEC(1.65 µg Abcam ab185226, 1 µg Abcam ab115569) and

combined with diluted lysate of ~1x10^6 cells and rotated overnight at 4 °C. Beads were then washed three times with RIPA-NR1 lysis buffer (20 mM Tris-HCl, pH 7.5, 150 mM NaCl, 1 mM EDTA, 0.5 mM EGTA, 0.4% sodium deoxycholate, 0.1% SDS, 1% NP40, 1x protease inhibitor cocktail, 1 mM PMSF), six times with LiCl-NR1 buffer (10 mM Tris-HCl, pH 7.5, 250 mM LiCl, 1 mM EDTA, 0.7% sodium deoxycholate, 1% NP-40 alternative, 1x protease inhibitor cocktail, 1 mM PMSF), three times with TET (10 mM Tris-HCl, pH 7.5, 1 mM EDTA, 0.2% Tween-20, protease inhibitor cocktail, 1 mM PMSF), and one time with IDTE (10 mM Tris-HCl, pH 80, 1 mM EDTA, 0.2% Tween-20, 1x protease inhibitor cocktail, 1 mM PMSF)

Bead complexes were resuspended in 25 µl TT (10 mM Tris-HCl, pH 8.0, 0.05% Tween-20, 1x protease inhibitor cocktail). Sequencing libraries were prepared using NEBNext Ultra II Library preparation kit (New England Biolabs) according to manufacturer's instructions. Libraries were eluted from the beads and crosslinking reversed by adding 20 µl of nuclease-free water, 4 µl 10% SDS, 4.5 µl 5 M NaCl, 3 µl 0.5 M EDTA, and 1 µl 20 mg/ml proteinase K (New England Biolabs) to the 46.5 µl NEBNext reaction. Samples were incubated at 55 °C for an hour, followed by 65 °C for 30 minutes. A magnet was used to remove Dynabeads from libraries. 2 µl of SpeedBeads 3 EDAC in 61 µl 20% PEG 8000/1.5 M NaCL were added to wash libraries and incubated for 10 minutes. SpeadBeads were then washed twice with 200 µl 80% ethanol for 1 minute each. After each wash, beads were collected with a magnet and ethanol removed. After the second wash, beads were air-dried and DNA eluted in 25 µl elution buffer (10 mM Tris-HCl, pH 8.0, 0.05% Tween-20). Libraries were amplified by PCR for 14 cycles using NEBNext Ultra II PCR master mix (New England Biolabs) and

Solexa 1GA and Solexa 1GB primers. Libraries were cleaned again with SpeedBeads using 36.5 µl 20% PEG 8000/1.5 M NaCl and 2 µl SpeedBeads. Ethanol washind and drying was repeated, the libraries eluted using 20 µl elution buffer. Next, libraries were size selected at 225-500 bp with gel extraction from 10% TBE acrylamide gels. Libraries were sequenced using either a NextSeq 500 or a NovaSeq 6000 sequencer (Illumina).

RNA-seq analysis

FASTQ files were mapped to the mouse mm10 genome using STAR (144). HOMER was used to create tag directories from aligned reads for analysis (76). Gene expression was calculated using HOMER by counting all strand-specific reads within exons. Reads were normalized to transcripts per million (TPM). Differential gene expression was assessed using DESeq2, using cutoffs for false discovery rate (FDR) of 0.05 or less and a fold-change of at least 1.5 (145).

ATAC-seq analysis

FASTQ files were mapped to the mouse mm10 genome using Bowtie2 (146). Peak-calling was carried out with HOMER (findPeaks) using parameters “-style factor -minDist 200 -size 200” (76). Peaks which contained at least 4 tags in one sample were used to identify differentially bound peaks by using DESeq2 (145).

ChIP-seq analysis

FASTQ files were mapped to the mouse genome with Bowtie2 (146). For H3K27ac ChIP-seq, ATAC-seq peaks were merged with the “mergePeaks” function in HOMER to create a file with all accessible enhancers in ER-HoxB8 cells. This peak file was used to identify binding of H3K27ac within a 1000 base pair region of an enhancers centered by the ATAC-seq peak. The HOMER function “findPeaks” was used with

parameters “-style -histone” to identify enhancers with H3K27 acetylation (76). Peaks which contained at least 16 counts in at least one sample were used to identify differentially acetylated enhancers with DESeq2 (145).

For transcription factor ChIP, DESeq2 was used to identify differentially bound areas of chromatin. Only peaks which contained at least 4 tag counts in one sample were used to identify differentially bound peaks.

Motif enrichment

The motif analysis function of HOMER (findMotifsGenome.pl) was used to identify motifs enriched in peak regions over background (76). The background sequences were either random genomic sequences or derived from a specific set of enhancers in the data set (e.g., with unchanged H3K27 acetylation between two conditions), as indicated in the text and figure legends.

Data Visualization

The UCSC genome browser was used to generate tracks indicating accessible enhancers in ATAC-seq or immunoprecipitated DNA in ChIP-seq (147). Prism (GraphPad, San Diego, CA), R, or Python were used create plots and graphs, and for statistical analysis. Figures 1, 16, and 17 were created using BioRender (BioRender.com).

Table 3: The guide RNA sequences used for CRISPR gene editing in this study.

Target	**gRNA sequence**
Intergenic enhancer of *Trem2*	1: ACATCCTGGCGAGAGTTAGA 2: ATGGTCACGCTAACCCAGAG
AP-1/ATF3 motif of the intergenic enhancer	GACTAGACTGGGCTAGATTT
TREM2	AACCTCCAAGCCGGTGACGC
TFEB	CAGCCCGATGCGTGACGCCA
ATF3	GGCGGTCGCACTGACTTCTG
Control gRNA	GCACTACCAGAGCTAACTCA

Acknowledgements:

Chapter 3 is coauthored with Nathanael Spann, Yohei Abe, Johannes Schlachetzki, Mohnish Alishala, Sydney O'Brien, Mashito Sakai, and Christopher Glass. The dissertation author was the primary author of this chapter.

CHAPTER 4: CONCLUSIONS AND FUTURE DIRECTIONS

TREM2 has recently been identified as a key regulator in multiple disease processes. First, it was identified as protective in Alzheimer's Disease in animal models and in humans by a genome-wide association study that found a missense variant of TREM2 that strongly associated with the development of Alzheimer's Disease (94-96). Additionally, it has been found to play a protective role in an animal model of metabolic syndrome and a detrimental role in cancer through immunosuppressive effects (95, 96). While it is highly expressed in Kupffer cells during NASH, the net effect of TREM2 is to date still undetermined (30, 87). Many open questions remained in regard to TREM2 signaling, especially how it is upregulated during times of tissue injury and how it exerts its effects on gene expression.

We addressed multiple open questions related to TREM2 in this study. First, with myocardial infarction, we identified a novel disease model where TREM2 is present and TREM2 itself or pathways upstream or downstream of TREM2 could potentially be used as therapeutic targets (Figure 16). Interestingly, treatment with a TREM2-activating antibody did not show an effect in an ischemia/reperfusion model. This may have multiple reasons as outlined in the discussion of chapter 2 but shows that it may be difficult to further activate TREM2 in certain *in vivo* settings. Future studies will need to address the functional effect deletion of TREM2 has in macrophages regarding gene expression, transcriptional regulation, and the effect this in turn has on cardiomyocyte function. Additionally, deletion or activation of transcription factors downstream of TREM2 should be tested in myocardial infarction models to test their role in modifying macrophage function and functional outcomes *in vivo*.

Second, we addressed the question on how the cell upregulates *Trem2* expression, as observed mostly during tissue injury or when macrophages are cultured in tissue culture (Figure 17). As the intergenic enhancer is accessible in our datasets only during high expression of *Trem2*, we expected this enhancer to be required for it. Surprisingly, in a cultured macrophage model *Trem2* was still highly expressed after deletion of the enhancer. This narrows down the regulation to either redundancy with the intronic enhancer (accessibility of one can compensate for the loss of the other) or that the intronic enhancer is the main regulator of *Trem2* expression. Future studies can add a deletion of the intronic enhancer to the cell line generated in this study and at the same time generate single deletions of the intronic enhancer to test which gene regulatory regions are most important for high expression of *Trem2*. Additionally, ER-HoxB8 cells could be generated from a TREM2 reporter mouse followed by a CRISPR screen to identify transcription factors or signaling pathways upstream of TREM2.

Third, while cells depending on TREM2 signaling have been identified through their gene expression by single-cell RNA-seq, little had been known about how TREM2 alters gene expression on a molecular level. In this study, we first identified enhancers that are more active (i.e., have increased H3K27 acetylation) when TREM2 is present. In these we found the motifs of MITF/TFE, AP-1, and MEF2 families enriched. We saw increased binding of most MITF/TFE family members and ATF3 (a member of the AP-1 family) in these enhancers with TREM2 present, suggesting that their binding to these enhancers is increased by TREM2. Interestingly, TFEC was an exception and showed decreased binding to these enhancers, pointing towards differing function and gene regulation by TFEC and the remaining MITF/TFE family in macrophages. Interestingly,

many TFEB peaks were lost in the TREM2 KO cells and many TFEC peaks were gained, suggesting opposing regulation by TREM2 signaling. Additionally, enhancer activation (by H3K27ac) was decreased in the lost TFEB peaks but also decreased in the gained TFEC peaks, indicating that TFEB binding is associated with enhancer activation and TFEC binding with enhancer repression in this context. Further gain and loss of function studies of these factor will be necessary to further elucidate the apparently diametral effects. Deletion of TFEB led to suppression of DAM/LAM/KC-N genes that are also increased when TREM2 is present, adding further evidence to the role of MITF/TFE factors mediating effects of TREM2 (Figure 17). Future studies may now address perturbations or double/triple knockout of family transcription factors in these cells to test redundancy, especially in the case of ATF3, where deletion showed minimal effects on gene expression. Additionally, inhibition/deletion or activation/overexpression of these factors can be tested in disease models to test whether they could play a role as therapeutic targets.

In summary, through the projects described we have identified an important role of TREM2 in an additional disease model and tested how expression of *Trem2* is regulated and how TREM2 itself regulates gene expression. This lays the foundation for multiple future in vitro and *in vivo* studies with the eventual future goal to modulate TREM2 signaling in macrophages as a therapy in disease processes. These diseases may include neurodegenerative disorders, myocardial infarction, metabolic syndrome, and cancer, as TREM2 has been shown to play a key role in the phenotype of these disease models.

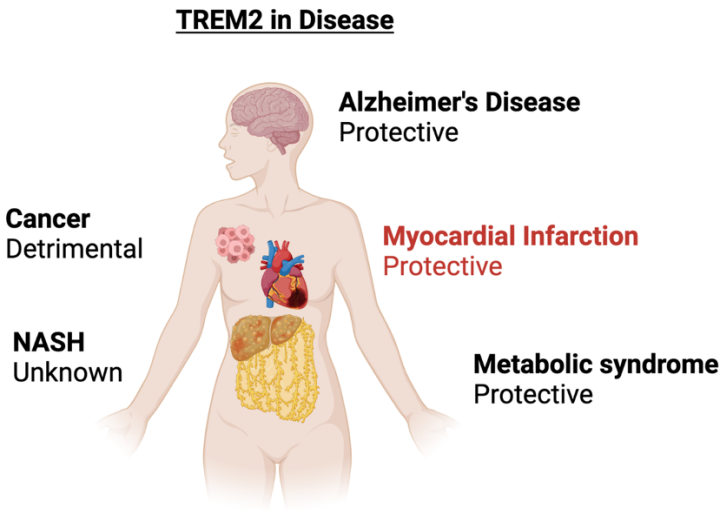

Figure 16: Disease models in which TREM2 is expressed and plays a role based on animal models or genome-wide association studies.
TREM2 has been identified as protective in Alzheimer's Disease by animal models and a genome-wide associate in humans. Additionally, it is protective in metabolic syndrome and detrimental in cancer. In this study, we identified its expression and a protective effect in a myocardial infarction model.

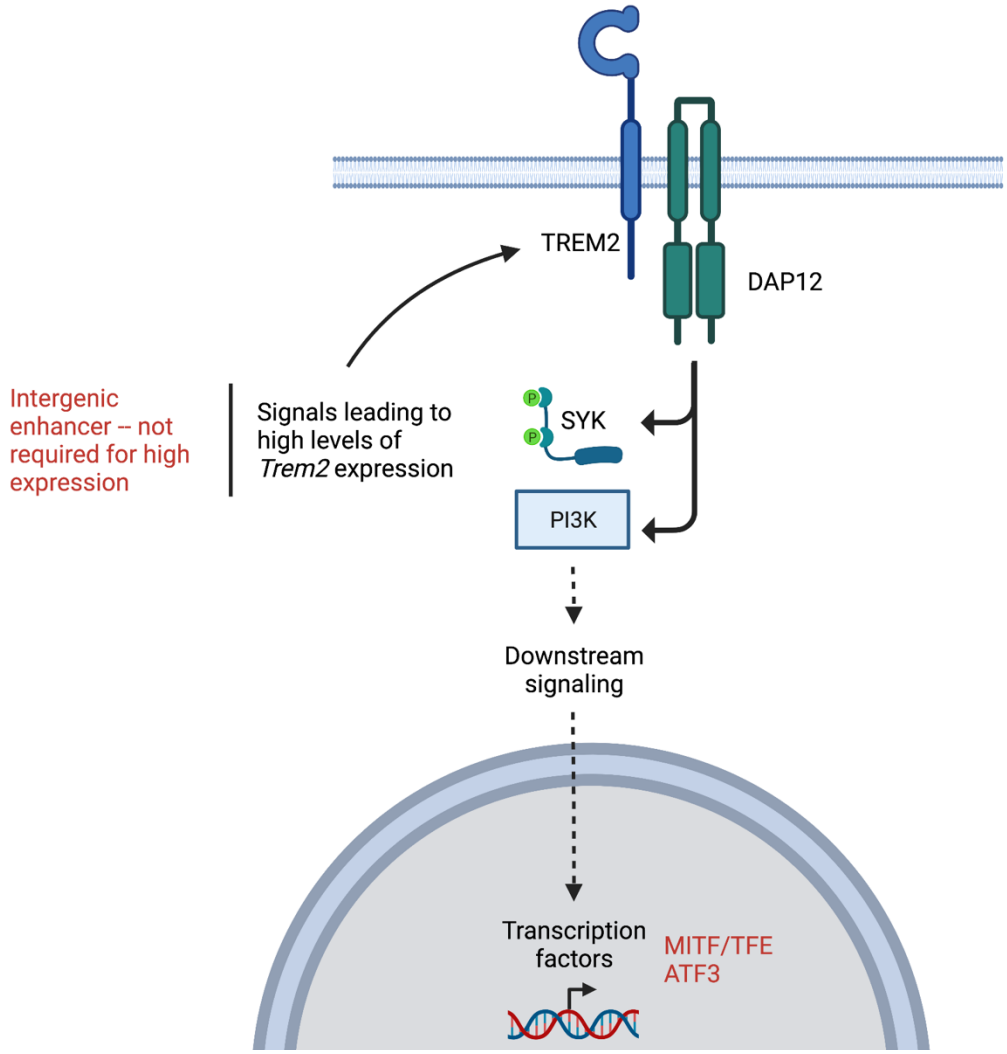

Figure 17: TREM2 signaling pathway with additional information identified in this study
Two important questions related to TREM2 signaling are how it is upregulated and how it mediates its effects on gene expression. In this study, we added evidence to these two questions. First, we discovered that the intergenic enhancer is not solely responsible or required for high expression of *Trem2* in a cultured macrophage model. Second, we identified the transcription factor family MITF/TFE family of transcription factors as well as the transcription factor ATF3 to be downstream of TREM2 by carrying out RNA-seq, ATAC-seq, ChIP-seq for H3K27ac, and ChIP-seq for transcription factors. Adapted from Dezykowska, Weiner, and Amit, *Cell* 2020 (80).

REFERENCES

1. Metchnikoff E. Untersuchungen über die mesodermalen Phagocyten einiger Wirbeltiere. Biol Zentralbl. 1883;3:560.

2. Ginhoux F, Guilliams M. Tissue-Resident Macrophage Ontogeny and Homeostasis. Immunity. 2016;44(3):439-49. Epub 2016/03/18. doi: 10.1016/j.immuni.2016.02.024. PubMed PMID: 26982352.

3. van Furth R, Cohn ZA. The origin and kinetics of mononuclear phagocytes. The Journal of experimental medicine. 1968;128(3):415-35. Epub 1968/09/01. doi: 10.1084/jem.128.3.415. PubMed PMID: 5666958; PMCID: PMC2138527.

4. Ginhoux F, Greter M, Leboeuf M, Nandi S, See P, Gokhan S, Mehler MF, Conway SJ, Ng LG, Stanley ER, Samokhvalov IM, Merad M. Fate mapping analysis reveals that adult microglia derive from primitive macrophages. Science. 2010;330(6005):841-5. Epub 2010/10/23. doi: 10.1126/science.1194637. PubMed PMID: 20966214; PMCID: PMC3719181.

5. Samokhvalov IM, Samokhvalova NI, Nishikawa S. Cell tracing shows the contribution of the yolk sac to adult haematopoiesis. Nature. 2007;446(7139):1056-61. Epub 2007/03/23. doi: 10.1038/nature05725. PubMed PMID: 17377529.

6. Schulz C, Gomez Perdiguero E, Chorro L, Szabo-Rogers H, Cagnard N, Kierdorf K, Prinz M, Wu B, Jacobsen SE, Pollard JW, Frampton J, Liu KJ, Geissmann F. A lineage of myeloid cells independent of Myb and hematopoietic stem cells. Science. 2012;336(6077):86-90. Epub 2012/03/24. doi: 10.1126/science.1219179. PubMed PMID: 22442384.

7. Gomez Perdiguero E, Klapproth K, Schulz C, Busch K, Azzoni E, Crozet L, Garner H, Trouillet C, de Bruijn MF, Geissmann F, Rodewald HR. Tissue-resident macrophages originate from yolk-sac-derived erythro-myeloid progenitors. Nature. 2015;518(7540):547-51. Epub 2014/12/04. doi: 10.1038/nature13989. PubMed PMID: 25470051; PMCID: PMC5997177.

8. McGrath KE, Frame JM, Fegan KH, Bowen JR, Conway SJ, Catherman SC, Kingsley PD, Koniski AD, Palis J. Distinct Sources of Hematopoietic Progenitors Emerge before HSCs and Provide Functional Blood Cells in the Mammalian Embryo. Cell reports. 2015;11(12):1892-904. Epub 2015/06/23. doi: 10.1016/j.celrep.2015.05.036. PubMed PMID: 26095363; PMCID: PMC4490098.

9. Epelman S, Lavine KJ, Beaudin AE, Sojka DK, Carrero JA, Calderon B, Brija T, Gautier EL, Ivanov S, Satpathy AT, Schilling JD, Schwendener R, Sergin I, Razani B, Forsberg EC, Yokoyama WM, Unanue ER, Colonna M, Randolph GJ, Mann DL.

Embryonic and adult-derived resident cardiac macrophages are maintained through distinct mechanisms at steady state and during inflammation. Immunity. 2014;40(1):91-104. Epub 2014/01/21. doi: 10.1016/j.immuni.2013.11.019. PubMed PMID: 24439267; PMCID: PMC3923301.

10. Zhao Y, Zou W, Du J, Zhao Y. The origins and homeostasis of monocytes and tissue-resident macrophages in physiological situation. J Cell Physiol. 2018;233(10):6425-39. Epub 2018/01/13. doi: 10.1002/jcp.26461. PubMed PMID: 29323706.

11. Brown MS, Goldstein JL. Lipoprotein metabolism in the macrophage: implications for cholesterol deposition in atherosclerosis. Annual review of biochemistry. 1983;52:223-61. Epub 1983/01/01. doi: 10.1146/annurev.bi.52.070183.001255. PubMed PMID: 6311077.

12. Suzuki H, Kurihara Y, Takeya M, Kamada N, Kataoka M, Jishage K, Ueda O, Sakaguchi H, Higashi T, Suzuki T, Takashima Y, Kawabe Y, Cynshi O, Wada Y, Honda M, Kurihara H, Aburatani H, Doi T, Matsumoto A, Azuma S, Noda T, Toyoda Y, Itakura H, Yazaki Y, Kodama T, et al. A role for macrophage scavenger receptors in atherosclerosis and susceptibility to infection. Nature. 1997;386(6622):292-6. Epub 1997/03/20. doi: 10.1038/386292a0. PubMed PMID: 9069289.

13. Mills CD. M1 and M2 Macrophages: Oracles of Health and Disease. Critical reviews in immunology. 2012;32(6):463-88. Epub 2013/02/23. doi: 10.1615/critrevimmunol.v32.i6.10. PubMed PMID: 23428224.

14. Nahrendorf M, Swirski FK. Abandoning M1/M2 for a Network Model of Macrophage Function. Circulation research. 2016;119(3):414-7. Epub 2016/07/28. doi: 10.1161/CIRCRESAHA.116.309194. PubMed PMID: 27458196; PMCID: PMC4965179.

15. Chavez-Galan L, Olleros ML, Vesin D, Garcia I. Much More than M1 and M2 Macrophages, There are also CD169(+) and TCR(+) Macrophages. Frontiers in immunology. 2015;6:263. Epub 2015/06/16. doi: 10.3389/fimmu.2015.00263. PubMed PMID: 26074923; PMCID: PMC4443739.

16. Cai B, Dongiovanni P, Corey KE, Wang X, Shmarakov IO, Zheng Z, Kasikara C, Davra V, Meroni M, Chung RT, Rothlin CV, Schwabe RF, Blaner WS, Birge RB, Valenti L, Tabas I. Macrophage MerTK Promotes Liver Fibrosis in Nonalcoholic Steatohepatitis. Cell metabolism. 2020;31(2):406-21 e7. Epub 2019/12/17. doi: 10.1016/j.cmet.2019.11.013. PubMed PMID: 31839486; PMCID: PMC7004886.

17. Keren-Shaul H, Spinrad A, Weiner A, Matcovitch-Natan O, Dvir-Szternfeld R, Ulland TK, David E, Baruch K, Lara-Astaiso D, Toth B, Itzkovitz S, Colonna M, Schwartz M, Amit I. A Unique Microglia Type Associated with Restricting Development of

Alzheimer's Disease. Cell. 2017;169(7):1276-90 e17. Epub 2017/06/13. doi: 10.1016/j.cell.2017.05.018. PubMed PMID: 28602351.

18. Vagnozzi RJ, Maillet M, Sargent MA, Khalil H, Johansen AKZ, Schwanekamp JA, York AJ, Huang V, Nahrendorf M, Sadayappan S, Molkentin JD. An acute immune response underlies the benefit of cardiac stem cell therapy. Nature. 2020;577(7790):405-9. Epub 2019/11/28. doi: 10.1038/s41586-019-1802-2. PubMed PMID: 31775156; PMCID: PMC6962570.

19. Hulsmans M, Clauss S, Xiao L, Aguirre AD, King KR, Hanley A, Hucker WJ, Wulfers EM, Seemann G, Courties G, Iwamoto Y, Sun Y, Savol AJ, Sager HB, Lavine KJ, Fishbein GA, Capen DE, Da Silva N, Miquerol L, Wakimoto H, Seidman CE, Seidman JG, Sadreyev RI, Naxerova K, Mitchell RN, Brown D, Libby P, Weissleder R, Swirski FK, Kohl P, Vinegoni C, Milan DJ, Ellinor PT, Nahrendorf M. Macrophages Facilitate Electrical Conduction in the Heart. Cell. 2017;169(3):510-22 e20. Epub 2017/04/22. doi: 10.1016/j.cell.2017.03.050. PubMed PMID: 28431249; PMCID: PMC5474950.

20. Mebius RE, Kraal G. Structure and function of the spleen. Nature Reviews Immunology. 2005;5(8):606-16. doi: 10.1038/nri1669. PubMed PMID: WOS:000230880900012.

21. Hoeffel G, Ginhoux F. Fetal monocytes and the origins of tissue-resident macrophages. Cell Immunol. 2018;330:5-15. Epub 2018/02/25. doi: 10.1016/j.cellimm.2018.01.001. PubMed PMID: 29475558.

22. Wolf AA, Yanez A, Barman PK, Goodridge HS. The Ontogeny of Monocyte Subsets. Frontiers in immunology. 2019;10:1642. Epub 2019/08/06. doi: 10.3389/fimmu.2019.01642. PubMed PMID: 31379841; PMCID: PMC6650567.

23. Hoeffel G, Wang Y, Greter M, See P, Teo P, Malleret B, Leboeuf M, Low D, Oller G, Almeida F, Choy SH, Grisotto M, Renia L, Conway SJ, Stanley ER, Chan JK, Ng LG, Samokhvalov IM, Merad M, Ginhoux F. Adult Langerhans cells derive predominantly from embryonic fetal liver monocytes with a minor contribution of yolk sac-derived macrophages. The Journal of experimental medicine. 2012;209(6):1167-81. Epub 2012/05/09. doi: 10.1084/jem.20120340. PubMed PMID: 22565823; PMCID: PMC3371735.

24. Teh YC, Ding JL, Ng LG, Chong SZ. Capturing the Fantastic Voyage of Monocytes Through Time and Space. Frontiers in immunology. 2019;10:834. Epub 2019/05/02. doi: 10.3389/fimmu.2019.00834. PubMed PMID: 31040854; PMCID: PMC6476989.

25. Mogensen TH. Pathogen recognition and inflammatory signaling in innate immune defenses. Clin Microbiol Rev. 2009;22(2):240-73, Table of Contents. Epub 2009/04/16. doi: 10.1128/CMR.00046-08. PubMed PMID: 19366914; PMCID: PMC2668232.

26. Kumar H, Kawai T, Akira S. Pathogen recognition by the innate immune system. Int Rev Immunol. 2011;30(1):16-34. Epub 2011/01/18. doi: 10.3109/08830185.2010.529976. PubMed PMID: 21235323.

27. Miller YI, Choi SH, Wiesner P, Fang L, Harkewicz R, Hartvigsen K, Boullier A, Gonen A, Diehl CJ, Que X, Montano E, Shaw PX, Tsimikas S, Binder CJ, Witztum JL. Oxidation-specific epitopes are danger-associated molecular patterns recognized by pattern recognition receptors of innate immunity. Circulation research. 2011;108(2):235-48. doi: 10.1161/CIRCRESAHA.110.223875. PubMed PMID: 21252151; PMCID: PMC3075542.

28. Tang D, Kang R, Coyne CB, Zeh HJ, Lotze MT. PAMPs and DAMPs: signal 0s that spur autophagy and immunity. Immunological reviews. 2012;249(1):158-75. Epub 2012/08/15. doi: 10.1111/j.1600-065X.2012.01146.x. PubMed PMID: 22889221; PMCID: PMC3662247.

29. Rock KL, Kono H. The inflammatory response to cell death. Annu Rev Pathol. 2008;3:99-126. Epub 2007/11/28. doi: 10.1146/annurev.pathmechdis.3.121806.151456. PubMed PMID: 18039143; PMCID: PMC3094097.

30. Seidman JS, Troutman TD, Sakai M, Gola A, Spann NJ, Bennett H, Bruni CM, Ouyang Z, Li RZ, Sun X, Vu BT, Pasillas MP, Ego KM, Gosselin D, Link VM, Chong LW, Evans RM, Thompson BM, McDonald JG, Hosseini M, Witztum JL, Germain RN, Glass CK. Niche-Specific Reprogramming of Epigenetic Landscapes Drives Myeloid Cell Diversity in Nonalcoholic Steatohepatitis. Immunity. 2020;52(6):1057-74 e7. Epub 2020/05/05. doi: 10.1016/j.immuni.2020.04.001. PubMed PMID: 32362324; PMCID: PMC7305990.

31. Nahrendorf M, Swirski FK, Aikawa E, Stangenberg L, Wurdinger T, Figueiredo JL, Libby P, Weissleder R, Pittet MJ. The healing myocardium sequentially mobilizes two monocyte subsets with divergent and complementary functions. The Journal of experimental medicine. 2007;204(12):3037-47. Epub 2007/11/21. doi: 10.1084/jem.20070885. PubMed PMID: 18025128; PMCID: PMC2118517.

32. Cooke JP. Inflammation and Its Role in Regeneration and Repair. Circulation research. 2019;124(8):1166-8. Epub 2019/04/12. doi: 10.1161/CIRCRESAHA.118.314669. PubMed PMID: 30973815; PMCID: PMC6578588.

33. Wynn TA, Vannella KM. Macrophages in Tissue Repair, Regeneration, and Fibrosis. Immunity. 2016;44(3):450-62. Epub 2016/03/18. doi: 10.1016/j.immuni.2016.02.015. PubMed PMID: 26982353; PMCID: PMC4794754.

34. Mack M. Inflammation and fibrosis. Matrix Biol. 2018;68-69:106-21. Epub 2017/12/03. doi: 10.1016/j.matbio.2017.11.010. PubMed PMID: 29196207.

35. Chimenti I, Sattler S, Del Monte-Nieto G, Forte E. Editorial: Fibrosis and Inflammation in Tissue Pathophysiology. Front Physiol. 2021;12:830683. Epub 2022/02/08. doi: 10.3389/fphys.2021.830683. PubMed PMID: 35126187; PMCID: PMC8814660.

36. Shi C, Pamer EG. Monocyte recruitment during infection and inflammation. Nature reviews Immunology. 2011;11(11):762-74. Epub 2011/10/11. doi: 10.1038/nri3070. PubMed PMID: 21984070; PMCID: PMC3947780.

37. Janeway CA, Jr., Medzhitov R. Innate immune recognition. Annual review of immunology. 2002;20:197-216. Epub 2002/02/28. doi: 10.1146/annurev.immunol.20.083001.084359. PubMed PMID: 11861602.

38. Oliveira-Nascimento L, Massari P, Wetzler LM. The Role of TLR2 in Infection and Immunity. Frontiers in immunology. 2012;3:79. Epub 2012/05/09. doi: 10.3389/fimmu.2012.00079. PubMed PMID: 22566960; PMCID: PMC3342043.

39. Duffield JS, Forbes SJ, Constandinou CM, Clay S, Partolina M, Vuthoori S, Wu S, Lang R, Iredale JP. Selective depletion of macrophages reveals distinct, opposing roles during liver injury and repair. The Journal of clinical investigation. 2005;115(1):56-65. Epub 2005/01/05. doi: 10.1172/JCI22675. PubMed PMID: 15630444; PMCID: PMC539199.

40. Chujo S, Shirasaki F, Kondo-Miyazaki M, Ikawa Y, Takehara K. Role of connective tissue growth factor and its interaction with basic fibroblast growth factor and macrophage chemoattractant protein-1 in skin fibrosis. J Cell Physiol. 2009;220(1):189-95. Epub 2009/03/12. doi: 10.1002/jcp.21750. PubMed PMID: 19277979.

41. Shimokado K, Raines EW, Madtes DK, Barrett TB, Benditt EP, Ross R. A significant part of macrophage-derived growth factor consists of at least two forms of PDGF. Cell. 1985;43(1):277-86. Epub 1985/11/01. doi: 10.1016/0092-8674(85)90033-9. PubMed PMID: 2416458.

42. Oishi Y, Manabe I. Macrophages in inflammation, repair and regeneration. International immunology. 2018;30(11):511-28. Epub 2018/08/31. doi: 10.1093/intimm/dxy054. PubMed PMID: 30165385.

43. Duewell P, Kono H, Rayner KJ, Sirois CM, Vladimer G, Bauernfeind FG, Abela GS, Franchi L, Nunez G, Schnurr M, Espevik T, Lien E, Fitzgerald KA, Rock KL, Moore KJ, Wright SD, Hornung V, Latz E. NLRP3 inflammasomes are required for atherogenesis and activated by cholesterol crystals. Nature. 2010;464(7293):1357-61. Epub 2010/04/30. doi: 10.1038/nature08938. PubMed PMID: 20428172; PMCID: PMC2946640.

44. Ridker PM, Everett BM, Thuren T, MacFadyen JG, Chang WH, Ballantyne C, Fonseca F, Nicolau J, Koenig W, Anker SD, Kastelein JJP, Cornel JH, Pais P, Pella D, Genest J, Cifkova R, Lorenzatti A, Forster T, Kobalava Z, Vida-Simiti L, Flather M, Shimokawa H, Ogawa H, Dellborg M, Rossi PRF, Troquay RPT, Libby P, Glynn RJ, Group CT. Antiinflammatory Therapy with Canakinumab for Atherosclerotic Disease. N Engl J Med. 2017;377(12):1119-31. Epub 2017/08/29. doi: 10.1056/NEJMoa1707914. PubMed PMID: 28845751.

45. Gortz B, Hayer S, Tuerck B, Zwerina J, Smolen JS, Schett G. Tumour necrosis factor activates the mitogen-activated protein kinases p38alpha and ERK in the synovial membrane in vivo. Arthritis Res Ther. 2005;7(5):R1140-7. Epub 2005/10/07. doi: 10.1186/ar1797. PubMed PMID: 16207331; PMCID: PMC1257441.

46. Weinblatt ME, Kremer JM, Bankhurst AD, Bulpitt KJ, Fleischmann RM, Fox RI, Jackson CG, Lange M, Burge DJ. A trial of etanercept, a recombinant tumor necrosis factor receptor:Fc fusion protein, in patients with rheumatoid arthritis receiving methotrexate. N Engl J Med. 1999;340(4):253-9. Epub 1999/01/28. doi: 10.1056/NEJM199901283400401. PubMed PMID: 9920948.

47. Bathon JM, Martin RW, Fleischmann RM, Tesser JR, Schiff MH, Keystone EC, Genovese MC, Wasko MC, Moreland LW, Weaver AL, Markenson J, Finck BK. A comparison of etanercept and methotrexate in patients with early rheumatoid arthritis. N Engl J Med. 2000;343(22):1586-93. Epub 2000/11/30. doi: 10.1056/NEJM200011303432201. PubMed PMID: 11096165.

48. Lipsky PE, van der Heijde DM, St Clair EW, Furst DE, Breedveld FC, Kalden JR, Smolen JS, Weisman M, Emery P, Feldmann M, Harriman GR, Maini RN, Anti-Tumor Necrosis Factor Trial in Rheumatoid Arthritis with Concomitant Therapy Study G. Infliximab and methotrexate in the treatment of rheumatoid arthritis. Anti-Tumor Necrosis Factor Trial in Rheumatoid Arthritis with Concomitant Therapy Study Group. N Engl J Med. 2000;343(22):1594-602. Epub 2000/11/30. doi: 10.1056/NEJM200011303432202. PubMed PMID: 11096166.

49. Investigators R-C, Gordon AC, Mouncey PR, Al-Beidh F, Rowan KM, Nichol AD, Arabi YM, Annane D, Beane A, van Bentum-Puijk W, Berry LR, Bhimani Z, Bonten MJM, Bradbury CA, Brunkhorst FM, Buzgau A, Cheng AC, Detry MA, Duffy EJ, Estcourt LJ, Fitzgerald M, Goossens H, Haniffa R, Higgins AM, Hills TE, Horvat CM, Lamontagne F, Lawler PR, Leavis HL, Linstrum KM, Litton E, Lorenzi E, Marshall JC,

Mayr FB, McAuley DF, McGlothlin A, McGuinness SP, McVerry BJ, Montgomery SK, Morpeth SC, Murthy S, Orr K, Parke RL, Parker JC, Patanwala AE, Pettila V, Rademaker E, Santos MS, Saunders CT, Seymour CW, Shankar-Hari M, Sligl WI, Turgeon AF, Turner AM, van de Veerdonk FL, Zarychanski R, Green C, Lewis RJ, Angus DC, McArthur CJ, Berry S, Webb SA, Derde LPG. Interleukin-6 Receptor Antagonists in Critically Ill Patients with Covid-19. N Engl J Med. 2021;384(16):1491-502. Epub 2021/02/26. doi: 10.1056/NEJMoa2100433. PubMed PMID: 33631065; PMCID: PMC7953461.

50. Pozzi LA, Maciaszek JW, Rock KL. Both dendritic cells and macrophages can stimulate naive CD8 T cells in vivo to proliferate, develop effector function, and differentiate into memory cells. Journal of immunology. 2005;175(4):2071-81. Epub 2005/08/06. doi: 10.4049/jimmunol.175.4.2071. PubMed PMID: 16081773.

51. Guerriero JL. Macrophages: Their Untold Story in T Cell Activation and Function. Int Rev Cell Mol Biol. 2019;342:73-93. Epub 2019/01/13. doi: 10.1016/bs.ircmb.2018.07.001. PubMed PMID: 30635094.

52. Tay TL, Mai D, Dautzenberg J, Fernandez-Klett F, Lin G, Sagar, Datta M, Drougard A, Stempfl T, Ardura-Fabregat A, Staszewski O, Margineanu A, Sporbert A, Steinmetz LM, Pospisilik JA, Jung S, Priller J, Grun D, Ronneberger O, Prinz M. A new fate mapping system reveals context-dependent random or clonal expansion of microglia. Nat Neurosci. 2017;20(6):793-803. Epub 2017/04/18. doi: 10.1038/nn.4547. PubMed PMID: 28414331.

53. Watanabe S, Alexander M, Misharin AV, Budinger GRS. The role of macrophages in the resolution of inflammation. The Journal of clinical investigation. 2019;129(7):2619-28. Epub 2019/05/21. doi: 10.1172/JCI124615. PubMed PMID: 31107246; PMCID: PMC6597225.

54. Boulter L, Govaere O, Bird TG, Radulescu S, Ramachandran P, Pellicoro A, Ridgway RA, Seo SS, Spee B, Van Rooijen N, Sansom OJ, Iredale JP, Lowell S, Roskams T, Forbes SJ. Macrophage-derived Wnt opposes Notch signaling to specify hepatic progenitor cell fate in chronic liver disease. Nature medicine. 2012;18(4):572-9. Epub 2012/03/06. doi: 10.1038/nm.2667. PubMed PMID: 22388089; PMCID: PMC3364717.

55. Tonkin J, Temmerman L, Sampson RD, Gallego-Colon E, Barberi L, Bilbao D, Schneider MD, Musaro A, Rosenthal N. Monocyte/Macrophage-derived IGF-1 Orchestrates Murine Skeletal Muscle Regeneration and Modulates Autocrine Polarization. Mol Ther. 2015;23(7):1189-200. Epub 2015/04/22. doi: 10.1038/mt.2015.66. PubMed PMID: 25896247; PMCID: PMC4817788.

56. Kaviratne M, Hesse M, Leusink M, Cheever AW, Davies SJ, McKerrow JH, Wakefield LM, Letterio JJ, Wynn TA. IL-13 activates a mechanism of tissue fibrosis that is completely TGF-beta independent. Journal of immunology. 2004;173(6):4020-9. Epub 2004/09/10. doi: 10.4049/jimmunol.173.6.4020. PubMed PMID: 15356151.

57. Wynn TA, Barron L. Macrophages: master regulators of inflammation and fibrosis. Semin Liver Dis. 2010;30(3):245-57. Epub 2010/07/29. doi: 10.1055/s-0030-1255354. PubMed PMID: 20665377; PMCID: PMC2924662.

58. Gibbons MA, MacKinnon AC, Ramachandran P, Dhaliwal K, Duffin R, Phythian-Adams AT, van Rooijen N, Haslett C, Howie SE, Simpson AJ, Hirani N, Gauldie J, Iredale JP, Sethi T, Forbes SJ. Ly6Chi monocytes direct alternatively activated profibrotic macrophage regulation of lung fibrosis. Am J Respir Crit Care Med. 2011;184(5):569-81. Epub 2011/06/18. doi: 10.1164/rccm.201010-1719OC. PubMed PMID: 21680953.

59. Pradere JP, Kluwe J, De Minicis S, Jiao JJ, Gwak GY, Dapito DH, Jang MK, Guenther ND, Mederacke I, Friedman R, Dragomir AC, Aloman C, Schwabe RF. Hepatic macrophages but not dendritic cells contribute to liver fibrosis by promoting the survival of activated hepatic stellate cells in mice. Hepatology. 2013;58(4):1461-73. Epub 2013/04/05. doi: 10.1002/hep.26429. PubMed PMID: 23553591; PMCID: PMC3848418.

60. Madala SK, Pesce JT, Ramalingam TR, Wilson MS, Minnicozzi S, Cheever AW, Thompson RW, Mentink-Kane MM, Wynn TA. Matrix metalloproteinase 12-deficiency augments extracellular matrix degrading metalloproteinases and attenuates IL-13-dependent fibrosis. Journal of immunology. 2010;184(7):3955-63. Epub 2010/02/26. doi: 10.4049/jimmunol.0903008. PubMed PMID: 20181883; PMCID: PMC3175622.

61. Masuda T, Sankowski R, Staszewski O, Bottcher C, Amann L, Sagar, Scheiwe C, Nessler S, Kunz P, van Loo G, Coenen VA, Reinacher PC, Michel A, Sure U, Gold R, Grun D, Priller J, Stadelmann C, Prinz M. Spatial and temporal heterogeneity of mouse and human microglia at single-cell resolution. Nature. 2019;566(7744):388-92. Epub 2019/02/15. doi: 10.1038/s41586-019-0924-x. PubMed PMID: 30760929.

62. Ramachandran P, Dobie R, Wilson-Kanamori JR, Dora EF, Henderson BEP, Luu NT, Portman JR, Matchett KP, Brice M, Marwick JA, Taylor RS, Efremova M, Vento-Tormo R, Carragher NO, Kendall TJ, Fallowfield JA, Harrison EM, Mole DJ, Wigmore SJ, Newsome PN, Weston CJ, Iredale JP, Tacke F, Pollard JW, Ponting CP, Marioni JC, Teichmann SA, Henderson NC. Resolving the fibrotic niche of human liver cirrhosis at single-cell level. Nature. 2019;575(7783):512-8. Epub 2019/10/10. doi: 10.1038/s41586-019-1631-3. PubMed PMID: 31597160; PMCID: PMC6876711.

63. Sajti E, Link VM, Ouyang Z, Spann NJ, Westin E, Romanoski CE, Fonseca GJ, Prince LS, Glass CK. Transcriptomic and epigenetic mechanisms underlying myeloid diversity in the lung. Nat Immunol. 2020;21(2):221-31. Epub 2020/01/22. doi: 10.1038/s41590-019-0582-z. PubMed PMID: 31959980; PMCID: PMC7667722.

64. Becher B, Schlitzer A, Chen J, Mair F, Sumatoh HR, Teng KW, Low D, Ruedl C, Riccardi-Castagnoli P, Poidinger M, Greter M, Ginhoux F, Newell EW. High-dimensional analysis of the murine myeloid cell system. Nat Immunol. 2014;15(12):1181-9. Epub 2014/10/13. doi: 10.1038/ni.3006. PubMed PMID: 25306126.

65. Sakai M, Troutman TD, Seidman JS, Ouyang Z, Spann NJ, Abe Y, Ego KM, Bruni CM, Deng Z, Schlachetzki JCM, Nott A, Bennett H, Chang J, Vu BT, Pasillas MP, Link VM, Texari L, Heinz S, Thompson BM, McDonald JG, Geissmann F, Glass CK. Liver-Derived Signals Sequentially Reprogram Myeloid Enhancers to Initiate and Maintain Kupffer Cell Identity. Immunity. 2019;51(4):655-70 e8. Epub 2019/10/08. doi: 10.1016/j.immuni.2019.09.002. PubMed PMID: 31587991; PMCID: PMC6800814.

66. Heinz S, Romanoski CE, Benner C, Glass CK. The selection and function of cell type-specific enhancers. Nat Rev Mol Cell Biol. 2015;16(3):144-54. Epub 2015/02/05. doi: 10.1038/nrm3949. PubMed PMID: 25650801; PMCID: PMC4517609.

67. Troutman TD, Kofman E, Glass CK. Exploiting dynamic enhancer landscapes to decode macrophage and microglia phenotypes in health and disease. Molecular cell. 2021;81(19):3888-903. Epub 2021/09/01. doi: 10.1016/j.molcel.2021.08.004. PubMed PMID: 34464593; PMCID: PMC8500948.

68. Creyghton MP, Cheng AW, Welstead GG, Kooistra T, Carey BW, Steine EJ, Hanna J, Lodato MA, Frampton GM, Sharp PA, Boyer LA, Young RA, Jaenisch R. Histone H3K27ac separates active from poised enhancers and predicts developmental state. Proceedings of the National Academy of Sciences of the United States of America. 2010;107(50):21931-6. Epub 2010/11/26. doi: 10.1073/pnas.1016071107. PubMed PMID: 21106759; PMCID: PMC3003124.

69. Fisher RC, Scott EW. Role of PU.1 in hematopoiesis. Stem Cells. 1998;16(1):25-37. Epub 1998/02/25. doi: 10.1002/stem.160025. PubMed PMID: 9474745.

70. Laiosa CV, Stadtfeld M, Xie H, de Andres-Aguayo L, Graf T. Reprogramming of committed T cell progenitors to macrophages and dendritic cells by C/EBP alpha and PU.1 transcription factors. Immunity. 2006;25(5):731-44. Epub 2006/11/08. doi: 10.1016/j.immuni.2006.09.011. PubMed PMID: 17088084.

71. Cirovic B, Schonheit J, Kowenz-Leutz E, Ivanovska J, Klement C, Pronina N, Begay V, Leutz A. C/EBP-Induced Transdifferentiation Reveals Granulocyte-Macrophage Precursor-like Plasticity of B Cells. Stem cell reports. 2017;8(2):346-59.

Epub 2017/01/24. doi: 10.1016/j.stemcr.2016.12.015. PubMed PMID: 28111277; PMCID: PMC5312250.

72. Mass E, Ballesteros I, Farlik M, Halbritter F, Gunther P, Crozet L, Jacome-Galarza CE, Handler K, Klughammer J, Kobayashi Y, Gomez-Perdiguero E, Schultze JL, Beyer M, Bock C, Geissmann F. Specification of tissue-resident macrophages during organogenesis. Science. 2016;353(6304). Epub 2016/08/06. doi: 10.1126/science.aaf4238. PubMed PMID: 27492475; PMCID: PMC5066309.

73. Tompa M, Li N, Bailey TL, Church GM, De Moor B, Eskin E, Favorov AV, Frith MC, Fu Y, Kent WJ, Makeev VJ, Mironov AA, Noble WS, Pavesi G, Pesole G, Regnier M, Simonis N, Sinha S, Thijs G, van Helden J, Vandenbogaert M, Weng Z, Workman C, Ye C, Zhu Z. Assessing computational tools for the discovery of transcription factor binding sites. Nature biotechnology. 2005;23(1):137-44. Epub 2005/01/08. doi: 10.1038/nbt1053. PubMed PMID: 15637633.

74. Boeva V. Analysis of Genomic Sequence Motifs for Deciphering Transcription Factor Binding and Transcriptional Regulation in Eukaryotic Cells. Front Genet. 2016;7:24. Epub 2016/03/05. doi: 10.3389/fgene.2016.00024. PubMed PMID: 26941778; PMCID: PMC4763482.

75. Ghisletti S, Barozzi I, Mietton F, Polletti S, De Santa F, Venturini E, Gregory L, Lonie L, Chew A, Wei CL, Ragoussis J, Natoli G. Identification and characterization of enhancers controlling the inflammatory gene expression program in macrophages. Immunity. 2010;32(3):317-28. Epub 2010/03/09. doi: 10.1016/j.immuni.2010.02.008. PubMed PMID: 20206554.

76. Heinz S, Benner C, Spann N, Bertolino E, Lin YC, Laslo P, Cheng JX, Murre C, Singh H, Glass CK. Simple combinations of lineage-determining transcription factors prime cis-regulatory elements required for macrophage and B cell identities. Molecular cell. 2010;38(4):576-89. Epub 2010/06/02. doi: 10.1016/j.molcel.2010.05.004. PubMed PMID: 20513432; PMCID: PMC2898526.

77. Lu YC, Yeh WC, Ohashi PS. LPS/TLR4 signal transduction pathway. Cytokine. 2008;42(2):145-51. Epub 2008/02/29. doi: 10.1016/j.cyto.2008.01.006. PubMed PMID: 18304834.

78. Glass CK, Natoli G. Molecular control of activation and priming in macrophages. Nat Immunol. 2016;17(1):26-33. Epub 2015/12/19. doi: 10.1038/ni.3306. PubMed PMID: 26681459; PMCID: PMC4795476.

79. Kober DL, Brett TJ. TREM2-Ligand Interactions in Health and Disease. Journal of molecular biology. 2017;429(11):1607-29. Epub 2017/04/23. doi: 10.1016/j.jmb.2017.04.004. PubMed PMID: 28432014; PMCID: PMC5485854.

80. Deczkowska A, Weiner A, Amit I. The Physiology, Pathology, and Potential Therapeutic Applications of the TREM2 Signaling Pathway. Cell. 2020;181(6):1207-17. Epub 2020/06/13. doi: 10.1016/j.cell.2020.05.003. PubMed PMID: 32531244.

81. Feuerbach D, Schindler P, Barske C, Joller S, Beng-Louka E, Worringer KA, Kommineni S, Kaykas A, Ho DJ, Ye C, Welzenbach K, Elain G, Klein L, Brzak I, Mir AK, Farady CJ, Aichholz R, Popp S, George N, Neumann U. ADAM17 is the main sheddase for the generation of human triggering receptor expressed in myeloid cells (hTREM2) ectodomain and cleaves TREM2 after Histidine 157. Neurosci Lett. 2017;660:109-14. Epub 2017/09/20. doi: 10.1016/j.neulet.2017.09.034. PubMed PMID: 28923481.

82. Filipello F, Goldsbury C, You SF, Locca A, Karch CM, Piccio L. Soluble TREM2: Innocent bystander or active player in neurological diseases? Neurobiol Dis. 2022;165:105630. Epub 2022/01/19. doi: 10.1016/j.nbd.2022.105630. PubMed PMID: 35041990.

83. Daws MR, Lanier LL, Seaman WE, Ryan JC. Cloning and characterization of a novel mouse myeloid DAP12-associated receptor family. European journal of immunology. 2001;31(3):783-91. Epub 2001/03/10. doi: 10.1002/1521-4141(200103)31:3<783::aid-immu783>3.0.co;2-u. PubMed PMID: 11241283.

84. Peng Q, Malhotra S, Torchia JA, Kerr WG, Coggeshall KM, Humphrey MB. TREM2- and DAP12-dependent activation of PI3K requires DAP10 and is inhibited by SHIP1. Sci Signal. 2010;3(122):ra38. Epub 2010/05/21. doi: 10.1126/scisignal.2000500. PubMed PMID: 20484116; PMCID: PMC2900152.

85. Mocsai A, Humphrey MB, Van Ziffle JA, Hu Y, Burghardt A, Spusta SC, Majumdar S, Lanier LL, Lowell CA, Nakamura MC. The immunomodulatory adapter proteins DAP12 and Fc receptor gamma-chain (FcRgamma) regulate development of functional osteoclasts through the Syk tyrosine kinase. Proceedings of the National Academy of Sciences of the United States of America. 2004;101(16):6158-63. Epub 2004/04/10. doi: 10.1073/pnas.0401602101. PubMed PMID: 15073337; PMCID: PMC395939.

86. Jaitin DA, Adlung L, Thaiss CA, Weiner A, Li B, Descamps H, Lundgren P, Bleriot C, Liu Z, Deczkowska A, Keren-Shaul H, David E, Zmora N, Eldar SM, Lubezky N, Shibolet O, Hill DA, Lazar MA, Colonna M, Ginhoux F, Shapiro H, Elinav E, Amit I. Lipid-Associated Macrophages Control Metabolic Homeostasis in a Trem2-Dependent Manner. Cell. 2019;178(3):686-98 e14. Epub 2019/07/02. doi: 10.1016/j.cell.2019.05.054. PubMed PMID: 31257031; PMCID: PMC7068689.

87. Xiong X, Kuang H, Ansari S, Liu T, Gong J, Wang S, Zhao XY, Ji Y, Li C, Guo L, Zhou L, Chen Z, Leon-Mimila P, Chung MT, Kurabayashi K, Opp J, Campos-Perez F, Villamil-Ramirez H, Canizales-Quinteros S, Lyons R, Lumeng CN, Zhou B, Qi L,

Huertas-Vazquez A, Lusis AJ, Xu XZS, Li S, Yu Y, Li JZ, Lin JD. Landscape of Intercellular Crosstalk in Healthy and NASH Liver Revealed by Single-Cell Secretome Gene Analysis. Molecular cell. 2019;75(3):644-60 e5. Epub 2019/08/10. doi: 10.1016/j.molcel.2019.07.028. PubMed PMID: 31398325; PMCID: PMC7262680.

88. Tsukamoto S, Takeuchi M, Kawaguchi T, Togasaki E, Yamazaki A, Sugita Y, Muto T, Sakai S, Takeda Y, Ohwada C, Sakaida E, Shimizu N, Nishii K, Jiang M, Yokote K, Bujo H, Nakaseko C. Tetraspanin CD9 modulates ADAM17-mediated shedding of LR11 in leukocytes. Exp Mol Med. 2014;46:e89. Epub 2014/04/05. doi: 10.1038/emm.2013.161. PubMed PMID: 24699135; PMCID: PMC3944444.

89. Hamerman JA, Jarjoura JR, Humphrey MB, Nakamura MC, Seaman WE, Lanier LL. Cutting edge: inhibition of TLR and FcR responses in macrophages by triggering receptor expressed on myeloid cells (TREM)-2 and DAP12. Journal of immunology. 2006;177(4):2051-5. Epub 2006/08/05. doi: 10.4049/jimmunol.177.4.2051. PubMed PMID: 16887962.

90. Turnbull IR, Gilfillan S, Cella M, Aoshi T, Miller M, Piccio L, Hernandez M, Colonna M. Cutting edge: TREM-2 attenuates macrophage activation. Journal of immunology. 2006;177(6):3520-4. Epub 2006/09/05. doi: 10.4049/jimmunol.177.6.3520. PubMed PMID: 16951310.

91. Takahashi K, Rochford CD, Neumann H. Clearance of apoptotic neurons without inflammation by microglial triggering receptor expressed on myeloid cells-2. The Journal of experimental medicine. 2005;201(4):647-57. Epub 2005/02/25. doi: 10.1084/jem.20041611. PubMed PMID: 15728241; PMCID: PMC2213053.

92. N'Diaye EN, Branda CS, Branda SS, Nevarez L, Colonna M, Lowell C, Hamerman JA, Seaman WE. TREM-2 (triggering receptor expressed on myeloid cells 2) is a phagocytic receptor for bacteria. J Cell Biol. 2009;184(2):215-23. Epub 2009/01/28. doi: 10.1083/jcb.200808080. PubMed PMID: 19171755; PMCID: PMC2654305.

93. Ulland TK, Song WM, Huang SC, Ulrich JD, Sergushichev A, Beatty WL, Loboda AA, Zhou Y, Cairns NJ, Kambal A, Loginicheva E, Gilfillan S, Cella M, Virgin HW, Unanue ER, Wang Y, Artyomov MN, Holtzman DM, Colonna M. TREM2 Maintains Microglial Metabolic Fitness in Alzheimer's Disease. Cell. 2017;170(4):649-63 e13. Epub 2017/08/13. doi: 10.1016/j.cell.2017.07.023. PubMed PMID: 28802038; PMCID: PMC5573224.

94. Wang Y, Cella M, Mallinson K, Ulrich JD, Young KL, Robinette ML, Gilfillan S, Krishnan GM, Sudhakar S, Zinselmeyer BH, Holtzman DM, Cirrito JR, Colonna M. TREM2 lipid sensing sustains the microglial response in an Alzheimer's disease model.

Cell. 2015;160(6):1061-71. Epub 2015/03/03. doi: 10.1016/j.cell.2015.01.049. PubMed PMID: 25728668; PMCID: PMC4477963.

95. Guerreiro R, Wojtas A, Bras J, Carrasquillo M, Rogaeva E, Majounie E, Cruchaga C, Sassi C, Kauwe JS, Younkin S, Hazrati L, Collinge J, Pocock J, Lashley T, Williams J, Lambert JC, Amouyel P, Goate A, Rademakers R, Morgan K, Powell J, St George-Hyslop P, Singleton A, Hardy J, Alzheimer Genetic Analysis G. TREM2 variants in Alzheimer's disease. N Engl J Med. 2013;368(2):117-27. Epub 2012/11/16. doi: 10.1056/NEJMoa1211851. PubMed PMID: 23150934; PMCID: PMC3631573.

96. Jonsson T, Stefansson H, Steinberg S, Jonsdottir I, Jonsson PV, Snaedal J, Bjornsson S, Huttenlocher J, Levey AI, Lah JJ, Rujescu D, Hampel H, Giegling I, Andreassen OA, Engedal K, Ulstein I, Djurovic S, Ibrahim-Verbaas C, Hofman A, Ikram MA, van Duijn CM, Thorsteinsdottir U, Kong A, Stefansson K. Variant of TREM2 associated with the risk of Alzheimer's disease. N Engl J Med. 2013;368(2):107-16. Epub 2012/11/16. doi: 10.1056/NEJMoa1211103. PubMed PMID: 23150908; PMCID: PMC3677583.

97. Paloneva J, Manninen T, Christman G, Hovanes K, Mandelin J, Adolfsson R, Bianchin M, Bird T, Miranda R, Salmaggi A, Tranebjaerg L, Konttinen Y, Peltonen L. Mutations in two genes encoding different subunits of a receptor signaling complex result in an identical disease phenotype. Am J Hum Genet. 2002;71(3):656-62. Epub 2002/06/25. doi: 10.1086/342259. PubMed PMID: 12080485; PMCID: PMC379202.

98. Bianchin MM, Capella HM, Chaves DL, Steindel M, Grisard EC, Ganev GG, da Silva Junior JP, Neto Evaldo S, Poffo MA, Walz R, Carlotti Junior CG, Sakamoto AC. Nasu-Hakola disease (polycystic lipomembranous osteodysplasia with sclerosing leukoencephalopathy--PLOSL): a dementia associated with bone cystic lesions. From clinical to genetic and molecular aspects. Cell Mol Neurobiol. 2004;24(1):1-24. Epub 2004/03/31. doi: 10.1023/b:cemn.0000012721.08168.ee. PubMed PMID: 15049507.

99. Molgora M, Esaulova E, Vermi W, Hou J, Chen Y, Luo J, Brioschi S, Bugatti M, Omodei AS, Ricci B, Fronick C, Panda SK, Takeuchi Y, Gubin MM, Faccio R, Cella M, Gilfillan S, Unanue ER, Artyomov MN, Schreiber RD, Colonna M. TREM2 Modulation Remodels the Tumor Myeloid Landscape Enhancing Anti-PD-1 Immunotherapy. Cell. 2020;182(4):886-900 e17. Epub 2020/08/14. doi: 10.1016/j.cell.2020.07.013. PubMed PMID: 32783918; PMCID: PMC7485282.

100. Katzenelenbogen Y, Sheban F, Yalin A, Yofe I, Svetlichnyy D, Jaitin DA, Bornstein C, Moshe A, Keren-Shaul H, Cohen M, Wang SY, Li B, David E, Salame TM, Weiner A, Amit I. Coupled scRNA-Seq and Intracellular Protein Activity Reveal an Immunosuppressive Role of TREM2 in Cancer. Cell. 2020;182(4):872-85 e19. Epub 2020/08/14. doi: 10.1016/j.cell.2020.06.032. PubMed PMID: 32783915.

101. Chang E, Pelosof L, Lemery S, Gong Y, Goldberg KB, Farrell AT, Keegan P, Veeraraghavan J, Wei G, Blumenthal GM, Amiri-Kordestani L, Singh H, Fashoyin-Aje L, Gormley N, Kluetz PG, Pazdur R, Beaver JA, Theoret MR. Systematic Review of PD-1/PD-L1 Inhibitors in Oncology: From Personalized Medicine to Public Health. Oncologist. 2021;26(10):e1786-e99. Epub 2021/07/02. doi: 10.1002/onco.13887. PubMed PMID: 34196068; PMCID: PMC8488782.

102. Virani SS, Alonso A, Aparicio HJ, Benjamin EJ, Bittencourt MS, Callaway CW, Carson AP, Chamberlain AM, Cheng S, Delling FN, Elkind MSV, Evenson KR, Ferguson JF, Gupta DK, Khan SS, Kissela BM, Knutson KL, Lee CD, Lewis TT, Liu J, Loop MS, Lutsey PL, Ma J, Mackey J, Martin SS, Matchar DB, Mussolino ME, Navaneethan SD, Perak AM, Roth GA, Samad Z, Satou GM, Schroeder EB, Shah SH, Shay CM, Stokes A, VanWagner LB, Wang NY, Tsao CW, American Heart Association Council on E, Prevention Statistics C, Stroke Statistics S. Heart Disease and Stroke Statistics-2021 Update: A Report From the American Heart Association. Circulation. 2021;143(8):e254-e743. Epub 2021/01/28. doi: 10.1161/CIR.0000000000000950. PubMed PMID: 33501848.

103. Glass CK, Witztum JL. Atherosclerosis. the road ahead. Cell. 2001;104(4):503-16. Epub 2001/03/10. doi: 10.1016/s0092-8674(01)00238-0. PubMed PMID: 11239408.

104. Anderson JL, Morrow DA. Acute Myocardial Infarction. N Engl J Med. 2017;376(21):2053-64. Epub 2017/05/26. doi: 10.1056/NEJMra1606915. PubMed PMID: 28538121.

105. Heusch G, Gersh BJ. The pathophysiology of acute myocardial infarction and strategies of protection beyond reperfusion: a continual challenge. Eur Heart J. 2017;38(11):774-84. Epub 2016/06/30. doi: 10.1093/eurheartj/ehw224. PubMed PMID: 27354052.

106. Fryar CD, Chen TC, Li X. Prevalence of uncontrolled risk factors for cardiovascular disease: United States, 1999-2010. NCHS Data Brief. 2012(103):1-8. Epub 2012/10/30. PubMed PMID: 23101933.

107. Bishu KG, Lekoubou A, Kirkland E, Schumann SO, Schreiner A, Heincelman M, Moran WP, Mauldin PD. Estimating the Economic Burden of Acute Myocardial Infarction in the US: 12 Year National Data. Am J Med Sci. 2020;359(5):257-65. Epub 2020/04/09. doi: 10.1016/j.amjms.2020.02.004. PubMed PMID: 32265010.

108. Han H, Wei X, He Q, Yu Y, Ruan Y, Wu C, Cao Y, Herzog E, He J. Comparison of In-Hospital Mortality and Length of Stay in Acute ST-Segment-Elevation Myocardial Infarction Among Urban Teaching Hospitals in China and the United States. Journal of the American Heart Association. 2019;8(22):e012054. Epub 2019/11/14. doi: 10.1161/JAHA.119.012054. PubMed PMID: 31718446; PMCID: PMC6915274.

109. Kaul P, Federspiel JJ, Dai X, Stearns SC, Smith SC, Jr., Yeung M, Beyhaghi H, Zhou L, Stouffer GA. Association of inpatient vs outpatient onset of ST-elevation myocardial infarction with treatment and clinical outcomes. JAMA. 2014;312(19):1999-2007. Epub 2014/11/17. doi: 10.1001/jama.2014.15236. PubMed PMID: 25399275; PMCID: PMC4266685.

110. Jernberg T, Johanson P, Held C, Svennblad B, Lindback J, Wallentin L, Swedeheart/Riks HIA. Association between adoption of evidence-based treatment and survival for patients with ST-elevation myocardial infarction. JAMA. 2011;305(16):1677-84. Epub 2011/04/28. doi: 10.1001/jama.2011.522. PubMed PMID: 21521849.

111. Puymirat E, Simon T, Steg PG, Schiele F, Gueret P, Blanchard D, Khalife K, Goldstein P, Cattan S, Vaur L, Cambou JP, Ferrieres J, Danchin N, Investigators UU, Investigators FM. Association of changes in clinical characteristics and management with improvement in survival among patients with ST-elevation myocardial infarction. JAMA. 2012;308(10):998-1006. Epub 2012/08/29. doi: 10.1001/2012.jama.11348. PubMed PMID: 22928184.

112. Hung J, Teng TH, Finn J, Knuiman M, Briffa T, Stewart S, Sanfilippo FM, Ridout S, Hobbs M. Trends from 1996 to 2007 in incidence and mortality outcomes of heart failure after acute myocardial infarction: a population-based study of 20,812 patients with first acute myocardial infarction in Western Australia. Journal of the American Heart Association. 2013;2(5):e000172. Epub 2013/10/10. doi: 10.1161/JAHA.113.000172. PubMed PMID: 24103569; PMCID: PMC3835218.

113. Sulo G, Igland J, Vollset SE, Nygard O, Ebbing M, Sulo E, Egeland GM, Tell GS. Heart Failure Complicating Acute Myocardial Infarction; Burden and Timing of Occurrence: A Nation-wide Analysis Including 86 771 Patients From the Cardiovascular Disease in Norway (CVDNOR) Project. Journal of the American Heart Association. 2016;5(1). Epub 2016/01/09. doi: 10.1161/JAHA.115.002667. PubMed PMID: 26744379; PMCID: PMC4859383.

114. Li W, Hsiao HM, Higashikubo R, Saunders BT, Bharat A, Goldstein DR, Krupnick AS, Gelman AE, Lavine KJ, Kreisel D. Heart-resident CCR2(+) macrophages promote neutrophil extravasation through TLR9/MyD88/CXCL5 signaling. JCI Insight. 2016;1(12). Epub 2016/08/19. doi: 10.1172/jci.insight.87315. PubMed PMID: 27536731; PMCID: PMC4985028.

115. Leuschner F, Nahrendorf M. Novel functions of macrophages in the heart: insights into electrical conduction, stress, and diastolic dysfunction. Eur Heart J. 2020;41(9):989-94. Epub 2019/04/05. doi: 10.1093/eurheartj/ehz159. PubMed PMID: 30945736; PMCID: PMC7778432.

116. Hilgendorf I, Gerhardt LM, Tan TC, Winter C, Holderried TA, Chousterman BG, Iwamoto Y, Liao R, Zirlik A, Scherer-Crosbie M, Hedrick CC, Libby P, Nahrendorf M, Weissleder R, Swirski FK. Ly-6Chigh monocytes depend on Nr4a1 to balance both inflammatory and reparative phases in the infarcted myocardium. Circulation research. 2014;114(10):1611-22. Epub 2014/03/15. doi: 10.1161/CIRCRESAHA.114.303204. PubMed PMID: 24625784; PMCID: PMC4017349.

117. King KR, Aguirre AD, Ye YX, Sun Y, Roh JD, Ng RP, Jr., Kohler RH, Arlauckas SP, Iwamoto Y, Savol A, Sadreyev RI, Kelly M, Fitzgibbons TP, Fitzgerald KA, Mitchison T, Libby P, Nahrendorf M, Weissleder R. IRF3 and type I interferons fuel a fatal response to myocardial infarction. Nature medicine. 2017;23(12):1481-7. Epub 2017/11/07. doi: 10.1038/nm.4428. PubMed PMID: 29106401; PMCID: PMC6477926.

118. Krishnamurthy P, Rajasingh J, Lambers E, Qin G, Losordo DW, Kishore R. IL-10 inhibits inflammation and attenuates left ventricular remodeling after myocardial infarction via activation of STAT3 and suppression of HuR. Circulation research. 2009;104(2):e9-18. Epub 2008/12/20. doi: 10.1161/CIRCRESAHA.108.188243. PubMed PMID: 19096025; PMCID: PMC2774810.

119. Majmudar MD, Keliher EJ, Heidt T, Leuschner F, Truelove J, Sena BF, Gorbatov R, Iwamoto Y, Dutta P, Wojtkiewicz G, Courties G, Sebas M, Borodovsky A, Fitzgerald K, Nolte MW, Dickneite G, Chen JW, Anderson DG, Swirski FK, Weissleder R, Nahrendorf M. Monocyte-directed RNAi targeting CCR2 improves infarct healing in atherosclerosis-prone mice. Circulation. 2013;127(20):2038-46. Epub 2013/04/26. doi: 10.1161/CIRCULATIONAHA.112.000116. PubMed PMID: 23616627; PMCID: PMC3661714.

120. DeBerge M, Yeap XY, Dehn S, Zhang S, Grigoryeva L, Misener S, Procissi D, Zhou X, Lee DC, Muller WA, Luo X, Rothlin C, Tabas I, Thorp EB. MerTK Cleavage on Resident Cardiac Macrophages Compromises Repair After Myocardial Ischemia Reperfusion Injury. Circulation research. 2017;121(8):930-40. Epub 2017/08/31. doi: 10.1161/CIRCRESAHA.117.311327. PubMed PMID: 28851810; PMCID: PMC5623080.

121. Nicolas-Avila JA, Lechuga-Vieco AV, Esteban-Martinez L, Sanchez-Diaz M, Diaz-Garcia E, Santiago DJ, Rubio-Ponce A, Li JL, Balachander A, Quintana JA, Martinez-de-Mena R, Castejon-Vega B, Pun-Garcia A, Traves PG, Bonzon-Kulichenko E, Garcia-Marques F, Cusso L, N AG, Gonzalez-Guerra A, Roche-Molina M, Martin-Salamanca S, Crainiciuc G, Guzman G, Larrazabal J, Herrero-Galan E, Alegre-Cebollada J, Lemke G, Rothlin CV, Jimenez-Borreguero LJ, Reyes G, Castrillo A, Desco M, Munoz-Canoves P, Ibanez B, Torres M, Ng LG, Priori SG, Bueno H, Vazquez J, Cordero MD, Bernal JA, Enriquez JA, Hidalgo A. A Network of Macrophages Supports Mitochondrial Homeostasis in the Heart. Cell. 2020;183(1):94-109 e23. Epub 2020/09/17. doi: 10.1016/j.cell.2020.08.031. PubMed PMID: 32937105.

122. Frangogiannis NG. The inflammatory response in myocardial injury, repair, and remodelling. Nature reviews Cardiology. 2014;11(5):255-65. Epub 2014/03/26. doi: 10.1038/nrcardio.2014.28. PubMed PMID: 24663091; PMCID: PMC4407144.

123. Heusch G. Cardioprotection: chances and challenges of its translation to the clinic. Lancet. 2013;381(9861):166-75. Epub 2012/10/26. doi: 10.1016/S0140-6736(12)60916-7. PubMed PMID: 23095318.

124. Yokota T, McCourt J, Ma F, Ren S, Li S, Kim TH, Kurmangaliyev YZ, Nasiri R, Ahadian S, Nguyen T, Tan XHM, Zhou Y, Wu R, Rodriguez A, Cohn W, Wang Y, Whitelegge J, Ryazantsev S, Khademhosseini A, Teitell MA, Chiou PY, Birk DE, Rowat AC, Crosbie RH, Pellegrini M, Seldin M, Lusis AJ, Deb A. Type V Collagen in Scar Tissue Regulates the Size of Scar after Heart Injury. Cell. 2020;182(3):545-62 e23. Epub 2020/07/06. doi: 10.1016/j.cell.2020.06.030. PubMed PMID: 32621799; PMCID: PMC7415659.

125. Mouton AJ, DeLeon-Pennell KY, Rivera Gonzalez OJ, Flynn ER, Freeman TC, Saucerman JJ, Garrett MR, Ma Y, Harmancey R, Lindsey ML. Mapping macrophage polarization over the myocardial infarction time continuum. Basic Res Cardiol. 2018;113(4):26. Epub 2018/06/06. doi: 10.1007/s00395-018-0686-x. PubMed PMID: 29868933; PMCID: PMC5986831.

126. Cavasin MA, Tao Z, Menon S, Yang XP. Gender differences in cardiac function during early remodeling after acute myocardial infarction in mice. Life sciences. 2004;75(18):2181-92. Epub 2004/08/25. doi: 10.1016/j.lfs.2004.04.024. PubMed PMID: 15325844.

127. Schlepckow K, Monroe KM, Kleinberger G, Cantuti-Castelvetri L, Parhizkar S, Xia D, Willem M, Werner G, Pettkus N, Brunner B, Sulzen A, Nuscher B, Hampel H, Xiang X, Feederle R, Tahirovic S, Park JI, Prorok R, Mahon C, Liang CC, Shi J, Kim DJ, Sabelstrom H, Huang F, Di Paolo G, Simons M, Lewcock JW, Haass C. Enhancing protective microglial activities with a dual function TREM2 antibody to the stalk region. EMBO Mol Med. 2020;12(4):e11227. Epub 2020/03/11. doi: 10.15252/emmm.201911227. PubMed PMID: 32154671; PMCID: PMC7136959.

128. Satija R, Farrell JA, Gennert D, Schier AF, Regev A. Spatial reconstruction of single-cell gene expression data. Nature biotechnology. 2015;33(5):495-502. Epub 2015/04/14. doi: 10.1038/nbt.3192. PubMed PMID: 25867923; PMCID: PMC4430369.

129. Butler A, Hoffman P, Smibert P, Papalexi E, Satija R. Integrating single-cell transcriptomic data across different conditions, technologies, and species. Nature biotechnology. 2018;36(5):411-20. Epub 2018/04/03. doi: 10.1038/nbt.4096. PubMed PMID: 29608179; PMCID: PMC6700744.

130. Wang GG, Calvo KR, Pasillas MP, Sykes DB, Hacker H, Kamps MP. Quantitative production of macrophages or neutrophils ex vivo using conditional Hoxb8. Nat Methods. 2006;3(4):287-93. Epub 2006/03/24. doi: 10.1038/nmeth865. PubMed PMID: 16554834.

131. Kanekiyo T, Bu G. The low-density lipoprotein receptor-related protein 1 and amyloid-beta clearance in Alzheimer's disease. Front Aging Neurosci. 2014;6:93. Epub 2014/06/07. doi: 10.3389/fnagi.2014.00093. PubMed PMID: 24904407; PMCID: PMC4033011.

132. Cheng J, Grassart A, Drubin DG. Myosin 1E coordinates actin assembly and cargo trafficking during clathrin-mediated endocytosis. Mol Biol Cell. 2012;23(15):2891-904. Epub 2012/06/08. doi: 10.1091/mbc.E11-04-0383. PubMed PMID: 22675027; PMCID: PMC3408416.

133. Rangaraju S, Dammer EB, Raza SA, Rathakrishnan P, Xiao H, Gao T, Duong DM, Pennington MW, Lah JJ, Seyfried NT, Levey AI. Identification and therapeutic modulation of a pro-inflammatory subset of disease-associated-microglia in Alzheimer's disease. Mol Neurodegener. 2018;13(1):24. Epub 2018/05/23. doi: 10.1186/s13024-018-0254-8. PubMed PMID: 29784049; PMCID: PMC5963076.

134. Zhang S, Hu L, Han C, Huang R, Ooi K, Qian X, Ren X, Chu D, Zhang H, Du D, Xia C. PLIN2 Mediates Neuroinflammation and Oxidative/Nitrosative Stress via Downregulating Phosphatidylethanolamine in the Rostral Ventrolateral Medulla of Stressed Hypertensive Rats. J Inflamm Res. 2021;14:6331-48. Epub 2021/12/10. doi: 10.2147/JIR.S329230. PubMed PMID: 34880641; PMCID: PMC8646230.

135. Loving BA, Tang M, Neal MC, Gorkhali S, Murphy R, Eckel RH, Bruce KD. Lipoprotein Lipase Regulates Microglial Lipid Droplet Accumulation. Cells. 2021;10(2). Epub 2021/01/28. doi: 10.3390/cells10020198. PubMed PMID: 33498265; PMCID: PMC7909280.

136. Irazoqui JE. Key Roles of MiT Transcription Factors in Innate Immunity and Inflammation. Trends in immunology. 2020;41(2):157-71. Epub 2020/01/22. doi: 10.1016/j.it.2019.12.003. PubMed PMID: 31959514; PMCID: PMC6995440.

137. La Spina M, Contreras PS, Rissone A, Meena NK, Jeong E, Martina JA. MiT/TFE Family of Transcription Factors: An Evolutionary Perspective. Front Cell Dev Biol. 2020;8:609683. Epub 2021/01/26. doi: 10.3389/fcell.2020.609683. PubMed PMID: 33490073; PMCID: PMC7815692.

138. Montague TG, Cruz JM, Gagnon JA, Church GM, Valen E. CHOPCHOP: a CRISPR/Cas9 and TALEN web tool for genome editing. Nucleic acids research.

2014;42(Web Server issue):W401-7. Epub 2014/05/28. doi: 10.1093/nar/gku410. PubMed PMID: 24861617; PMCID: PMC4086086.

139. Labun K, Montague TG, Gagnon JA, Thyme SB, Valen E. CHOPCHOP v2: a web tool for the next generation of CRISPR genome engineering. Nucleic acids research. 2016;44(W1):W272-6. Epub 2016/05/18. doi: 10.1093/nar/gkw398. PubMed PMID: 27185894; PMCID: PMC4987937.

140. Labun K, Montague TG, Krause M, Torres Cleuren YN, Tjeldnes H, Valen E. CHOPCHOP v3: expanding the CRISPR web toolbox beyond genome editing. Nucleic acids research. 2019;47(W1):W171-W4. Epub 2019/05/21. doi: 10.1093/nar/gkz365. PubMed PMID: 31106371; PMCID: PMC6602426.

141. Gosselin D, Skola D, Coufal NG, Holtman IR, Schlachetzki JCM, Sajti E, Jaeger BN, O'Connor C, Fitzpatrick C, Pasillas MP, Pena M, Adair A, Gonda DD, Levy ML, Ransohoff RM, Gage FH, Glass CK. An environment-dependent transcriptional network specifies human microglia identity. Science. 2017;356(6344). Epub 2017/05/27. doi: 10.1126/science.aal3222. PubMed PMID: 28546318; PMCID: PMC5858585.

142. Link VM, Duttke SH, Chun HB, Holtman IR, Westin E, Hoeksema MA, Abe Y, Skola D, Romanoski CE, Tao J, Fonseca GJ, Troutman TD, Spann NJ, Strid T, Sakai M, Yu M, Hu R, Fang R, Metzler D, Ren B, Glass CK. Analysis of Genetically Diverse Macrophages Reveals Local and Domain-wide Mechanisms that Control Transcription Factor Binding and Function. Cell. 2018;173(7):1796-809 e17. Epub 2018/05/22. doi: 10.1016/j.cell.2018.04.018. PubMed PMID: 29779944; PMCID: PMC6003872.

143. Heinz S, Texari L, Hayes MGB, Urbanowski M, Chang MW, Givarkes N, Rialdi A, White KM, Albrecht RA, Pache L, Marazzi I, Garcia-Sastre A, Shaw ML, Benner C. Transcription Elongation Can Affect Genome 3D Structure. Cell. 2018;174(6):1522-36 e22. Epub 2018/08/28. doi: 10.1016/j.cell.2018.07.047. PubMed PMID: 30146161; PMCID: PMC6130916.

144. Dobin A, Davis CA, Schlesinger F, Drenkow J, Zaleski C, Jha S, Batut P, Chaisson M, Gingeras TR. STAR: ultrafast universal RNA-seq aligner. Bioinformatics. 2013;29(1):15-21. Epub 2012/10/30. doi: 10.1093/bioinformatics/bts635. PubMed PMID: 23104886; PMCID: PMC3530905.

145. Love MI, Huber W, Anders S. Moderated estimation of fold change and dispersion for RNA-seq data with DESeq2. Genome Biol. 2014;15(12):550. Epub 2014/12/18. doi: 10.1186/s13059-014-0550-8. PubMed PMID: 25516281; PMCID: PMC4302049.

146. Langmead B, Salzberg SL. Fast gapped-read alignment with Bowtie 2. Nat Methods. 2012;9(4):357-9. Epub 2012/03/06. doi: 10.1038/nmeth.1923. PubMed PMID: 22388286; PMCID: PMC3322381.

147. Kent WJ, Sugnet CW, Furey TS, Roskin KM, Pringle TH, Zahler AM, Haussler D. The human genome browser at UCSC. Genome Res. 2002;12(6):996-1006. Epub 2002/06/05. doi: 10.1101/gr.229102. PubMed PMID: 12045153; PMCID: PMC186604.